

© 2018

ABDULEMAM ABU-SAIBIA

ALL RIGHTS RESERVED

FLEXURAL BEHAVIOR OF CONTINUOUS CONCRETE BEAMS  
PRESTRESSED WITH BONDED AND UNBONDED TENDONS

by

ABDULEMAM K. ABU-SAIBIA

A dissertation submitted to the

School of Graduate Studies

Rutgers, The State University of New Jersey

In partial fulfillment of the requirements

For the degree of

Doctor of Philosophy

Graduate Program in Civil and Environmental Engineering

Written under the direction of

Hani H. Nassif

And approved by

---

---

---

---

New Brunswick, New Jersey

OCTOBER, 2018

## ABSTRACT OF THE DISSERTATION

Flexural Behavior of Continuous Concrete Beams Prestressed with

Bonded and Unbonded Tendons

by ABDULEMAM ABU-SAIBIA

Dissertation Director:

Hani Nassif

Post-tensioning techniques have become very popular and a primary method in long spans continuous bridges and other structures due to their excellent performance in controlling cracking and excessive deflection. Moreover, the use of continuous prestressed concrete beams leads to shallower cross-sections, requires less maintenance cost, and enhances the durability of concrete in the negative moment region. Since using post-tensioned unbonded tendon requires particular analysis methods to predict the stress in the unbonded tendon because of the bond lack between the tendon and the adjacent concrete, thus this research presents an analytical approach to estimate the stress in the tendon and provide full-range of load versus deformation at different location of the span length at various load levels. The model used a *trussed-beam* system in addition to moment and force equilibrium equations to find the unknowns which include the stress in the unbonded tendon, deflection, and neutral axis depth. The analytical part included analyzing and estimating the stress in the unbonded tendon for beams subjected to a third-point and single-point load.

The proposed approach was validated with results from the performed beam tests in addition to test data in the literature. The experimental part included 20-ft long continuous High Strength Concrete (HSC) beams post-tensioned internally with bonded and unbonded tendons. The experimental approach included casting, instrumenting, and load testing of 8 continuous span beams at various levels of prestressing and combination of tendons. Various design parameters such as the area of non-prestressed steel in tension at the maximum positive and negative moment locations and effective prestress in the bonded, and unbonded tendons are considered.

Both models show a good correlation between predicted and experimental results. Furthermore, the effect of different design parameters on the flexural response was investigated. This study demonstrates that some design parameters have a significant influence on the results while the impact of other variables can be ignored.



## **ACKNOWLEDGEMENTS**

First, I would like to thank my committee members Dr. Tsakalakos, Dr. Najm, and Dr. Wang for their assistance and appreciated suggestions and comments.

Special appreciation and gratitude go to my advisor, Dr. Nassif for his guidance, assistance and valuable comments throughout the research study.

Great appreciations for the people in our RIME group who helped me performing the beam tests and ordering materials for the experimental research.

In addition, I would like to thanks the supplier companies who helped me get the materials that needed for the beam tests especially Jersey Precast, General Technology Inc. (GTI), Micro-Measurements, Precision-Hayes International and Clayton in Edison-New Jersey.

Finally, my deepest appreciation goes to my wife, children, and my big family in Iraq for their support and patience during my research study.

# TABLE OF CONTENTS

<b>ABSTRACT</b> .....	ii
<b>ACKNOWLEDGEMENTS</b> .....	iv
<b>TABLE OF CONTENTS</b> .....	v
<b>LIST OF TABLES</b> .....	viii
<b>LIST OF FIGURES</b> .....	ix
<b>LIST OF SYMBOLS</b> .....	xviii
<b>CHAPTER</b>	
<b>I. INTRODUCTION</b> .....	1
1.1 General Overview .....	1
1.2 Problem Statement .....	2
1.3 Scope .....	3
1.4 Organization of the Dissertation .....	4
<b>II. LITERATURE REVIEW</b> .....	6
2.1 Introduction .....	6
2.2 Behavior of Simply Supported Concrete Beams With Unbonded Tendons .....	7
2.3 Behavior of Continuous Concrete Beams with Unbonded Tendons .....	10
<b>III. EXPERIMENTAL PROGRAM</b> .....	17
3.1 Introduction .....	17
3.2 Experimental Program and Test Parameters .....	17
3.3 Materials Properties .....	24
3.3.1 High Strength Concrete .....	24
3.3.2 Non-prestressing Steel .....	30
3.3.3 Prestressing Steel .....	44
3.3.3.1 Unbonded Tendon .....	45

3.3.3.2 Bonded Tendon.....	46
3.3.3.3 Cable Grout .....	47
3.4 Instrumentation .....	50
3.4.1 Load Cells .....	50
3.4.2 Linear Voltage Differential Transducers (LVDTs) .....	51
3.4.3 Strain Gauges .....	52
3.5 Loading Frame Setup.....	54
3.5.1 Middle Support Steel Frame .....	57
<b>IV. EXPERIMENTAL RESULTS AND DISCUSSION .....</b>	<b>59</b>
4.1 Introduction.....	59
4.2 Crack Behavior .....	59
4.3 Modes of Failure and Plastic Hinge Formation .....	67
4.4 Load-Deformation Behavior .....	69
4.4.1 Load-Deflection Relationship.....	69
4.4.2 Load-Strain Relationship .....	81
4.4.3 Stress in Prestressing Steel.....	92
<b>V. ANALYTICAL INVESTIGATION .....</b>	<b>100</b>
5.1 Introduction.....	100
5.2 Methodology Background .....	101
5.3 Trussed-Beam Model for Continuous Beams .....	101
5.3.1 Main Assumptions .....	102
5.3.2 Mathematical Formulation for Two-Span Continuous Beam with Third-Point Loading.....	105
5.3.2.1 Derivation of Calculating the Strain in the Unbonded Tendon using Energy Conservation with Third-Point Loading .....	112
5.3.2.1 Deflection Calculation from Curvature Diagram using Moment-Area Integration with Third-Point Loading .....	119
5.3.3 Mathematical Formulation for Two-Span Continuous Beam with Single-Point Loading at Midspan.....	129

5.3.3.1 Derivation of Calculating the Strain in the Unbonded Tendon using Energy Conservation with Single-Point Loading .....	130
5.3.3.2 Deflection Calculation from Curvature Diagram using Moment-Area Integration with Single-Point Loading .....	135
5.4 Flow Chart Analysis .....	140
5.5 Moment-Deformation Relationship .....	142
<b>VI. MODEL VALIDATION AND COMPARISON OF RESULTS.....</b>	<b>142</b>
6.1 Introduction.....	142
6.2 Validation of the Proposed Model using Load-Deformation Curves .....	143
6.3 Comparison of Stress in Unbonded Tendon .....	158
6.4 Study the Effect of Design Parameters .....	160
<b>VII. CONCLUSIONS .....</b>	<b>169</b>
7.1 Summary .....	169
7.2 Conclusions.....	171
<b>REFERENCES.....</b>	<b>173</b>

## LIST OF TABLES

<b>3.1</b>	Prestressing and Reinforcement Details of Test Specimens.....	19
<b>3.2</b>	Typical concrete mix proportions per one cubic yard. ....	25
<b>3.3</b>	Summary of Compression, Tension, and Modulus of Concrete for all Beam Tests .....	28
<b>3.4</b>	Concrete Strength of the Typical Concrete Mix at Various Ages .....	28
<b>3.5</b>	Summary of Steel Details for all Beam Tests .....	31
<b>3.6</b>	Summary of $f_y$ , $E_s$ , $f_u$ and $\epsilon_u$ for Tensile Steel at positive Locations .....	34
<b>3.7</b>	Summary of $f_y$ , $E_s$ , $f_u$ and $\epsilon_u$ for Tensile Steel at Middle Support Location .....	34
<b>3.8</b>	Summary of Compression Strength for Cable Grout Samples at Different Ages. ....	49
<b>4.1</b>	Summary of Results for Crack Width and no. of Cracks. ....	66
<b>4.2</b>	Summary of Location of First Crack and Cracking Load.....	68
<b>4.3</b>	Summary of Beam Camber due to Bonded and Unbonded Tendons .....	70
<b>4.4</b>	Summary of Stress Increase $\Delta f_{psU}$ and Stress $f_{psU}$ in the Unbonded Tendon at Failure .....	68
<b>5.1</b>	Failure Mechanisms of Two-Span Continuous Beam due to Loading Type.....	104
<b>5.2</b>	Summary of Unknowns and Provided Relationships .....	105
<b>6.1</b>	Experimental and Predicted Comparison of Stress in Unbonded Tendon.....	159
<b>6.2</b>	Material Properties and Dimensions of Case Study Beams.....	162
<b>6.3</b>	Summary of Stress Increase in the Unbonded Tendon for the First Proposed Model .....	167
<b>6.4</b>	Summary of Stress Increase in the Unbonded Tendon for the Second Proposed Model.....	168

## LIST OF FIGURES

<b>3.1</b>	(a) Typical Cross-Section at L/3, (b) at Middle Support, (c) Two-Span Continuous Beam Test Layout .....	23
<b>3.2</b>	Vibrators for 4 x 8 in. Concrete Cylinders.....	26
<b>3.3</b>	Concrete Tests Setup.....	29
<b>3.4</b>	Reinforcement Details at Middle Support .....	30
<b>3.5</b>	a) and b) Test Setup for Tension Test of Steel Rebar, c) P3 Strain Indicator and Recorder, d) Strain Gauge Setup e) Fracture of Steel Rebar at Fracture .....	33
<b>3.6</b>	Stress versus Strain Relationship from Bottom Rebar Tension Test, Beam 1 .....	35
<b>3.7</b>	Stress versus Strain Relationship from Top Rebar Tension Test, Beam 1 .....	35
<b>3.8</b>	Stress versus Strain Relationship from Bottom Rebar Tension Test, Beam 2 .....	36
<b>3.9</b>	Stress versus Strain Relationship from Top Rebar Tension Test, Beam 2 .....	36
<b>3.10</b>	Stress versus Strain Relationship from Bottom Rebar Tension Test, Beam 3 .....	37
<b>3.11</b>	Stress versus Strain Relationship from Top Rebar Tension Test, Beam 3 .....	37
<b>3.12</b>	Stress versus Strain Relationship from Bottom Rebar Tension Test, Beam 4 .....	38
<b>3.13</b>	Stress versus Strain Relationship from Top Rebar Tension Test, Beam 4 .....	38
<b>3.14</b>	Stress versus Strain Relationship from Bottom Rebar Tension Test, Beam 5 .....	39
<b>3.15</b>	Stress versus Strain Relationship from Top Rebar Tension Test, Beam 5 .....	39

<b>3.16</b>	Stress versus Strain Relationship from Bottom Rebar	
	Tension Test, Beam 6 .....	40
<b>3.17</b>	Stress versus Strain Relationship from Top Rebar	
	Tension Test, Beam 6 .....	40
<b>3.18</b>	Stress versus Strain Relationship from Bottom Rebar	
	Tension Test, Beam 7 .....	41
<b>3.19</b>	Stress versus Strain Relationship from Top Rebar	
	Tension Test, Beam 7 .....	41
<b>3.20</b>	Stress versus Strain Relationship from Bottom Rebar	
	Tension Test, Beam 8 .....	42
<b>3.21</b>	Stress versus Strain Relationship from Top Rebar	
	Tension Test, Beam 8 .....	42
<b>3.22</b>	Typical Longitudinal and Shear Reinforcement for Beam Specimen .....	43
<b>3.23</b>	Stress versus Strain Relationship for 5/16" Prestressing Strands .....	44
<b>3.24</b>	PVC Pipe for Unbonded Tendon, a) Before Casting	
	b) After Casting.....	45
<b>3.25</b>	Plastic Corrugated Tube.....	46
<b>3.26</b>	Mono-Strand Anchorage System.....	47
<b>3.27</b>	Cable Grout Specimens, (a) After Demolding, (b) Compression Test.....	48
<b>3.28</b>	Typical Bonded and Unbonded Tendons Cross Sections .....	49
<b>3.29</b>	Typical Load Cell Used to Monitor Applied Load.....	50
<b>3.30</b>	Typical Load Cell Used with Bonded and Unbonded Tendon .....	51
<b>3.31</b>	Linear Voltage Differential Transducer, a) 6-in Range LVDT	
	b) 2-in Range LVDT .....	52
<b>3.32</b>	Stain Gauge Installation Kits .....	53
<b>3.33</b>	Strain Gauges installation in the Longitudinal Steel.....	53
<b>3.34</b>	Location of the Strain Gauges on the Reinforcing Rebar .....	54
<b>3.35</b>	Loading Frame before Rotation .....	55
<b>3.36</b>	New Loading Frame Setup and Beam Test .....	57
<b>3.37</b>	Middle Support Steel Frame, (a) Before Placing Beam Test,	
	(b) After Placing Beam Test .....	58

<b>4.1</b>	Students Observing Cracks during Beam Testing .....	60
<b>4.2</b>	(a) Microscope for Cracks Measurements, (b) Magnified Crack using Microscope .....	60
<b>4.3</b>	Plastic Hinges Locations for Third-Point Loading .....	61
<b>4.4</b>	Plastic Hinge Locations for Single Point Loading at Midspan.....	61
<b>4.5</b>	Crack Patterns at Failure for All Test Specimens.....	65
<b>4.6</b>	Relationship between Applied Load and Deflection at Different locations for Beam 1.....	71
<b>4.7</b>	Relationship between Applied Load and Deflection at Different locations for Beam 2.....	71
<b>4.8</b>	Relationship between Applied Load and Deflection at Different locations for Beam 3.....	72
<b>4.9</b>	Relationship between Applied Load and Deflection at Different locations for Beam 4.....	72
<b>4.10</b>	Relationship between Applied Load and Deflection at Different locations for Beam 5.....	73
<b>4.11</b>	Relationship between Applied Load and Deflection at Different locations for Beam 6.....	73
<b>4.12</b>	Relationship between Applied Load and Deflection at Different locations for Beam 7.....	74
<b>4.13</b>	Relationship between Applied Load and Deflection at Different locations for Beam 8.....	74
<b>4.14</b>	Relationship between Applied Load and Deflection at Maximum Positive Moment in both Spans for Beam 1.....	75
<b>4.15</b>	Relationship between Applied Load and Deflection at Maximum Positive Moment in both Spans for Beam 2.....	75
<b>4.16</b>	Relationship between Applied Load and Deflection at Maximum Positive Moment in both Spans for Beam 3.....	76
<b>4.17</b>	Relationship between Applied Load and Deflection at Maximum Positive Moment in both Spans for Beam 4.....	76
<b>4.18</b>	Relationship between Applied Load and Deflection at	



	Maximum Positive Moment in both Spans for Beam 5.....	77
<b>4.19</b>	Relationship between Applied Load and Deflection at Maximum Positive Moment in both Spans for Beam 6.....	77
<b>4.20</b>	Relationship between Applied Load and Deflection at Maximum Positive Moment in both Spans for Beam 7.....	78
<b>4.21</b>	Relationship between Applied Load and Deflection at Maximum Positive Moment in both Spans for Beam 8.....	78
<b>4.22</b>	Relationship between Applied Load and Deflection for varying $f_{pe}$ .....	79
<b>4.23</b>	Relationship between Applied Load and Deflection for varying $A_{s2}$ .....	79
<b>4.24</b>	Relationship between Applied Load and Deflection for varying $A_{s1}$ .....	80
<b>4.25</b>	Relationship between Applied Load and Deflection for varying <i>cross-section</i> .....	80
<b>4.26</b>	Relationship between Applied Load and Rebar Tensile Strain for Beam 1 .....	82
<b>4.27</b>	Relationship between Applied Load and Rebar Compressive Strain for Beam 1 .....	82
<b>4.28</b>	Relationship between Applied Load and Rebar Tensile Strain for Beam 2 .....	83
<b>4.29</b>	Relationship between Applied Load and Rebar Compressive Strain for Beam 2 .....	83
<b>4.30</b>	Relationship between Applied Load and Rebar Tensile Strain for Beam 3 .....	84
<b>4.31</b>	Relationship between Applied Load and Rebar Compressive Strain for Beam 3 .....	84
<b>4.32</b>	Relationship between Applied Load and Rebar Tensile Strain for Beam 4 .....	85
<b>4.33</b>	Relationship between Applied Load and Rebar Compressive Strain for Beam 4 .....	85

<b>4.34</b>	Relationship between Applied Load and Rebar Tensile Strain for Beam 5 .....	86
<b>4.35</b>	Relationship between Applied Load and Rebar Compressive Strain for Beam 5 .....	86
<b>4.36</b>	Relationship between Applied Load and Rebar Tensile Strain for Beam 6 .....	87
<b>4.37</b>	Relationship between Applied Load and Rebar Compressive Strain for Beam 6 .....	87
<b>4.38</b>	Relationship between Applied Load and Rebar Tensile Strain for Beam 7 .....	88
<b>4.39</b>	Relationship between Applied Load and Rebar Compressive Strain for Beam 7 .....	88
<b>4.40</b>	Relationship between Applied Load and Rebar Tensile Strain for Beam 8 .....	89
<b>4.41</b>	Relationship between Applied Load and Rebar Compressive Strain for Beam 8 .....	89
<b>4.42</b>	Relationship between Applied Load and Rebar Tensile Strain for varying $f_{pe}$ .....	90
<b>4.43</b>	Relationship between Applied Load and Rebar Tensile Strain for varying $A_{s2}$ .....	90
<b>4.44</b>	Relationship between Applied Load and Rebar Tensile Strain for varying $A_{s1}$ .....	91
<b>4.45</b>	Relationship between Applied Load and Rebar Tensile Strain for varying <i>cross-section</i> .....	91
<b>4.46</b>	Relationship between Applied Load and Stress Increase in Unbonded Tendon for Beam 1.....	94
<b>4.47</b>	Relationship between Applied Load and Stress Increase in Unbonded Tendon for Beam 2.....	94
<b>4.48</b>	Relationship between Applied Load and Stress Increase in Unbonded Tendon for Beam 3.....	95
<b>4.49</b>	Relationship between Applied Load and Stress Increase	

	in Unbonded Tendon for Beam 4.....	95
<b>4.50</b>	Relationship between Applied Load and Stress Increase in Unbonded Tendon for Beam 5.....	96
<b>4.51</b>	Relationship between Applied Load and Stress Increase in Unbonded Tendon for Beam 6.....	96
<b>4.52</b>	Relationship between Applied Load and Stress Increase in Unbonded Tendon for Beam 7.....	97
<b>4.53</b>	Relationship between Applied Load and Stress Increase in Unbonded Tendon for Beam 8.....	97
<b>4.54</b>	Relationship between Applied Load and Stress Increase in Unbonded Tendon for varying $f_{pe}$ .....	98
<b>4.55</b>	Relationship between Applied Load and Stress Increase in Unbonded Tendon for varying $A_{s2}$ .....	98
<b>4.56</b>	Relationship between Applied Load and Stress Increase in Unbonded Tendon for varying $A_{s1}$ .....	99
<b>4.57</b>	Relationship between Applied Load and Stress Increase in Unbonded Tendon for varying <i>cross-section</i> .....	99
<b>5.1</b>	Concrete Stress-Strain Curve.....	108
<b>5.2</b>	Typical Cross Section Used in the Analysis .....	109
<b>5.3</b>	Typical Stress-Strain Relationship for Non-prestressed Steel .....	110
<b>5.4</b>	Stress-Strain Relationships for; (a) Prestressed Steel Tendon, (b) Prestressed FRP Tendon.....	110
<b>5.5</b>	Failure Mechanism of Two-Span Continuous Beam with Third-Point Loading.....	112
<b>5.6</b>	Beam Tendon Profile and Collapse Mechanism under Third-Point Loading: (a) Beam Unbonded Tendon Profile; (b) Collapse Mechanism, (c) Plastic Hinge at Positive Moment at Ultimate; and (d) Plastic Hinge at Negative Moment at Ultimate.....	115
<b>5.7</b>	Typical Stress-Strain Relationship for Prestressing Tendon .....	118
<b>5.8</b>	Curvature Distribution of Continuous Beam at Cracking Concrete in Tension .....	120

<b>5.9</b>	Curvature Distribution of Continuous Beam at Yielding of Non-Prestressed Steel .....	121
<b>5.10</b>	Curvature Distribution of Continuous Beam at Yielding of Prestressing Tendon .....	123
<b>5.11</b>	Simplified Curvature Distribution of Continuous Beam at Yielding of Prestressing Tendon .....	124
<b>5.12</b>	Curvature Distribution of Continuous Beam at Crushing of Concrete in Compression .....	127
<b>5.13</b>	Simplified Curvature Distribution of Continuous Beam at Crushing of Concrete in Compression .....	127
<b>5.14</b>	Failure Mechanism of Two-Span Continuous Beam with Single-Point Load at Midspan .....	129
<b>5.15</b>	Beam Tendon Profile and Collapse Mechanism: (a) Beam Unbonded Tendon Profile; (b) Collapse Mechanism, (c) Plastic Hinge at Positive Moment at Ultimate; and (d) Plastic Hinge at Negative Moment at Ultimate.....	133
<b>5.16</b>	Curvature Distribution for a) Two-Span Beams under Single Point Load, b) At Cracking, c) after Cracking until Ultimate, and d) Idealized Curvature at Ultimate .....	138
<b>5.17</b>	Flow Chart for Analysis of Two-Span Continuous Beam .....	140
<b>5.18</b>	Moment versus Deformation Relationship of Beams Prestressed with Bonded and Unbonded Tendons.....	141
<b>6.1</b>	Applied load and deflection relationship of beam no. 1 in this Investigation: Analytical and experimental results.....	145
<b>6.2</b>	Applied load and deflection relationship of beam no. 1 in this Investigation: Analytical and experimental results.....	145
<b>6.3</b>	Applied load and deflection relationship of beam no. 1 in this Investigation: Analytical and experimental results.....	146
<b>6.4</b>	Applied load and deflection relationship of beam no. 2 in this Investigation: Analytical and experimental results.....	146
<b>6.5</b>	Applied load and deflection relationship of beam no. 2 in this	

	Investigation: Analytical and experimental results.....	147
<b>6.6</b>	Applied load and deflection relationship of beam no. 2 in this	
	Investigation: Analytical and experimental results.....	147
<b>6.7</b>	Applied load and deflection relationship of beam no. 3 in this	
	Investigation: Analytical and experimental results.....	148
<b>6.8</b>	Applied load and deflection relationship of beam no. 3 in this	
	Investigation: Analytical and experimental results.....	148
<b>6.9</b>	Applied load and deflection relationship of beam no. 3 in this	
	Investigation: Analytical and experimental results.....	149
<b>6.10</b>	Applied load and deflection relationship of beam no. 4 in this	
	Investigation: Analytical and experimental results.....	149
<b>6.11</b>	Applied load and deflection relationship of beam no. 4 in this	
	Investigation: Analytical and experimental results.....	150
<b>6.12</b>	Applied load and deflection relationship of beam no. 4 in this	
	Investigation: Analytical and experimental results.....	150
<b>6.13</b>	Applied load and deflection relationship of beam no. 5 in this	
	Investigation: Analytical and experimental results.....	151
<b>6.14</b>	Applied load and deflection relationship of beam no. 5 in this	
	Investigation: Analytical and experimental results.....	151
<b>6.15</b>	Applied load and deflection relationship of beam no. 5 in this	
	Investigation: Analytical and experimental results.....	152
<b>6.16</b>	Applied load and deflection relationship of beam no. 6 in this	
	Investigation: Analytical and experimental results.....	152
<b>6.17</b>	Applied load and deflection relationship of beam no. 6 in this	
	Investigation: Analytical and experimental results.....	153
<b>6.18</b>	Applied load and deflection relationship of beam no. 6 in this	
	Investigation: Analytical and experimental results.....	153
<b>6.19</b>	Applied load and deflection relationship of beam no. 7 in this	
	Investigation: Analytical and experimental results.....	154

<b>6.20</b>	Applied load and deflection relationship of beam no. 7 in this Investigation: Analytical and experimental results.....	154
<b>6.21</b>	Applied load and deflection relationship of beam no. 7 in this Investigation: Analytical and experimental results.....	155
<b>6.22</b>	Applied load and deflection relationship of beam no. 8 in this Investigation: Analytical and experimental results.....	155
<b>6.23</b>	Applied load and deflection relationship of beam C2 Tested by Tan and Tjandra (2007): Analytical and experimental results.....	156
<b>6.24</b>	Applied load and deflection relationship of beam YLB3 Tested by Lou et al. (2016): Analytical and experimental results.....	156
<b>6.25</b>	Applied load and deflection relationship of beam YLC3 Tested by Lou et al. (2016): Analytical and experimental results.....	157
<b>6.26</b>	Relationship Between Applied Load and Deflection at L/3 from Exterior Support for varying Reinforcing Steel $A_{sI}$ .....	163
<b>6.27</b>	Relationship Between Applied Load and Deflection at L/3 from Exterior Support for varying Unbonded Tendon Area $A_{psU}$ .....	163
<b>6.28</b>	Relationship Between Applied Load and Deflection at L/3 from Exterior Support for varying Bonded Tendon Area $A_{psB}$ .....	164
<b>6.29</b>	Relationship Between Applied Load and Deflection at L/3 from Exterior Support for varying Effective Stress $f_{pe}$ .....	164
<b>6.30</b>	Relationship Between Applied Load and Deflection at Midspan for varying Reinforcing Steel $A_{sI}$ .....	165
<b>6.31</b>	Relationship Between Applied Load and Deflection at Midspan for varying Unbonded Tendon Area $A_{psU}$ .....	165
<b>6.32</b>	Relationship Between Applied Load and Deflection at Midspan for varying Bonded Tendon Area $A_{psB}$ .....	166
<b>6.33</b>	Relationship Between Applied Load and Deflection at Midspan for varying Effective Stress $f_{pe}$ .....	166

## LIST OF SYMBOLS

$a$	depth of equivalent rectangular stress block as defined in ACI 318-05
$A_g$	gross area of the concrete section at midspan
$A_{psb}$	area of bonded prestressing steel
$A_{psu}$	area of unbonded prestressing steel (also used as $A_{ps}$ )
$A_{s1}$	area of non-prestressing tensile steel at midspan
$A_{s2}$	area of non-prestressing tensile steel at middle support
$A_s'$	area of non-prestressing compressive steel
$b$	width of the section
$b_w$	thickness of the web (for flanged sections)
$c$	depth of the neutral axis measured from top concrete fiber
$\Delta\epsilon_{ps}$	change in the strain in the prestressing tendons
$\Delta f_{ps}$	change in the stress in the prestressing tendons
$\Delta f_s$	change in the stress in the non-prestressing steel
$d_{ps}$	depth of the prestressing steel measured from top concrete fiber
$d_s$	depth of bonded non-prestressed steel measured from top concrete fiber
$e_m$	eccentricity of the tendon at midspan (also used as $e$ )
$e_s$	eccentricity of the tendon at support
$e_u^*$	eccentricity of the tendon at $L_h$ distance from the support
$E_{ps}$	modulus of elasticity of prestressing steel
$E_s$	modulus of elasticity of non-prestressing steel
$f$	load geometry factor=10, 3, 6 for 1point, 2point and uniform loading
$f'_c$	concrete compressive stress
$f_{cu}$	concrete compressive stress obtained from a cube test
$f_{pe}$	effective prestress in prestressing tendons after all losses
$f_{ps}$	stress at ultimate in prestressing tendons
$f_{pu}$	tensile strength of prestressing tendons
$f_{py}$	yield stress of prestressing tendons
$f_r$	modulus of rupture of plain concrete

$f_s$	stress in the non-prestressing tensile reinforcement
$f_y$	yield stress of non-prestressing tensile reinforcement
$h$	height of section
$h_f$	thickness of the flange
$I_g$	gross moment of inertia of uncracked section
$L$	span length
$L_a$	theoretical constant moment length = $L/f$
$L_h$	distance to the plastic hinge measured from the support
$L_p$	length of the plastic hinge
$M$	maximum moment applied on the beam
$M_{cr}$	the cracking moment
$M_{ph}$	moment at the plastic hinge
$PPR$	partial prestressing ratio
$Z$	the distance from the critical section to the point of contraflexure
$r^2$	radius of gyration
$\alpha$	$0.85 \beta_1$
$\beta_1$	ACI 318-05 stress block reduction factor
$\epsilon_c$	strain in the concrete
$\epsilon_{cu}$	strain in the concrete top fiber at ultimate
$\epsilon_{pe}$	effective prestrain in prestressing tendons after all losses
$\epsilon_{ps}$	strain at ultimate in prestressing tendons
$\epsilon_{pu}$	tensile strain of prestressing tendons at failure
$\delta$	elongation of tendon length between end anchorages
$\Delta$	midspan deflection
$\theta$	angle of rotation between the horizontal and the midspan
$\rho_{ps}$	prestressing steel reinforcing ratio = $A_{ps}/bd_{ps}$
$\rho_s$	non-prestressing tensile steel reinforcing ratio = $A_s/bd_s$



$\omega$	combined reinforcing index at ultimate = $\omega_{ps} + \omega_s - \omega'_s$
$\omega_{ps}$	reinforcing index of prestressing tendons at ultimate
$\omega_s$	reinforcing index of non-prestressing tensile steel
$\omega'_s$	reinforcing index of non-prestressing compressive steel
$w_c$	density of concrete

***Sub/superscripts***

$t$	top fiber
$b$	bottom fiber
$u$	unbonded tendon
$b$	bonded tendon
$c$	used for concrete properties
$s$	non-prestressing steel
$ps$	prestressing tendon
$cr$	cracking of concrete
$y$	yielding of non-prestressing steels
$py$	yielding of prestressing tendons
$u$	ultimate load, concrete failure in compression
$i$	iteration index number

# CHAPTER I

## INTRODUCTION

### 1.1 GENERAL OVERVIEW

Post-tensioning has become very popular applicability and a primary method in long spans bridges and other structures due to their excellent performance for cracking control and reduction of excessive deflection. There are many key advantages to using post-tensioning and have made it widely used includes: improving seismic behavior, reducing vibration, longer spans, decreasing dead load due to using thinner concrete members, etc. Moreover, the growing concerns about existed concrete structures that need more flexural resistance after the construction have increased rehabilitation using prestressing steel. Also, it has been widely used in the construction of segmental box girder bridges with longer spans. Post-tensioned concrete structures can be post-tensioning with bonded or unbonded tendons or both (hybrid tendons). The unbonded tendons can be stressed externally or internally.

Because of the widespread use of the post-tensioning unbonded tendon, especially strengthen the foundations, parking garages, and bridge; many types of research have investigated unbonded prestressing. Many investigators have focused on studying the behavior of the post-tensioned simple span concrete beams, but few of them studied the continuous beams. Continuous beams have become more preferred than simple span beams in construction especially in bridges because continuous girders have fewer joints, which require less maintenance cost and avoid corrosion issue at the negative moment region.

Furthermore, using continuous beams leads to smaller cross-sections, less deflection due to the advantages of moment redistribution.

## **1.2 PROBLEM STATEMENT**

In terms of the analysis, prestressed concrete beams with unbonded tendons behave differently when compare with beams with bonded tendons. Since the bond between the tendon and the concrete around the tendon is a lack or no bonding, the strain compatibility equations are not applicable because the axial strain in the tendon due to prestressing force and the applied loads is different from the strain in the concrete. The strain increases in unbonded tendons beyond the effective prestress depend on the total stress of the unbonded prestressing tendons between the anchorages location. It can be concluded that analysis of concrete beams prestressed with unbonded tendons is beam analysis rather than section analysis.

Many researchers proposed equations for calculating the stress of bonded, unbonded and hybrid tendons using different approaches applies for simple span only, however, an accurate analysis method that applies to continuous beams is needed. Also, the code equations are very conservative in comparison with experimental data. Accordingly, a new approach for the analysis of continuous beams prestressed with bonded and unbonded tendon is in demand.

Moreover, the previous investigations mostly have focused on simple span beams, while using continuous beams have become widely applied in parking garages and bridges.

Thus, the major goal of this study is to find out calculating the stress in the hybrid tendons at ultimate for two-span continuous concrete beams.

### **1.3 SCOPE**

The main objective of this study is to produce a model for calculating the stress in the unbonded tendons at different limit states for prestressed continuous concrete beams with bonded and unbonded tendons. The model applies for the beam at different types of load and various tendon profiles. Theoretical models will be developed to study the flexural behavior of the beams with a combination of prestressed bonded, prestressed unbonded and non-prestressed reinforcements at cracking, yielding of non-prestressing steel, yielding of prestressing tendon limit states. Several design parameters will be investigated in the analytical model. The theoretical results will be validated and compared with the results from experiments.

Finally, two-span continuous concrete specimens with bonded and unbonded tendons will be conducted to validate the presented analytical model. Nine beam specimens will be tested till failure occurs. Moreover, the design parameters that have significant effects on the proposed design equations will be investigated.

## **1.4 ORGANIZATION OF THE DISSERTATION**

The study was organized into five chapters to achieve the objectives of this study.

Chapter I presents the introduction which includes the overview of the study, problem statement, and objectives of the research. A brief description of all chapters in this dissertation is presented.

Chapter II is the literature review which covers the previous studies done by different investigators related to the stress at ultimate in unbonded tendons and the effective of the moment of inertia. Also, the previous technical papers that achieved about prestressed continuous concrete beams with bonded and/or unbonded tendons will be reviewed. The most updated code provisions for calculating the stress at ultimate are presented.

Chapter III presented the experimental programs for building two-span continuous beams. This includes the design parameters, materials properties that used, tests set-up and instrumentations. The experimental results that include strains stressed and load carrying capacity for all beams will be presented too.

Chapter IV shows all the experimental results which include crack pattern, load versus deflection relationship at a different location of the span length, load versus tensile strain in the rebar and load versus stress increase in the unbonded tendon. Also, all results are discussed in this chapter.

Chapter V proposed the two analytical models that applied to two-span concrete beams post-tensioned with bonded and unbonded tendon. The first model is applied for

beams subjected to a third-point load, while the other one for single-point load. The flowchart of the analysis steps is shown in this chapter.

Chapter VI presents the validation of the proposed approaches with experimental results that conducted in the laboratory. The reliability of the models is investigated herein. Case studies that show the influence of some design parameters on the flexural response of the beam is examined in this chapter.

Chapter VII introduces the most important conclusions that have accomplished in this study and the recommendations for the further studies.

## CHAPTER II

### LITERATURE REVIEW

#### 2.1 INTRODUCTION

Since the post-tensioned concrete structures turned into broadly used in construction, understanding the analysis and behavior of this kind of structural element became mandatory. A considerable amount of literature on the prestressed concrete simple-span beams with unbonded tendons has been undertaken. The reason for this interest is mainly to understand the behavior and performance of those members at different load levels. As it is noted in chapter one that the strain compatibility equations cannot be applied because of the lack of bond between the unbonded tendon and the surrounding concrete, new methods are needed despite finding relationships among the unknown parameters.

Since the design code equation requires the stress in the unbonded tendons at ultimate limit state to calculate the moment capacity of the prestressed members, most of the investigators have focused on finding the stress in the unbonded tendons  $f_{psU}$  at ultimate load level. The researchers have presented some methodologies to calculate the stress in the unbonded tendon with simplicity and more accuracy. Some researchers have developed new approaches for calculating the short-time deflection at various load levels.

In this chapter, an overview of the most studies that have published recently about the prestressing with unbonded tendons is presented. The first part introduces the most recent literature on the behavior of the simply supported concrete beams with unbonded

tendon while the second part presents studies that deal with the behavior of continuous beams with unbonded tendons.

## **2.2 BEHAVIOR OF SIMPLY-SUPPORTED CONCRETE BEAMS WITH UNBONDED TENDONS**

Park et al. (2006) proposed two numerical models to study the numerical procedure for analysis of prestressed concrete structures; both models were based on the finite element method. The first model represents the interaction between the tendon and the surrounding concrete, the friction and bond effect at the interface of tendon and the concrete is represented by the other model. The procedure was able to predict the elastic and plastic deformation, cracking, pretensioned bonded and unbonded post-tensioned response and patterns damage throughout their service life. The study verified the numerical results with experimental and analytical results and showed reasonably represent the nonlinear behavior of all limit states.

Harajli (2006) proposed a comprehensive assessment of the main parameters for the stress in unbonded tendons beyond the effective stress. The evaluation of current design expressions is conducted based on an extensive experimental database. Moreover, the author introduced an accurate expression for evaluating the equivalent plastic hinge length for simply supported and continuous members. Three alternative design methods were proposed to explain the sensitivity of stress in unbonded tendons based on this expression. These alternative design equations can be summarized as:



Alternative I:

$$f_{ps} = E_{ps} \varepsilon_{ps} \left( Q + \frac{1-Q}{\left[ 1 + \left( \frac{E_{ps} \varepsilon_{ps}}{K f_{py}} \right)^N \right]^{1/N}} \right) \quad (2.1)$$

Where: Q is the ratio of the slope of the post-yield branch of the stress-strain curve to the modulus of elasticity.

$$Q = \frac{f_{pu} - K f_{py}}{E_{ps} \varepsilon_{ps} - K f_{py}} \quad (2.2)$$

Then assuming the characteristic coefficients N=7 and K=1.0 that estimated by (Naaman 1983) to calculate the  $f_{ps}$ .

Alternative II:

$$f_{ps} = f_{pe} + \phi_{ps} E_{ps} \varepsilon_{ps} \left( \frac{d_p - c_y}{L_a / n_p} \right) \left( \frac{20.7}{f} + 10.5 \right) \leq f_{py} \quad (2.3)$$

Where

$$c_y = \frac{A_{ps} f_{py} + A_s f_y}{0.85 \beta_1 f_c' b} \quad (2.4)$$

Alternative III:

$$f_{ps} = \frac{f_{pe} + K_a E_{ps} \epsilon_{cu} \left[ d_p - \frac{\rho_s d_s f_y}{0.85 \beta_1 f_c'} \right]}{1 + \frac{K_a E_{ps} \epsilon_{cu} \rho_p d_p}{0.85 \beta_1 f_c'}} \quad (2.5)$$

According to the study results, the author concluded that most of the design equations for predicting the stress in the unbonded tendon at ultimate spread out from experimental data. Also, it is found that the equivalent plastic hinge length depends mostly on the neutral axis depth and type of load application. In comparison, the author concludes that the ACI equation for predicting the stress in the unbonded tendons is over conservative for simply supported members and the AASHTO LRFD approach is more rational than the ACI approach.

Ozkul (2007) proposed a general method for the analysis of simply supported beams prestressed with bonded and unbonded tendons. The analytical method uses four basic concepts; force and moment equilibrium, compatibility of deflection and work-energy principle. The model can calculate the stress in the unbonded tendon as well as calculating deflection at different limit states. Also, a finite element analysis was performed to validate the proposed approach. Thirteen high strength concrete simply supported beams prestressed with unbonded tendons were conducted. The presented model was validated using the beam tests results in addition to test data from the literature. The proposed approach shows good agreement at cracking, yielding of reinforcing steel, yielding of prestressing tendon and ultimate limit states.

Ozkul et al. (2008) presented a rational approach for predicting the stress in the unbonded tendon at different limit states. The method called *trussed-beam* model which

divides the prestressed beam with unbonded tendon into two elements, the first element is the reinforced concrete elements which include all components such as concrete, reinforcing steel and bonded tendon. However, the second element represents the unbonded tendon as a trussed element. Also, a finite element model was performed. To validate the proposed approach, twenty-five simply supported concrete beams prestressed with unbonded tendon were used. The model results show a very good agreement with the experimental results at all load levels.

### **2.3 BEHAVIOR OF CONTINUOUS BEAM WITH UNBONDED TENDON**

Machida and Bamrungwong (1999) investigated the flexural behavior of partially prestressed concrete beams. Three partially continuous prestressed concrete beams, one monolithically continuous beam and one single span beam, were conducted. Also, the non-linear analytical model was developed to predict the flexural behavior of the beams. Based on the experimental specimens results, the flexural behavior of partially prestressed concrete beams represented the transitional region between the monolithic beams and the simply supported beams. It showed that the degree of continuity was disclosed the negative moment value, especially in the linear range. Moreover, the study showed that there was a relationship between the force in the external tendon and the degree of continuity of the beam, the more continuity, the higher external tendon force.

Harajli et al. (2002) studied the experimental and analytical behavior of post-tensioned continuous beams prestressed using external tendons. Nine two-spans continuous beams were tested, all beams failed in flexural mode by forming collapse mechanism except one beam failed in shear after yielding the bonded reinforcement. It

was shown that beams with external prestressing behave similarly to the beams with internal prestressing. Also, it showed that the tendon profile affects load-carrying capacity, beams with straight tendons had lower load-carrying capacity comparing with those with draped tendons due to second-order effects. The analytical model showed that the plastic region lengths had a significant effect on stress increase in tendons, the tendon stress increase due to the rotational capacity and larger plastic-region lengths.

Tan and Tjandra (2003) tested four specimens consisting of two simple-span T-sections beams with expand to the rectangular section at the middle support and connecting using external prestressing tendons. The external tendon length equals the distance between the points of Contraflexure from the elastic bending moment diagram. The experimental results demonstrated that using the external tendons over the intermediate support enhances the capacity and serviceability of the beams for instance; increasing the load-carry capacity, reducing joint opening and the ductility as well. On the other side, reinforcing the positive regions with the external tendons leads to higher ultimate load, less deflection, and rotation over the interior support and smaller crack width. Additionally, the study showed the flexural behavior is not changing when CFRP tendon is used compared with steel tendon.

Aravinthan et al. (2005) studied the flexural behavior of continuous beams prestressed with highly external tendons. Nine specimens with a rectangular cross-section include six specimens two-span, and three simple-span were conducted. The results showed that for all loading stages, the linear transformation of tendon profile does not affect the flexural behavior of the beams. Also, yielding of prestressing tendons occurs at the ultimate loading stage due to the high eccentricity. Furthermore, the test results showed

that the tendon profile and load pattern influence the moment redistribution in unsymmetrical loading.

Tan and Tjandra (2007) tested twelve two-span externally prestressed continuous T-beams with different tendon types and profile. This study presented design charts to be used for strengthening two-span beams using external prestressing. Furthermore, the test results showed that using tendon overlapping especially at the negative moment can significantly enhance the strength of the entire continuous beam. Also, the ultimate load, deflection, and stress in the tendon are not be affected by the tendon type.

Chan (2008) investigated post-tensioned concrete beams experimentally and numerically. Eighteen two-span continuous beams partially prestressed with external tendons were conducted. Steel tendons were used in some of the beams, while other beams prestressed using Parafil ropes (kind of AFRP). A numerical model from literature was developed and used for the analysis in addition to the FEM. The test results showed that forming the first plastic hinge represents the ultimate capacity of the concrete beams with unbonded tendons. Also, the moment redistribution affects the shear forces in the continuous beams with unbonded tendons.

Decheng (2009) studied the strengthening of simple-span, continuous concrete beams and beams in reinforced concrete frames using external post-tensioning tendons. Furthermore, the study carried out the effect of the strengthening using external tendons on the secondary moments and moment redistribution in continuous concrete beams. Two sets of equations, Refined and Simplified, were proposed and verified with experimental results from the literature, in addition to seven continuous beams were conducted. The Refined

Equations showed good accuracy in comparison with the experimental results for estimating the load-carry capacity of the beams, on the other side, the Simplified Equations conservatively predict the capacity of the beams. The experimental results showed that for most of the tested beams, moment redistribution occurs in the interior support section. For strengthening reinforced concrete frames with external prestressing, the concept of bond reduction coefficients can be applied in the analysis.

Zheng et al. (2009) conducted an experimental study using internal unbonded carbon fiber reinforced polymer (CFRP) tendon, four partially simple spans, and nine partially two-span continuous beams were conducted. Also, according to the experimental results, an equation for calculating the length of the plastic hinge was produced. Furthermore, a formula for estimating the stress in unbonded CFRP tendon and coefficient of moment modification for partially prestressed continuous beams were introduced.

Kim and Lee (2012) proposed a new flexural behavior model for continuous beams with unbonded post-tensioning tendons. The research used the idealized curvature distribution of simply supported beam and extended to continuous beams. The authors validated the proposed model with experimental specimens that done by other researchers. The authors concluded that the proposed model shows good accuracy for estimating the overall flexural behavior of the continuous unbonded post-tensioned beam for different loading types. In addition, the study showed the flexibility on applying it on internal and external post-tensioning tendons.

Ghallab (2013) reviewed the past literature equations of calculating the stress increase in tendons at the failure. Also, a simple method for calculating the stress in

external tendons for two-span continuous beams for different load patterns is proposed. The presented equation was compared with thirty-seven experimental beam results from the literature. Different parameters such as tendon and loading type, span to depth ratio, eccentricity to depth ratio, prestressing force in tendons and non-prestressing reinforcement were studied. In general, the study showed better agreement than the reviewed methods with the need for more improvement. Moreover, it was found that BS8110 <sup>(2)</sup> and ACI-318 <sup>(3)</sup> equations were rationally accurate for eccentricities within the section depth. Otherwise, lack agreement was found. The study suggested that previous research can be applied to FRP tendon with considering the ultimate strength of beams with FRP tendons is equivalent to the yielding stress of the steel tendons.

Lou et al. (2013) numerically investigated the flexural behavior of the experimental continuous beams externally prestressed that were conducted by previous research. The increase in stress in the external tendon, moment redistribution and secondary moments were studied. A finite-element model was used for analysis of continuous beams with external tendons. The study showed that the presence of plastic hinges in continuous beams affect the stress increase in external tendons. Also, it was found that there is a linear relationship between the secondary moments and the force in external tendons. Moreover, a lower degree of moment redistribution at the interior support occurs under symmetrical loads on each span.

Zhou and Zheng (2014) presented an evaluation procedure for predicting the stress in the unbonded tendon in the continuous beams. Sixteen two-span continuous beam specimens were conducted and tested under static loading to validate the proposed procedure. The model was developed from the equilibrium of the ultimate flexural

capacity and adjusted using the experimental results. The rotation capacity of the plastic hinges was affected by several variables includes the prestressing reinforcement, the total reinforcement at the supports and the midspan, span-depth ratio. It was shown that the presented model is more accurate than the ACI code and China specification for predicting the stress at ultimate in the unbonded tendons in continuous beams. Also, the study showed a linear relationship between the stresses in the unbonded tendons and the stresses in normal reinforcements.

Chan and Au (2015) studied the behavior of continuous concrete beams with externally prestressing unbonded tendons. Nine two-span continuous concrete beams partially prestressed with external tendons were conducted. In order to study the behavior of preloaded reinforced concrete beams, two of them were loaded prior prestressing the tendons. All the beams were tested up to a failure to investigate the full-range behavior of the beams. The test result showed that the failure of continuous concrete beams with unbonded tendon occurs when any of the formed plastic hinges reaches its ultimate curvature. Also, the study explained that the direction of the moment redistribution in continuous concrete beams is not specified because the plastic hinge locations are varied, while in reinforced concrete beams assumed away from the critical section. Moreover, it was shown that the curvature ductility factor is a function of reinforcement ratio and span to depth ratio, where it decreases when the reinforcement ratio increases. And because the tendon remains elastic beyond forming of the plastic hinges, residual stiffness in continuous concrete beams with unbonded tendon cannot be negligible.

Maghsudi and Askari (2015) investigated the stress increase in unbonded tendons for two-span continuous post-tensioned self-compacting concrete beams with external



CFRP sheets. Two continuous post-tensioned I-section high strength normal concrete beams and other two using high strength self-compacting concrete were conducted. Different design codes were examined and compared with the experimental results. It was found that ACI 318-11 gives better estimates than AASHTO-2010, and this one provides better results than BS 8110-97. Also, the experimental results showed that the stress increase in the unbonded tendons in strengthened beams with bonded external FRP sheets is lower than non-strengthened beams. Moreover, the strengthened post-tensioned beams showed an obvious reduction in flexural crack width beyond yielding of tensile steel.

Six (2015) studied the stress increase in the unbonded tendon for three-span continuous concrete slabs prestressed with the unbonded tendon. Four full-scale specimens were built and tested until failure. The stress increase in the tendon was monitored at the ends and at various locations along the length of the strand using load cells and strain gauges. All slabs were tested under a third-point load. The experimental results were compared with other research and with the American Concrete Institute (ACI) and the American Association of State Highway and Transportation Officials Load and Resistance Factor Design (AASHTO LRFD) Bridge Design Specifications. The test results showed that both ACI and AASHTO design prediction methods are conservative. Also, it was found that the plastic hinge length, cracking distribution and deformation behavior is significantly affected by non-prestressed steel.

## **CHAPTER III**

### **EXPERIMENTAL PROGRAM**

#### **3.1 Introduction**

In the previous chapter, it was found that most of the reviewed literature were investigated studying the behavior of continuous concrete beams prestressed with external tendons, but there were no few studies investigated the behavior of continuous concrete beams prestressed internally with bonded and unbonded tendons. Therefore, this chapter presents the experimental program which includes casting, instrumenting and testing two-span continuous beam specimens prestressed internally with bonded and unbonded tendons. The analytical results that presented using this approach need to be validated and compared with experimental specimens. Therefore, several specimens were conducted at the civil engineering laboratory, Rutgers University to validate the proposed model. Thus, this chapter mainly covers the experimental program in details which includes; the test parameters, material properties, beam fabrication, instrumentation and the test procedure.

#### **3.2 Experimental Program and Test Parameters**

Eight two-span continuous concrete beams partially prestressed with bonded and unbonded tendons were conducted and loaded to failure with a significant deflection to investigate the full-range behavior. Each beam has two spans, 10 ft. each and has three supports two at the ends and one at the mid-point between the exterior supports. The beams are divided into three groups. Each group has a different cross-section and test parameters to study the effect of each parameter individually. The first group specimens with constant

T-section over two equal spans, while the second group is similar to the first group with extended 1 ft. I-section on both sides over the middle support to increase the ductility at the negative moment location and provide a similar section effect as at the midspan. Finally, the third group with constant I-section over two spans. The summary of the test specimens properties and design variables are shown in Table 3.1. All the groups were post-tensioned internally for both bonded and unbonded tendons. The first seven beams were tested under third-point loading for each span; however, the eighth beam was loaded under a single concentrated loading at midspan.

Table 3.1 Prestressing and Reinforcement Details of Test Specimens

Beam no.	(+ve) Moment section								(-ve) Moment section			
	Non-Prestressing Reinforcement				Bonded using Grout		Unbonded		Non-Prestressing Reinforcement			
	$A_s$ (in <sup>2</sup> )	$d_s$ (in)	$A_s'$ (in <sup>2</sup> )	$d_s'$ (in)	$A_{psB}$ (in <sup>2</sup> )	$d_{psB}$ (in)	$A_{psU}$ (in <sup>2</sup> )	$d_{psU}$ (in)	$A_s$ (in <sup>2</sup> )	$d_s$ (in)	$A_s'$ (in <sup>2</sup> )	$d_s'$ (in)
1	0.22	9.25	0.098	0.90	0.058	8.5	0.058	7.0	0.098	9.0	0.22	0.75
2	0.22	9.25	0.22	1.00	0.058	8.5	0.058	7.0	0.22	9.0	0.22	0.75
3	0.22	9.25	0.098	0.90	0.058	8.5	0.058	7.0	0.098	9.0	0.22	0.75
4	0.22	9.25	0.098	0.90	0.058	8.5	0.058	7.0	0.498	8.75	0.22	0.75
5	0.33	9.25	0.098	0.90	0.058	8.125	0.058	6.625	0.429	9.0	0.33	0.75
6	0.22	9.25	0.098	0.90	0.058	8.5	0.058	7.0	0.538	9.0	0.22	0.75
7	0.22	9.25	0.098	0.90	0.058	8.5	0.058	7.0	0.538	9.0	0.22	0.75
8	0.22	9.25	0.098	0.90	0.058	8.5	0.058	7.0	0.538	9.0	0.22	0.75

Table 3.1 Continued

(-ve) Moment section				single span Length (in)	$f_{peB}/f_{pu}$	$f_{peU}/f_{pu}$	L/ $d_{psB}$	L/ $d_{psu}$	Tendon Profile	Cross-section
Bonded using Grout		Unbonded								
$A_{psB}$ (in <sup>2</sup> )	$d_{psB}$ (in)	$A_{psU}$ (in <sup>2</sup> )	$d_{psU}$ (in)							
0.058	7.125	0.058	8.875	120	0.6	0.6	14.55	17.14	harped-2-point	T-section
0.058	7.125	0.058	8.875	120	0.65	0.65	14.55	17.14	harped-2-point	T-section
0.058	7.125	0.058	8.875	120	0.7	0.7	14.55	17.14	harped-2-point	T-section
0.058	7.125	0.058	8.875	120	0.7	0.7	14.55	17.14	harped-2-point	I-section at the middle support only
0.058	6.75	0.058	8.5	120	0.7	0.7	14.55	17.14	harped-2-point	I-section at the middle support only
0.058	7.125	0.058	8.875	120	0.7	0.7	14.55	17.14	harped-2-point	I-section at the middle support only
0.058	7.125	0.058	8.875	120	0.72	0.72	14.55	17.14	harped-2-point	I-section
0.058	7.125	0.058	8.875	120	0.72	0.72	14.55	17.14	harped-1-point	I-section

Several design parameters were investigated including the compressive concrete strength  $f_c'$ , non-prestressed reinforcement  $A_s$ , at the positive and negative region (middle support), the ratio of the effective prestressed tendon to the ultimate stress  $f_{pe}/f_{pu}$ , and the cross-section shape. The area of prestressed reinforcement  $A_{ps}$  was not been a variable in this investigation since using bigger tendon sizes exceed the limit of the testing machine in the laboratory. In partially prestressed members, the following formula is used to quantify the partial prestressing ratio ( $PPR$ ):

$$PPR = \frac{A_{ps}f_{ps}\left(d_p - \frac{a}{2}\right)}{A_{ps}f_{ps}\left(d_p - \frac{a}{2}\right) + A_sf_y\left(d_s - \frac{a}{2}\right)} \quad (3.1)$$

Then, the amount of the nonprestressing reinforcement  $\omega$  and the prestressing reinforcement  $\omega_p$  would be as follows:

$$\omega + \omega_p = \frac{\rho_sf_y}{f_c'} + \frac{\rho_{ps}f_{ps}}{f_c'} = \frac{A_sf_y}{bd_sf_c'} + \frac{A_{ps}f_{ps}}{bd_{ps}f_c'} \quad (3.2)$$

T-section was selected as the typical cross-section for all beam specimens. The dimensions of the section are; the depth is 10 in. and 2.25 in. as flange depth, while 12 in. and 5 in. represent the flange and web width, respectively. The span length of the continuous beams is 20 ft. each span is 10 ft. long with 1 ft. extension beyond the external supports at the ends (22 ft total length) to provide a room for anchorages and the coils to prevent crushing of concrete at the ends. Three steel supports are used to carry the beam weight and the external loads, one at each end and one at the middle. Two points harped tendon profile was considered for both bonded and unbonded tendons. Upper and lower layer of non-prestressed reinforcing bars were placed into the steel cages for the entire beam length.

Size no. 3 and 4 deformed bars were used for the tension side, and no. 2 plain bars were used for the compression side. The centroid of the top layer of non-prestressed reinforcement is located at a depth of 0.9 in. from the extreme compression fiber, while the bottom layer is located at a depth of 9.25 in. from the extreme top fiber. All beams were designed to avoid shear failure. Thus, shear stirrups were made of no. 2 plain bars provided at 1.5 in. for 40 in. from the center of the supports and 3 in. between the point loads in each span. Steel coils made of no. 2 plain bar were used at both ends of the beam to prevent crushing of the concrete due to the high prestressing force during the tendons post-tensioning. High capacity 250-kN load cells were used for each tendon placed at the dead end of the tendon to measure the change of the prestressing force during the prestressing and applying the external loads. Fig. 3.1 shows the typical cross-sections at  $L/3$  from the exterior support and the beam layout.

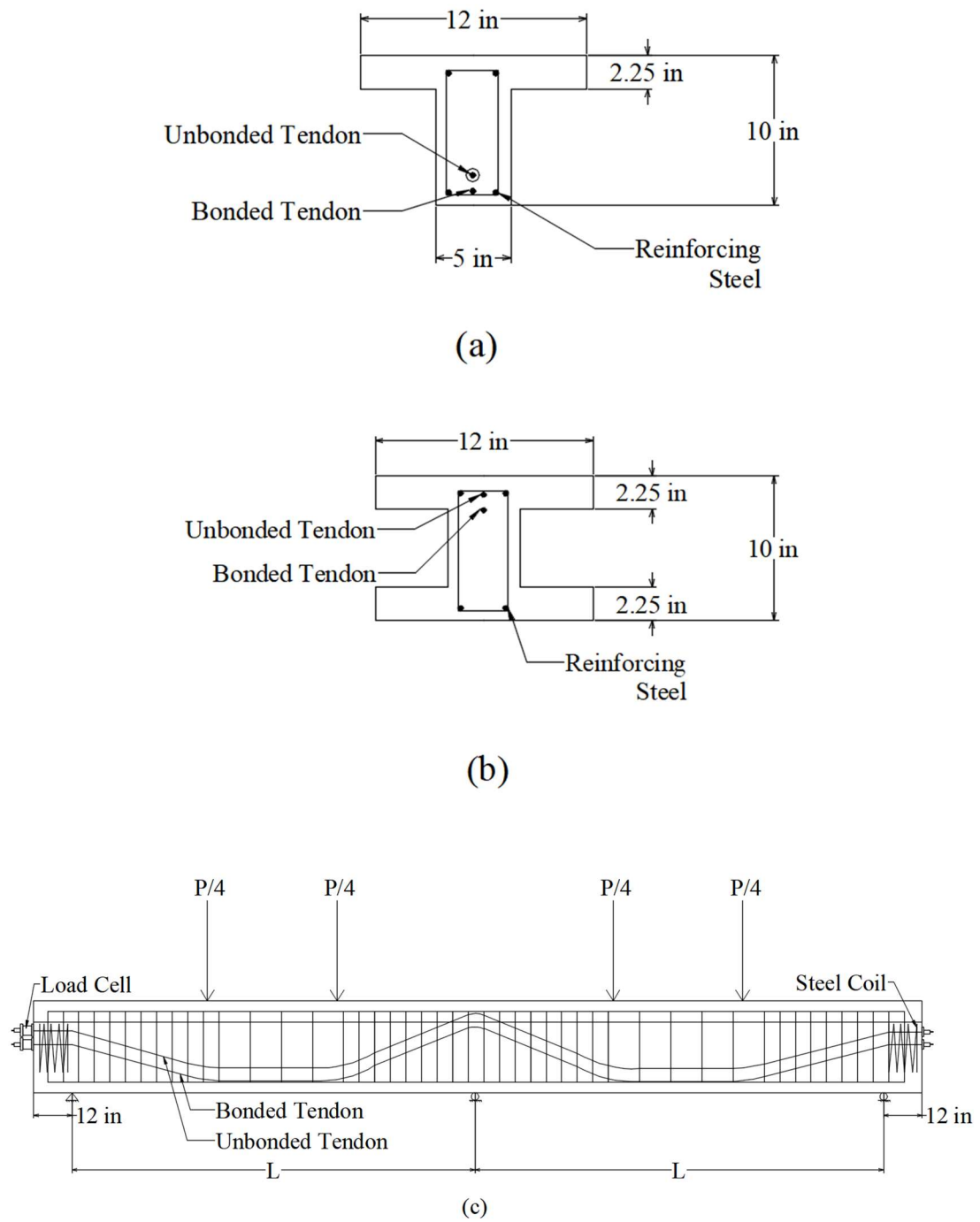


**Fig. 3.1 (a) Typical Cross-Section at  $L/3$ , (b) at Middle Support,**

**(c) Two-Span Continuous Beam Test Layout**



### 3.3 Materials Properties

#### 3.3.1 High Strength Concrete

The high strength concrete was used for all the test specimens. Because of the beams dimensions and length, the amount of concrete that is required to cast each specimen exceeds the capacity of the available concrete mixer in the laboratory. Thus, two similar batches were made at the same time for each beam. Two mixes were poured in sequence and vibrated after the second mix to satisfy making a rough surface between the two mixes and avoiding forming a cold joint between the two layers. The components of the typical concrete mix include Portland cement type I, sand, 3/8 in. crushed stone aggregate, 28% water to cement ratio with 10% of silica fume and about 18.5 ounces per 100 lb. of cementitious material as shown in Table 3.2.

The similar concrete mixture which was used by Ozkul (2007) was modified to achieve a minimum target concrete compressive strength  $f_c'$  of 10 ksi for all beam at 28 days. The ultimate compressive strength was determined by taking the average strength of three 4 x 8 in. cylinders from each mix then take the ultimate concrete compressive strength average of all mixes per each beam.

In order to achieve minimum concrete compressive strength at the time of demolding the beam, the compression tests were performed at age 3 days when the time for demolding the beams which require moving the beam from the hooks using the laboratory crane. Usually, the beam at an early age using this design mix gains about 80-85% of the ultimate compressive strength which is about 9 ksi which much bigger the modulus of rupture, and that's enough to move the beam safely without appearing any crack.

**Table 3.2 Typical concrete mix proportions per one cubic yard.**

<b>Mix Components</b>	<b>Amount / yd<sup>3</sup></b>
<b><u>Cement</u></b> Allentown Portland Cement Type I Bulk Specific Gravity=3.15	1120 lbs./yd <sup>3</sup>
<b><u>Aggregate</u></b> Local Maximum size=3/8 in Bulk specific gravity (oven dry)=2.81 Dry-rodded unit weight=98.11 lbs/ft <sup>3</sup> Absorption based on oven dry weight=1.2%	1722 lbs./yd <sup>3</sup>
<b><u>Sand</u></b> Local Fineness Modulus=2.9 Bulk specific gravity (oven dry)=2.56 Dry-rodded unit weight=107.17 lbs/ft <sup>3</sup> Absorption based on oven dry weight=0.36%	924 lbs./yd <sup>3</sup>
<b><u>Silica Fume</u></b> W.R. Grace Corp. –Force 10000D Bulk Specific Gravity=2.22	108 lbs./yd <sup>3</sup>
<b><u>Water</u></b> Tap water at room temperature	314 lbs./yd <sup>3</sup>
<b><u>Superplasticizer</u></b> W.R. Grace Corp. –Daracem 19	18.5 oz./cwt

All 4 x 8 in. cylinders were taken from each mix and put on the vibrators as shown in Fig. 3.2. The concrete was cast in the cylinders in two layers, the cylinders were filled half of the height then vibrated for 3-4 seconds, then they filled to the top and vibrated again to achieve the maximum density.



**Fig. 3.2 Vibrators for 4 x 8 in. Concrete Cylinders**

In order to achieve a flat and smooth surface at the end of the cylinders, sulfur capping for concrete compressive and modulus of elasticity tests were used as shown in Figs. 3.3a and 3.3b.

The concrete modulus of rupture  $f_r$  was measured on the day of testing to find the maximum tensile stress of the concrete. The 4 x 8 in. split cylinder tests were performed for the day of testing to compare the results with the stresses at the extreme concrete fibers in tension zones of the beams. The cylinders were fully supported by rigid plates from the top and bottom for the entire length as shown in Fig. 3.3c.

To calculate the modulus of rupture from the splitting test, the following formula is used:

$$f_{r, measured} = \frac{2P}{\pi DL} \quad (3.3)$$

where  $P$  is the applied load read out from Tinius Olsen,  $L$  is the height of the cylinder specimen, and  $D$  is the diameter of the concrete cylinder. The values from Eq. (3.3) were compared with the results from ACI 318-14 equation as follows:

$$f_{r, calculated} (psi) = 7.5\sqrt{f'_c (psi)} \quad (3.4)$$

To perform the concrete modulus of elasticity was measured by calculating the slope of the stress-strain diagram using six points within the elastic limit (40% of the ultimate compressive strength). The calculated value of the concrete modulus of elasticity was computed using the ACI 363R-10 formula as follow:

$$E_{c, calculated} = 39.9\sqrt{f'_c (psi)} + 1730 \quad (3.5)$$

The experimental and predicted values of compression and tension test in addition to the modulus of elasticity of concrete for all beams specimens are shown in Table 3.3.

**Table 3.3 Summary of Compression, Tension, and Modulus of Concrete for all Beam Tests**

Beam No.	Measured			Calculated	
	$f'_c$ (ksi)	$E_c$ (ksi)	$f_r$ (ksi)	$E_c^{\dagger}$ (ksi)	$f_r^{\dagger\dagger}$ (ksi)
1	10.2	5149	0.72	5760	0.76
2	10.6	5325	0.79	5830	0.77
3	11.2	5966	0.82	5953	0.79
4	12.4	6135	0.81	6173	0.84
5	10.8	5419	0.75	5877	0.78
6	10.7	5523	0.73	5857	0.78
7	12.5	6364	0.85	6191	0.84
8	12.3	5957	0.81	6155	0.83

A typical concrete mix was made to cast cylinders and perform compression, tension and modulus of elasticity tests at different concrete ages to show the variation of test results with the time. Table 3.3 shows the results of concrete tests at one, three, seven, fourteen and 28 days. The concrete compression, tension, and elastic modulus test setup are shown in Fig. 3.4.

**Table 3.4 Concrete Strength of the Typical Concrete Mix at Various Ages**

Age (day)	$f'_c$ (ksi)	$E_c$ (ksi)	$f_r$ (ksi)
1	7.4	4327	0.45
3	8.3	4754	0.52
7	8.8	4820	0.60
14	9.4	4860	0.66
28	10.1	5075	0.74



**(a) Compressive Strength Test Setup**

**(b) Modulus of Elasticity Test Setup**



**(c) Splitting Tensile Strength Test Setup**

**Fig. 3.3 Concrete Tests Setup**

### 3.3.2 Non-Prestressing Steel

Grade 60 # 2 plain bar and deformed bars sizes # 3 and 4 were used as non-prestressed reinforcement. Two # 2 plain bars were used as top reinforcement for all test beams except beam 2 where # 3 was used. Also all shear stirrups and anchorage reinforcement at the beam ends were made of # 2 plain bar. Two # 3 deformed bars were used as bottom reinforcement for all test beams except beam 5 where three # 3 bars were used. Moreover, additional bars 40 inch (between the inflection points) in length were used at the middle support location as tensile reinforcement to resist the negative moment at the middle support. Fig. 3.4 shows the typical reinforcement details at the middle support location. No. of bars and bar size of the top and bottom steel for all beams are summarized in Table 3.5.

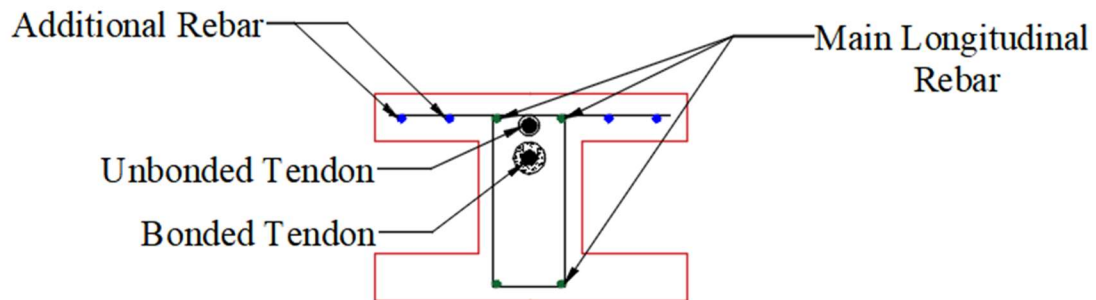


**Fig. 3.4 Reinforcement Details at Middle Support**

**Table 3.5 Summary of Steel Details for all Beam Tests**

<b>Beam No.</b>	<b>Bottom Steel</b>	<b>Top Steel</b>	<b>Addition Top Steel at Middle Support</b>	<b>Stirrups</b>
1	2 # 3	2 # 2	-----	# 2
2	2 # 3	2 # 3	-----	# 2
3	2 # 3	2 # 2	-----	# 2
4	2 # 3	2 # 2	2 # 4	# 2
5	3 # 3	2 # 2	3 # 3	# 2
6	2 # 3	2 # 2	4 # 3	# 2
7	2 # 3	2 # 2	4 # 3	# 2
8	2 # 3	2 # 2	4 # 3	# 2

Samples of 24 inch in length from each longitudinal bar placed in the steel cage for all test beam were collected for tension tests. Then, the tension tests were performed using the Test Resources machine. Since there is no an extensometer available in the laboratory; a foil strain gauge was installed at the middle of the gauge length of each sample. This strain gauge was connected to P3 strain indicator and recorder to measure the strain in the rebar during the test. Then, the load readings from the machine and the strain readings from the strain indicator were videotaped. The typical gauge length was 17 inch (the clear distance face to face between the grips). The strain gauges were stopped at 0.032 in/in, which approximately 2.1-inch elongation. The tension machine report provides the tensile stress and the elongation up to failure. The strain from the testing machine can be found by dividing the elongation over the gauge length. Since the elongation from the machine in the elastic stage is higher than actual strain (strain gauge reading), therefore the strain gauge readings were adopted until the strain gauge stopped, then, the machine readings were adopted until failure. The average values of yielding stress  $f_y$ , elastic modulus  $E_s$ , stress at



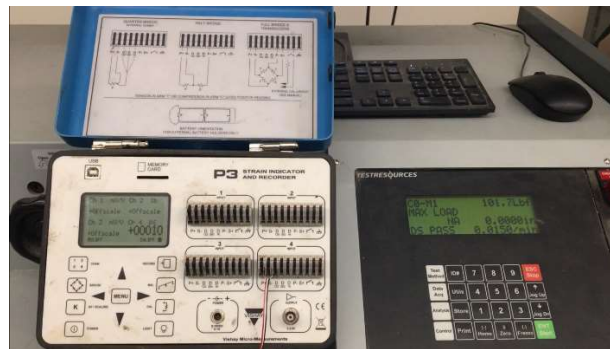
rupture  $f_u$  and the strain at rupture  $\varepsilon_u$  for positive and negative locations are presented in Table 3.6 and 3.7 respectively. The test set up and the sample after failure are shown in Fig 3.5. The stress-strain relationships are plotted to show the stress and stress at yielding and failure, in addition, to calculate the modulus of elasticity as shown in Fig 3.6 to 3.21.



(a)



(b)



(c)



(d)



(e)

**Fig. 3.5 a) and b) Test Setup for Tension Test of Steel Rebar, c) P3 Strain Indicator and Recorder, d) Strain Gauge Setup e) Fracture of Steel Rebar at Fracture**

**Table 3.6 Summary of  $f_y$ ,  $E_s$ ,  $f_u$  and  $\epsilon_u$  for Tensile Steel at positive Locations**

<b>Beam No.</b>	<b><math>f_y</math> (ksi)</b>	<b><math>E_s</math> (ksi)</b>	<b><math>f_u</math> (ksi)</b>	<b><math>\epsilon_u</math> (in/in)</b>
1	76.4	27284	116	0.08
2	78.6	28089	130	0.11
3	68.4	27677	107	0.09
4	66.5	27097	108	0.10
5	69.0	28297	103	0.12
6	80.0	28832	120	0.10
7	76.8	27453	114	0.09
8	85.5	28335	123	0.09

**Table 3.7 Summary of  $f_y$ ,  $E_s$ ,  $f_u$  and  $\epsilon_u$  for Tensile Steel at Middle Support Location**

<b>Beam No.</b>	<b><math>f_y</math> (ksi)</b>	<b><math>E_s</math> (ksi)</b>	<b><math>f_u</math> (ksi)</b>	<b><math>\epsilon_u</math> (in/in)</b>
1	71.5	27778	77	0.04
2	69.0	28672	108	0.09
3	66.5	27836	74	0.04
4	64.0	28444	89	0.12
5	70.5	28218	102	0.10
6	69.0	27405	109	0.09
7	70.2	27903	109	0.11
8	87.3	28176	131	0.10

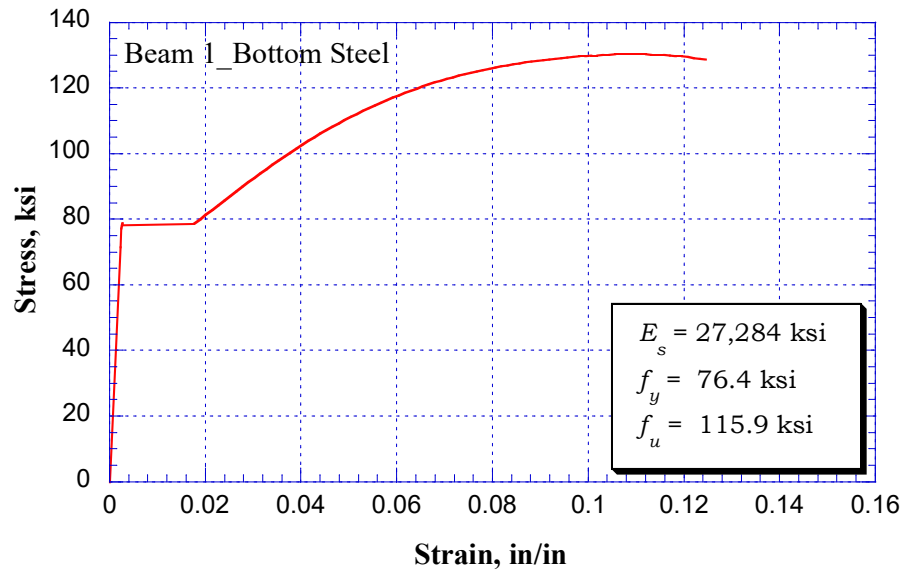


**Fig. 3.6 Stress versus Strain Relationship from Bottom Rebar Tension Test,  
Beam 1**

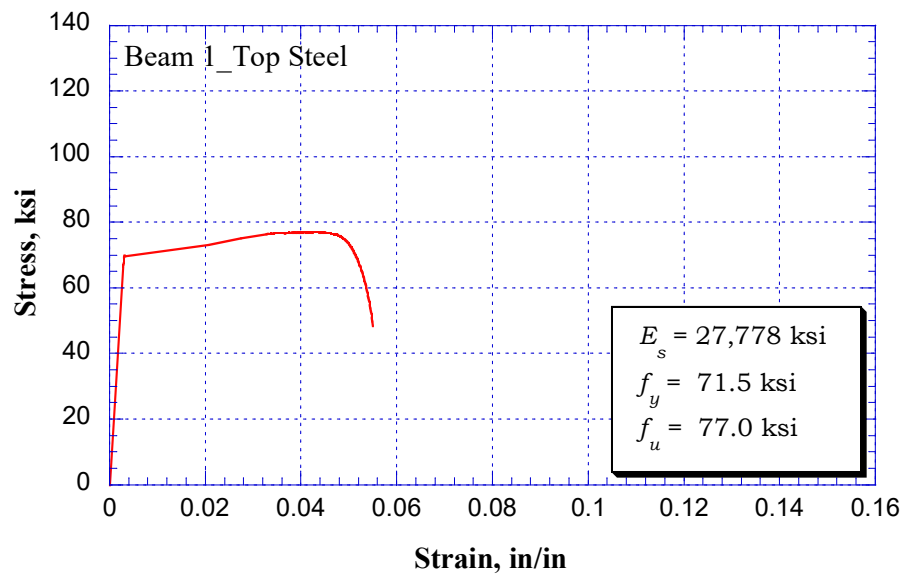


**Fig. 3.7 Stress versus Strain Relationship from Top Rebar Tension Test, Beam 1**

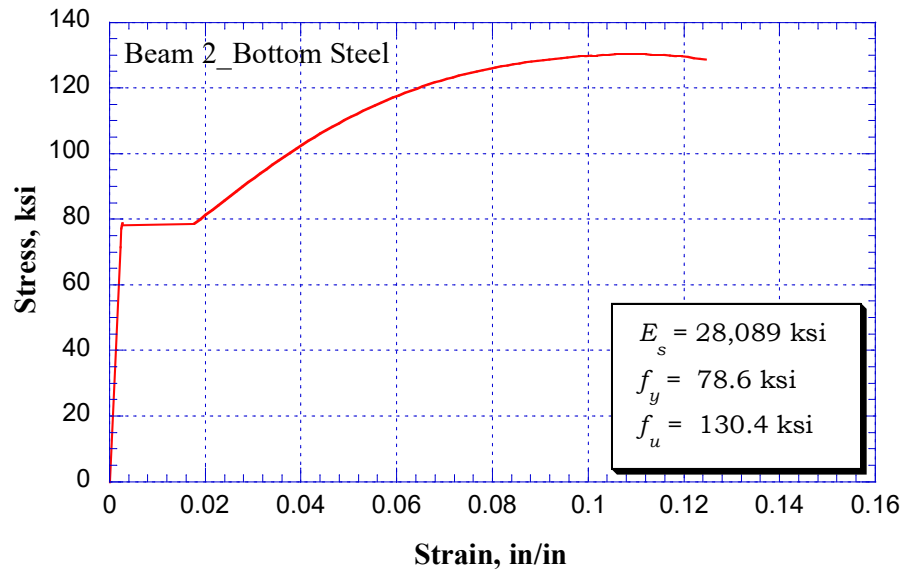


**Fig. 3.8 Stress versus Strain Relationship from Bottom Rebar Tension Test,  
Beam 2**

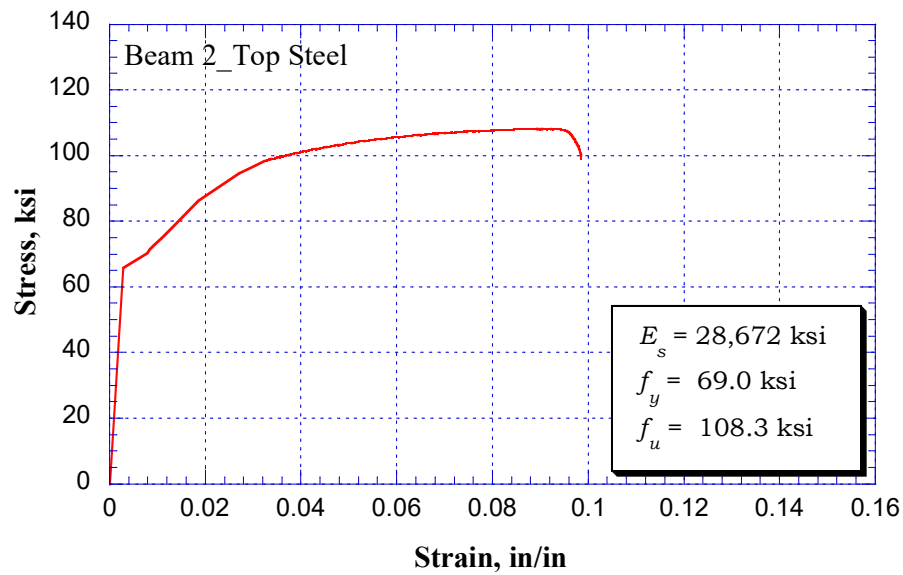


**Fig. 3.9 Stress versus Strain Relationship from Bottom Top Tension Test, Beam 2**

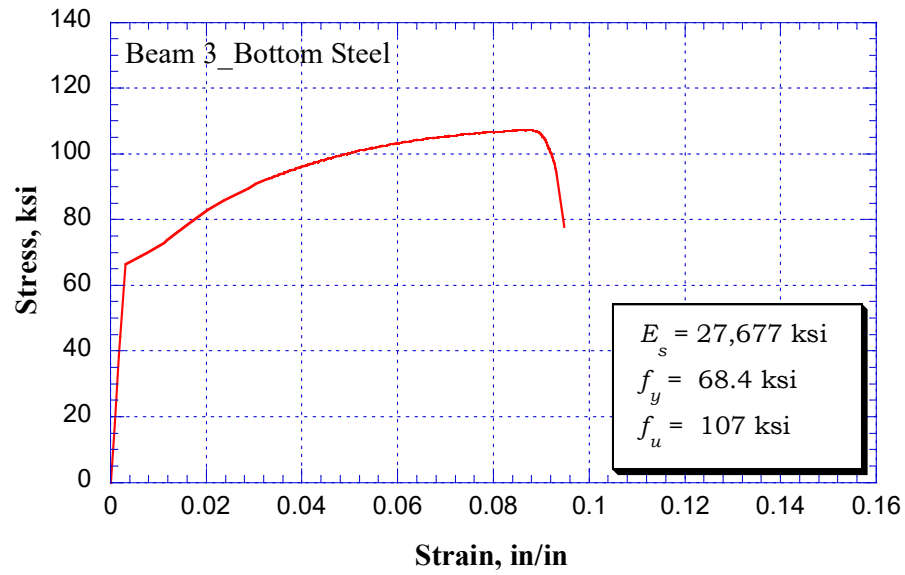


**Fig. 3.10 Stress versus Strain Relationship from Bottom Rebar Tension Test,**

**Beam 3**

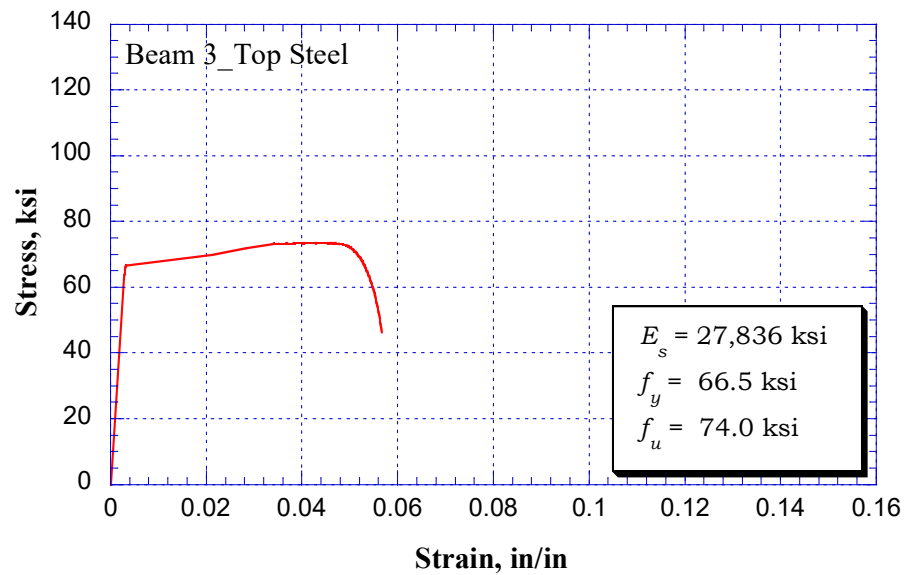


**Fig. 3.11 Stress versus Strain Relationship from Top Rebar Tension Test,**

**Beam 3**

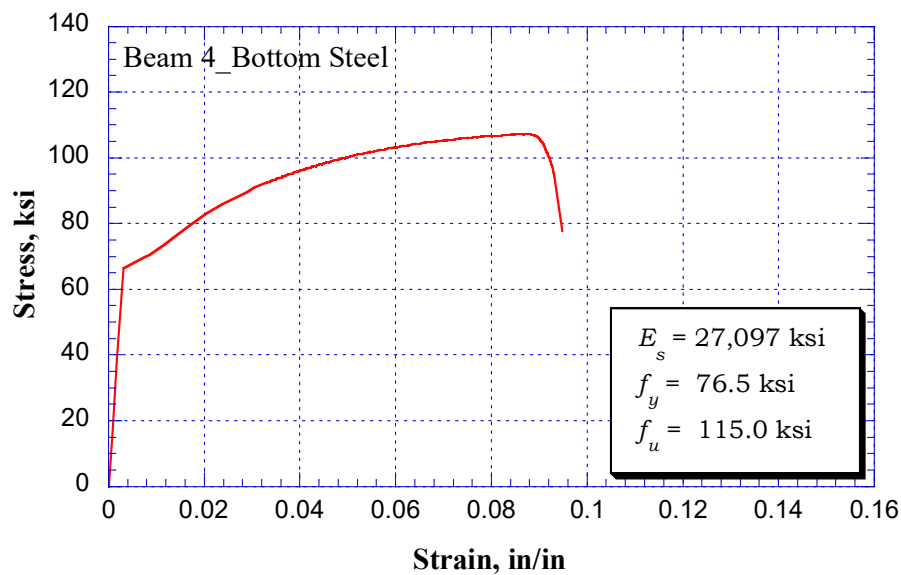


**Fig. 3.12 Stress versus Strain Relationship from Bottom Rebar Tension Test,**

**Beam 4**

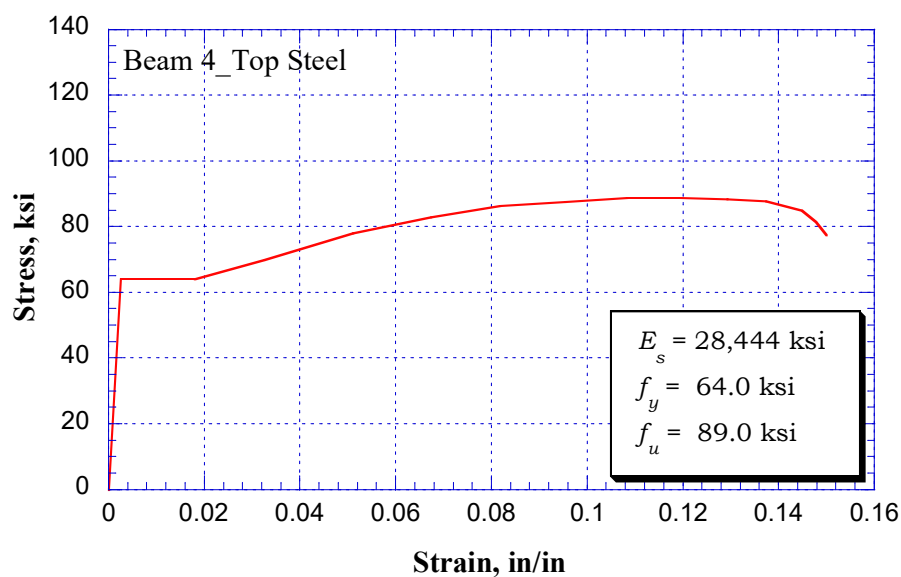


**Fig. 3.13 Stress versus Strain Relationship from Top Rebar Tension Test,**

**Beam 4**

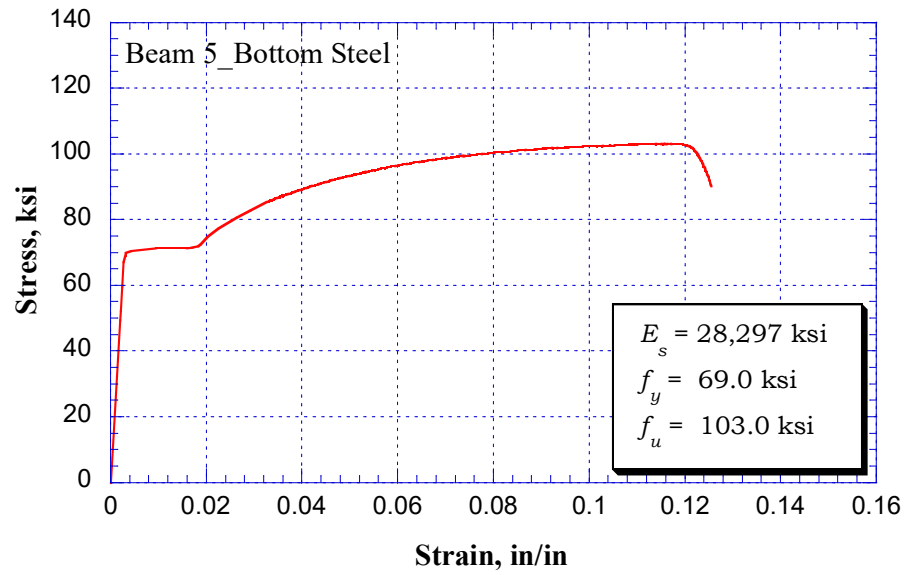


**Fig. 3.14 Stress versus Strain Relationship from Bottom Rebar Tension Test,  
Beam 5**

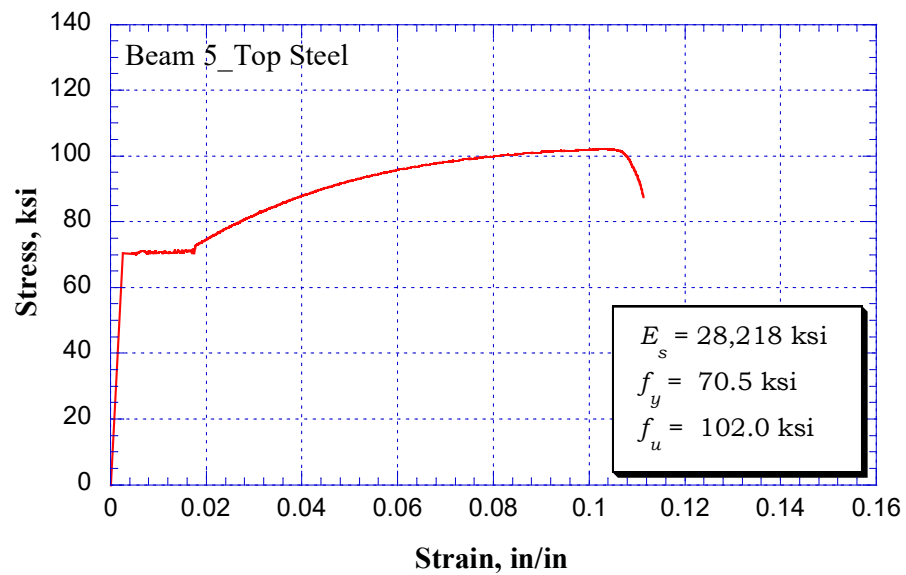


**Fig. 3.15 Stress versus Strain Relationship from Top Rebar Tension Test,  
Beam 5**



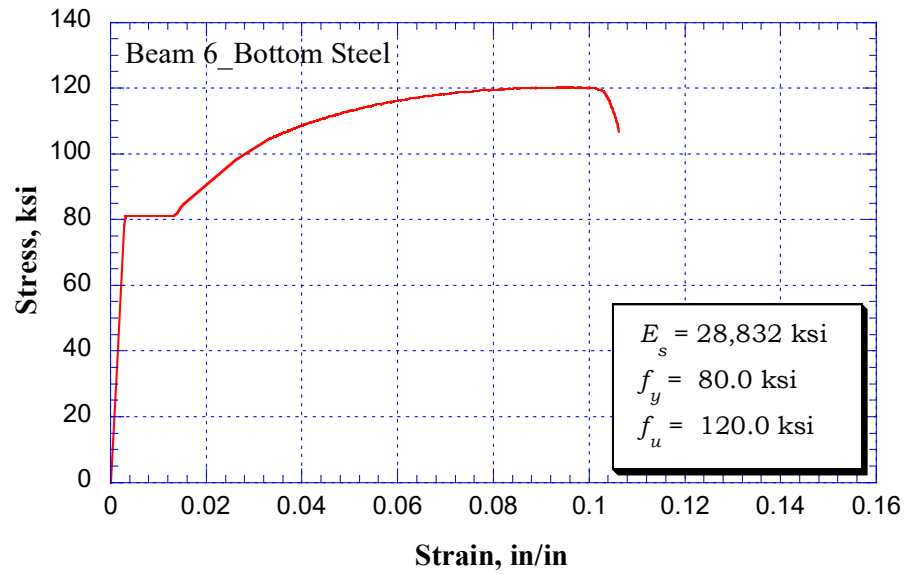


**Fig. 3.16 Stress versus Strain Relationship from Bottom Rebar Tension Test,  
Beam 6**

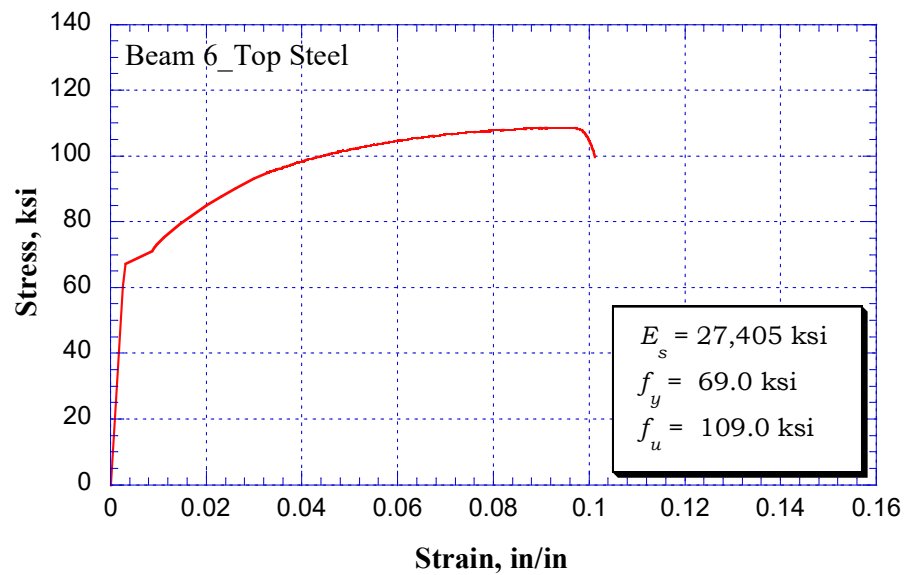


**Fig. 3.17 Stress versus Strain Relationship from Top Rebar Tension Test,  
Beam 6**

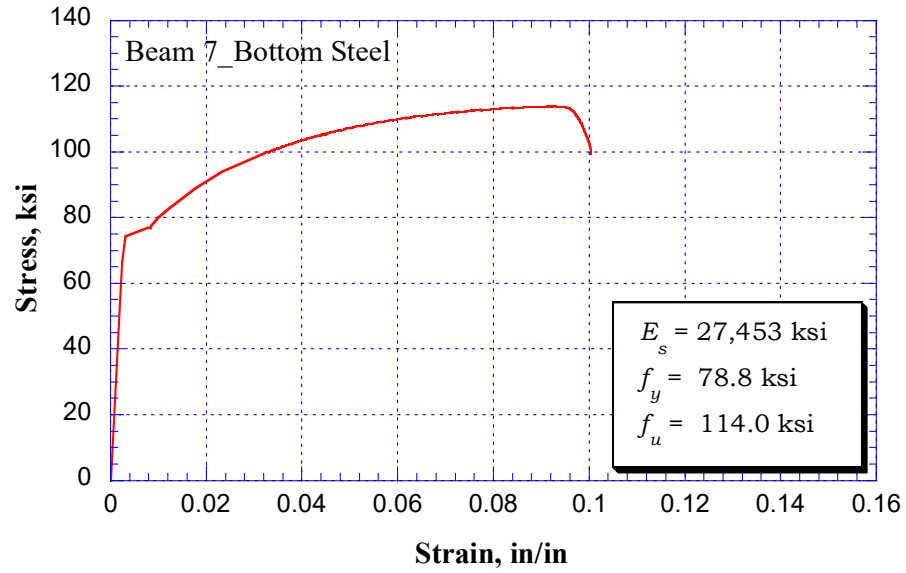


**Fig. 3.18 Stress versus Strain Relationship from Bottom Rebar Tension Test,  
Beam 7**

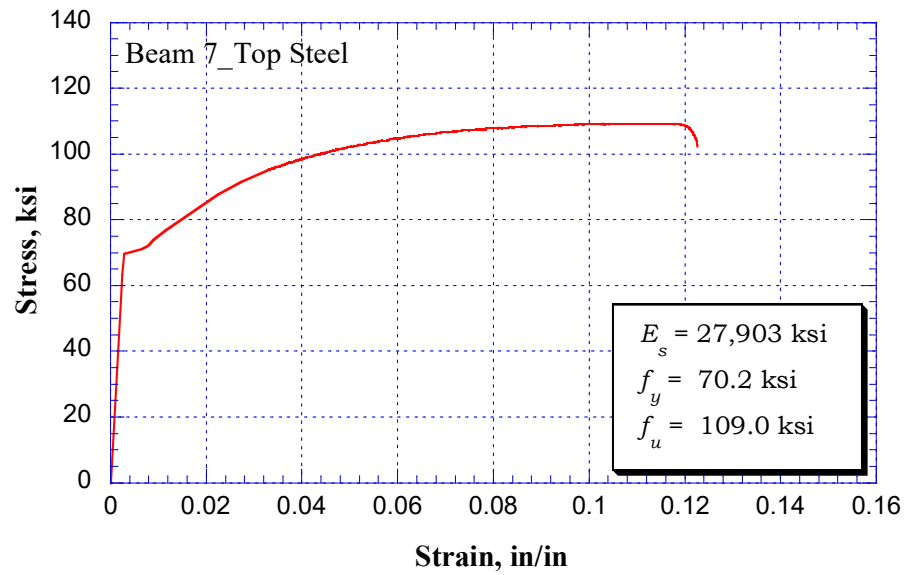


**Fig. 3.19 Stress versus Strain Relationship from Top Rebar Tension Test,  
Beam 7**

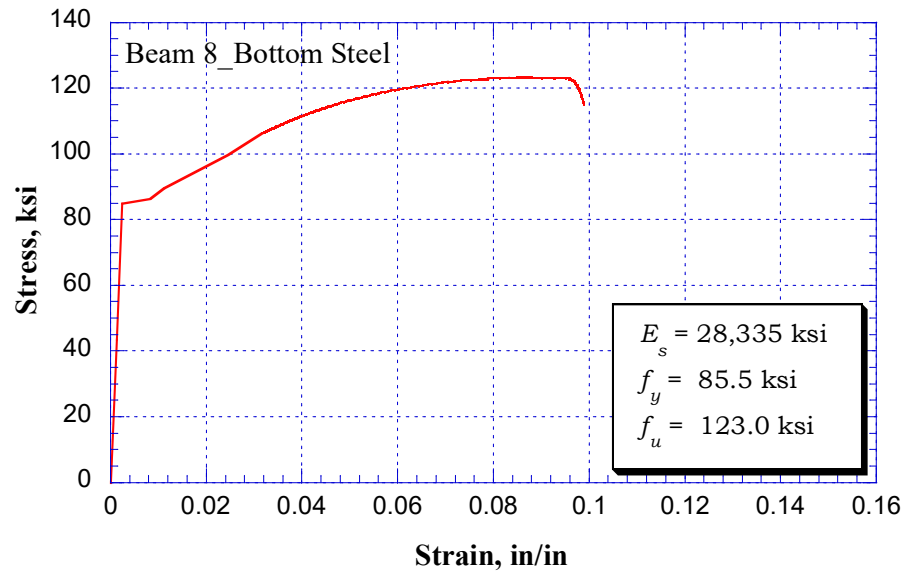


**Fig. 3.20 Stress versus Strain Relationship from Bottom Rebar Tension Test,  
Beam 8**

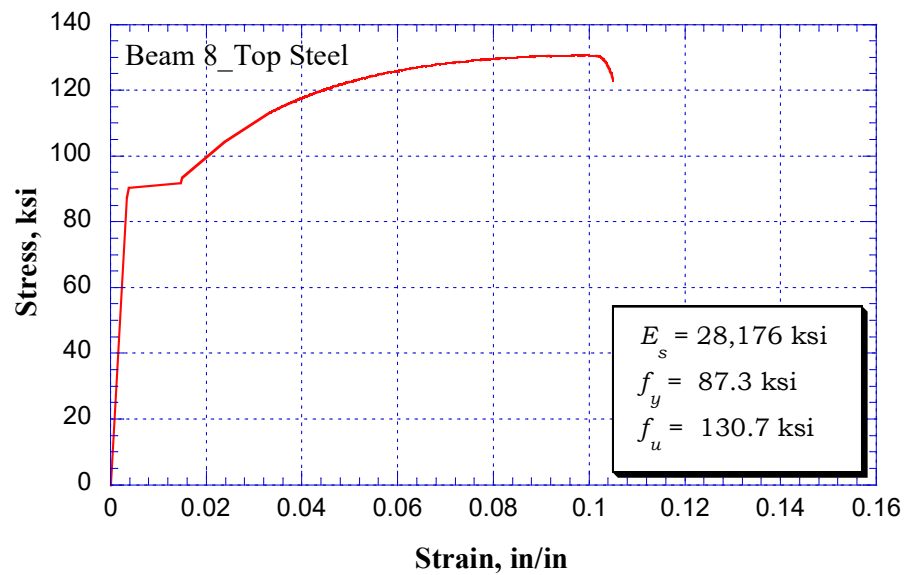


**Fig. 3.21 Stress versus Strain Relationship from Top Rebar Tension Test,  
Beam 8**

The steel cages for all beam specimens were made by connecting the upper and lower layer of the longitudinal rebar with stirrups. Fig 3.22 illustrates the typical longitudinal and stirrups use in the beam specimen. The stirrups width at 1 ft. from each beam specimen end is wider than the stirrups at rest of the entire beam and that to provide more room for installing the anchorage of the prestressing bonded tendon.

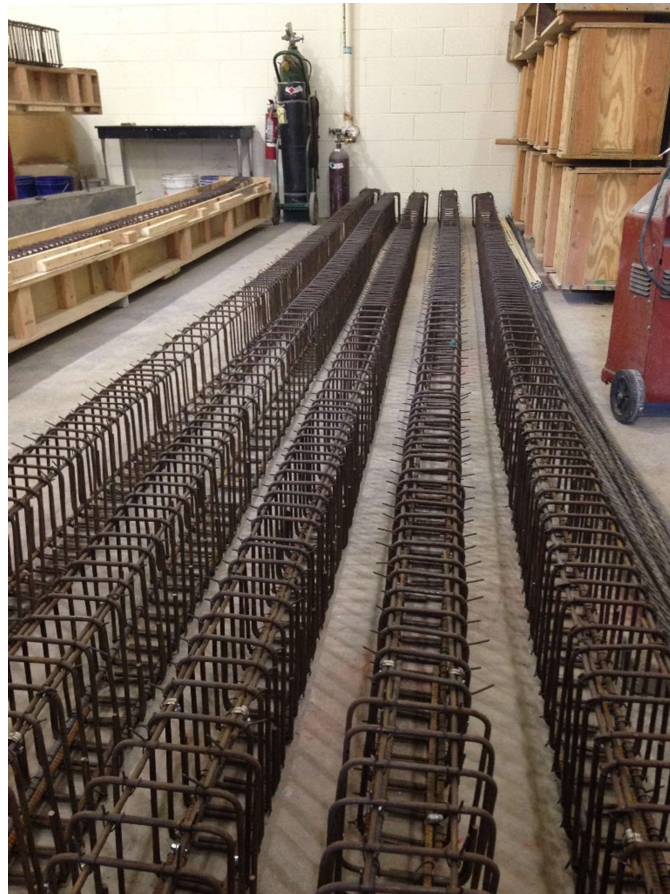


**Fig 3.22 Typical Longitudinal and Shear Reinforcement for Beam Specimen**

### 3.3.3 Prestressing Steel

All beam specimens, two 5/16 inch diameter with a nominal area of 0.058 sq. in. and ultimate strength 270 ksi (reported) strands were used. The strands were donated from Jersey Precast Company, a local precast/prestressed concrete plant in New Jersey. To determine the material properties of the strand, a tensile test was performed using Test Resources Machine for two samples of the used strand. The test results showed that the actual strength of the strands was higher than the reported value. Also, the stress-strain relationship demonstrates that the average yield and ultimate strength of the strand were 265 and 300 ksi as shown in Fig. 3.23.

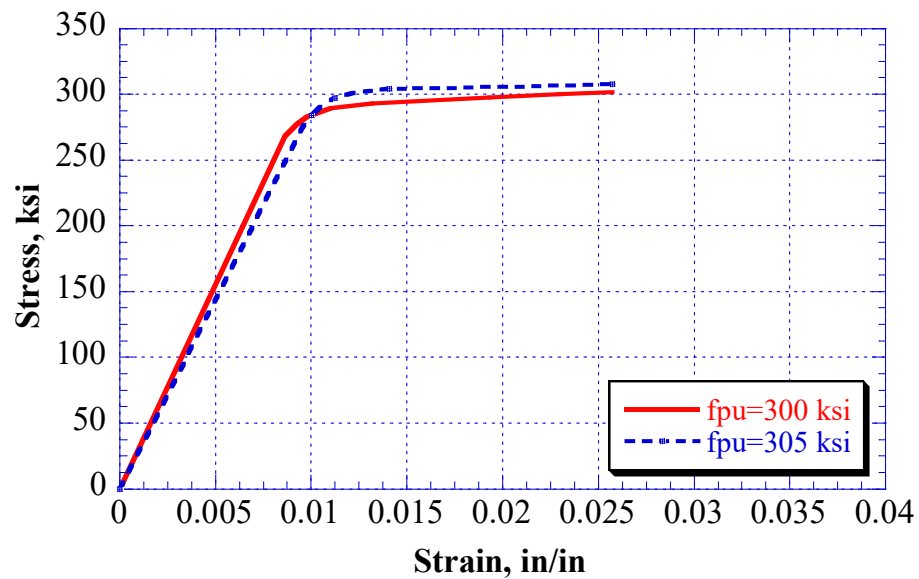
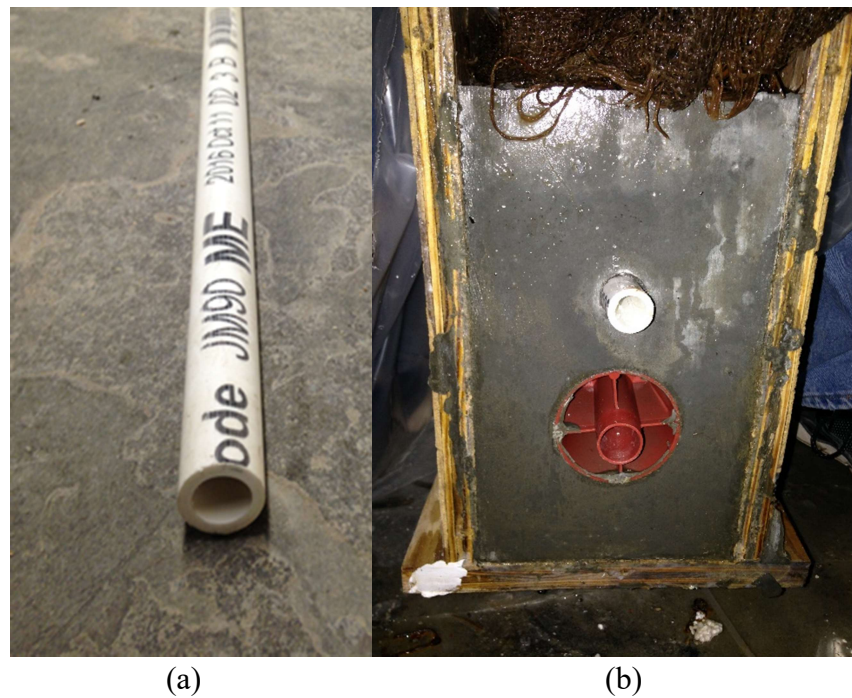


Fig. 3.23 Stress versus Strain Relationship for 5/16" Prestressing Strands

### 3.3.3.1 Unbonded Tendon

To provide debonding between the strand and adjacent concrete, 0.5-inch inner diameter PVC pipe was used. The PVC pipe was placed inside the steel cage in the level of the tendon profile. The pipe before and after casting the beam is shown in Fig. 3.24. The tendon eccentricity at a different location was made by using a U-shape size no. 2 plain bar connected to the vertical stirrups with hose clamps. The length of each PVC segment is 8 ft. from the manufacturer, therefore couplers were used to connect each piece with the others.



**Fig 3.24 PVC Pipe for Unbonded Tendon, a) Before Casting**

**b) After Casting**

### 3.3.3.2 Bonded Tendon

The bond between the strand and surrounding concrete has a significant effect on the flexural response for the prestressed concrete beam (Laco and Borzovic 2017). Therefore, a different procedure was applied to provide a bond between the strand and the adjacent concrete. A sheathing duct was donated from Jersey Precast. The plastic corrugated tube with 0.9-inch inner diameter was used for the bonded tendon for all beam specimens as shown in Fig. 3.25.



**Fig 3.25 Plastic Corrugated Tube**

A mono-bonded anchorage was used to connect the sheathing pipe with beam specimen end. Fig. 3.26 illustrates the pieces of the anchorage used with the bonded tendon.





**Fig 3.26 Mono-Strand Anchorage System**

The procedure for installing the bonded strand can be described as follows:

The first stage was installing the corrugated duct inside the steel cage in a way that follows the unbonded tendon profile using the same hangers that used to hold the PVC pipe for the unbonded tendon.

the second stage was fixing the strand at one end (dead end) using a mono-bonded anchorage system as shown in Fig. 3.26, then applying the prestressing force at the other end (the free end) until reaching the target force, then lock the strand using the same anchorage that used at the dead end.

### **3.3.3.3 Cable Grout**

To provide the bond between the strand and the sheathing duct, a cable grout was used. A mix of 50 lb. grout to 1.5 gal. of water was made as directed by the manufacturer. Samples 2x2 inch of grout mix were collected, cured and tested for compression at different



ages to know the actual strength. The samples and compression test setup are shown in Fig. 3.27. The compression strength results of the samples at various ages are shown in Table 3.8. The cable grout mix was injecting the grout material into the corrugated tube throughout the access vents that placed before casting the beam. These vents were placed at both ends of the beam tests and at the points with the highest elevation on the tendon profile (for two-span continuous beam the highest elevation of the tendon located at the interior support location). The specifications require 0.24-inch minimum thickness cover of grout around the strand which was satisfied when using 5/16 inch diameter strand. Fig. 3.28 illustrates the typical cross-section of the bonded and unbonded tendons and locations at the midspan.

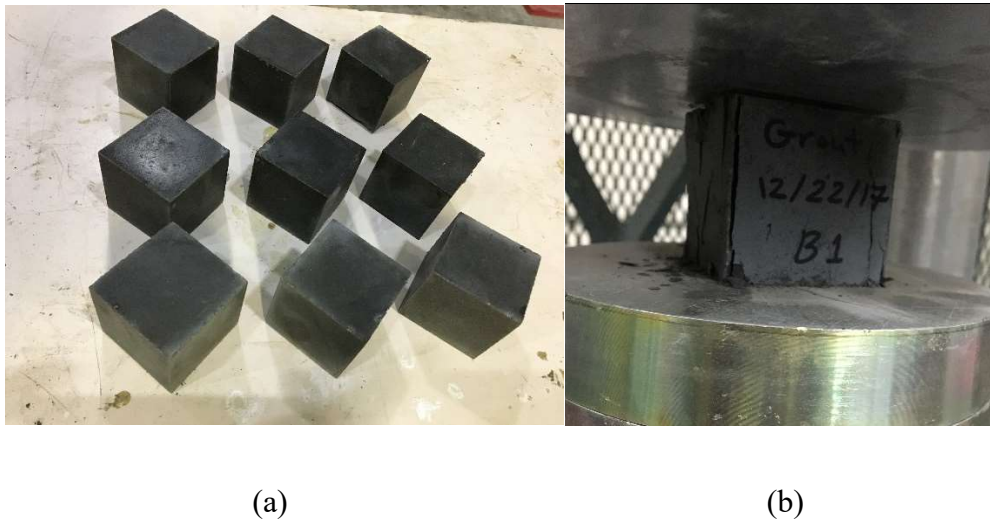


**Fig. 3.27 Cable Grout Specimens, (a) After Demolding, (b) Compression Test**

**Table 3.8 Summary of Compression Strength for Cable Grout Samples at Different Ages**

Age	Ave. Force (lb)	Ave. strength (psi)
1 day	14933	3733
3 day	18600	4650
7 day	24867	6217
14 day	27833	6958
28 day	29300	7325

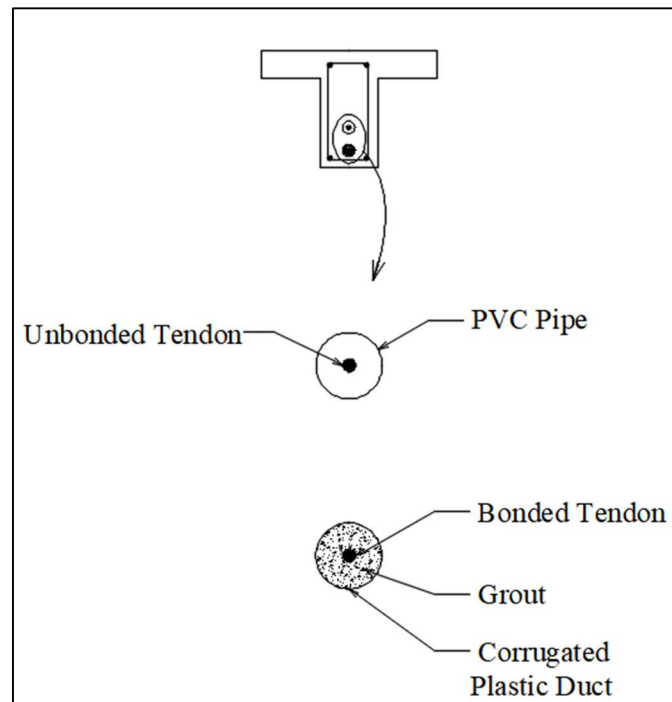


**Fig 3.28 Typical Bonded and Unbonded Tendons Cross Sections**

### 3.4 Instrumentation

There are three types of electrical devices were used to monitor the deformations and forces in the beams test. The devices were connected to a data logger (CR3000) from Campbell Scientific Company to collect data. These devices include:

#### 3.4.1 Load Cells

Two types of load cells were used in the beam tests, 250-kips and 50-kips capacity. The 250-kips load cell measures the total external applied load on the beam; this load cell was attached to the hydraulic actuator of the loading machine. A 50-kips load cell was used measures the force in the prestressing bonded and unbonded tendons. These load cells were placed at the live end of the beam to observe the prestressing force for both tendons. The typical load cells used in the test are shown in Fig. 3.29 and 3.30.



**Fig 3.29 Typical Load Cell Used to Monitor Applied Load**



**Fig 3.30 Typical Load Cell Used with Bonded and Unbonded Tendon**

### **3.4.2 Linear Voltage Differential Transducers (LVDTs)**

The linear voltage differential transducer (LVDT) usually uses to monitor the displacements. Thus two types of LVDTs were used according to the range capacity, 6-in and 2-in range capacity, as shown in Fig. 3.31.

The 6-in range LVDT was installed to measure deflections of the beam at different locations, under the load points and midspan for both spans. Also, the 6-in range LVDTs were placed to measure the camber during post-tensioning of the strands.

While the 2-in range LVDT was placed to measure the strain of the extreme fiber at midspan. Since LVDT measures displacement, not strains, an initial gauge length was measured in advance, then the strain computed by dividing the current reading over the initial gauge length.

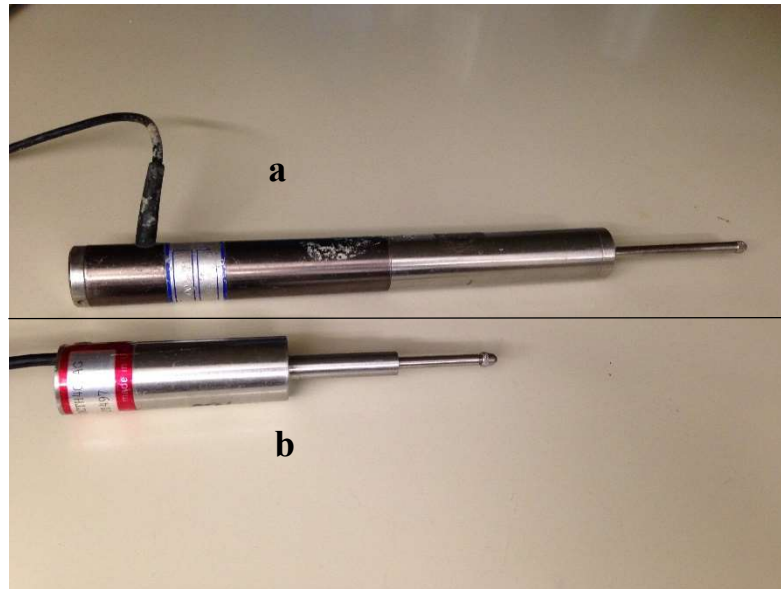


**Fig 3.31 Linear Voltage Differential Transducer, a) 6-in Range LVDT**

**b) 2-in Range LVDT**

### **3.4.3 Strain Gauges**

Foil strain gauges were used to measure the strain in the longitudinal non-prestressing steel and strains in the bonded and unbonded strands. Type L2A-06-125LW-120 (resistance 120 ohms; gauge factor 2.13, transverse sensitivity 0.5%; at 24°C) was purchased from Micro-Measurements. All the installation kits as shown in Fig. 3.32 that required to prepare contact surface and satisfy bond were purchased from the same company. Strain gauges installation includes grinding the rebar surface, smooth it with sandpaper to satisfy enough contact area between the rebar and strain gauge, then clean several times to remove the particles due to grinding. Once the surface becomes fully clean, conditioner and neutralizer were applied. After preparing the surface, strain gauges were glued using the adhesive kit to provide the bond; a firm pressure should be applied at this

stage. Fig. 3.33 shows the strain gauge installation on the steel bars. The locations of the strain gauges on the steel reinforcement are shown in Fig. 3.34.



**Fig 3.32 Stain Gauge Installation Kits**



**Fig 3.33 Strain Gauges installation in the Longitudinal Steel**

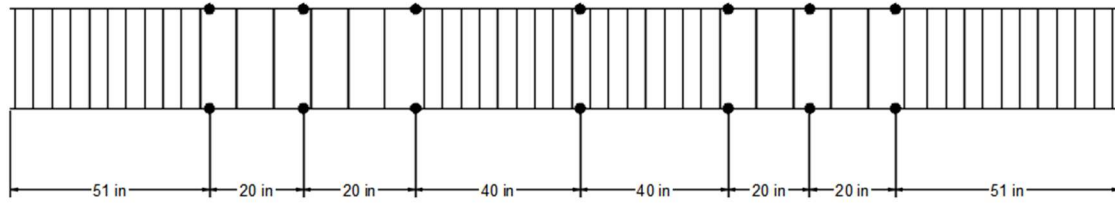


**Fig 3.34 Location of the Strain Gauges on the Reinforcing Rebar**



### 3.5 Loading Frame Setup

The civil engineering laboratory has a loading frame as shown in Fig. 3.34, which was set up in a way that the tested beam was perpendicular in the short direction of the testing room. Since each test specimen was 22 ft. the length which requires enough room for casting, prestressing and testing. Therefore the decision was made to rotate the loading frame 90 degrees to make the long side of the room is parallel to the length of the beam test.



**Fig 3.35 Loading Frame before Rotation**



The instrument Maker and repairer of the civil engineering laboratory were able to rotate the loading frame and fixed to the ground through the insert that already built on the concrete floor. The new set up capable of fitting test specimen up to 30 ft in length, in addition, this set up make moving the specimen easily because the test beam became parallel with the top crane movement.

In addition to rotating the loading frame, new modifications were required on some parts of the frame to be able to test two-span continuous beam. These changes were placed on the big loading beam and the supports. Since the applied loads of the specimen contain two point-load on each span, thus, a long loading beam and two more short beams one for each span were required. Three steel supports, two exterior and one interior were designed to carry beam tests and the external loads. The current supports can be used as exterior supports after moving them farther from the center of frame, but a new steel fabrication was required to make the interior support. Fig. 3.35 shows the new frame design after the modifications.



**Fig 3.36 New Loading Frame Setup and Beam Test**

### **3.5.1 Middle Support Steel Frame**

Once the strands post-tensioned, the beam cambers up at the positive moment locations due to the eccentricities of the prestressing forces of the bonded and unbonded tendons. The beam at the middle support location is held by a steel frame which allows for free rotation and prevents any differential vertical movement at the supports. This frame was set up after placing the test beam on the supports and before post-tensioning the strands. The frame consists of two vertical threaded rods connected with steel channels underneath the transverse beams under the middle support and connected with the transverse channel at the top of the test beam. The test beam was placed on a roller and held by a roller from the top which compressed by tightening the nuts of the threaded rods

on both sides of the test beam. The middle support frame before and after placing beam test is shown in Fig. 3.36.



(a)

(b)

**Fig. 3.37 Middle Support Steel Frame, (a) Before Placing Beam Test, (b) After Placing Beam Test**

## **CHAPTER IV**

### **EXPERIMENTAL RESULTS AND DISCUSSION**

#### **4.1 Introduction**

The eight 20 ft. long two-span continuous concrete beams that were conducted in the laboratory were loaded until failure and observed by different measurements types at the critical locations on the beam to fully understand the behavior of the continuous beams internally prestressed with bonded and unbonded tendons. The collected data include cracking behavior, modes of failure, load-deflection under the loading points and midspan, moment-curvature relationship, strain in prestressing and reinforcing steel and the effective stress in the unbonded tendon. Since all the specimens have two spans right and left, the left span is the span next to the live prestressing end, while the right span is the one next to the dead end.

#### **4.2 Cracking Behavior**

All test continuous concrete beams were observed for cracking appearance at three locations, between the point loads of the right span, left span and at the location of the middle support. To observe cracks on the beam test, all the beams were white painted and grid and numbered to identify the location of the crack then present it in AutoCAD drawings. The location, path, and propagation of any crack on the test beams with applied load increases were observed by five people as shown in Fig. 4.1. Two microscopes that were connected to computers were used to identify little cracks and measuring the cracks by magnifying the crack width to 20 times the width as shown in Fig. 4.2.

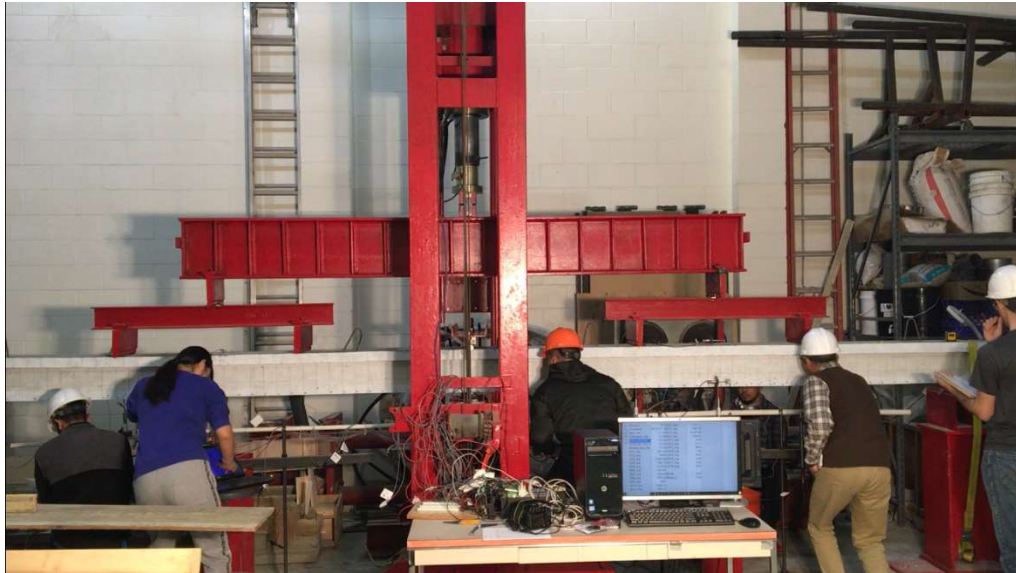
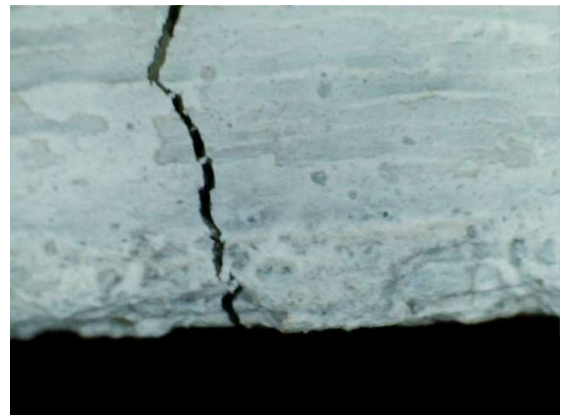


**Fig. 4.1 Students Observing Cracks during Beam Testing**



**(a)**



**(b)**

**Fig. 4.2 (a) Microscope for Cracks Measurements, (b) Magnified Crack using Microscope**

As it is obvious that the crack appears at the tension zones, thus the cracks at the positive moment locations start from the extreme bottom concrete fiber, while they appear from the extreme top fiber at the middle support location. As it is obvious that the first crack appears at the plastic hinges locations, where the maximum moments located (explained in chapter five). Since beam 1 to 7 were tested under the third- point load, the plastic hinges were located at the exterior point load and the middle support. While beam no. 8 was tested under a single load at midspan, so the plastic hinges were at midspan and the middle support as shown in Fig. 4.3 and Fig. 4.4, respectively.



**Fig. 4.3 Plastic Hinges Locations for Third-Point Loading**

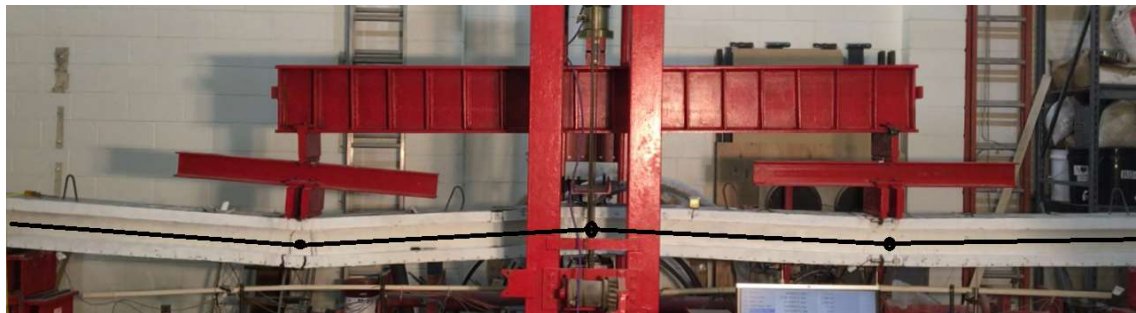


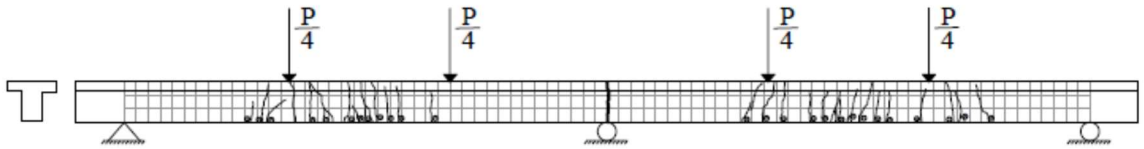
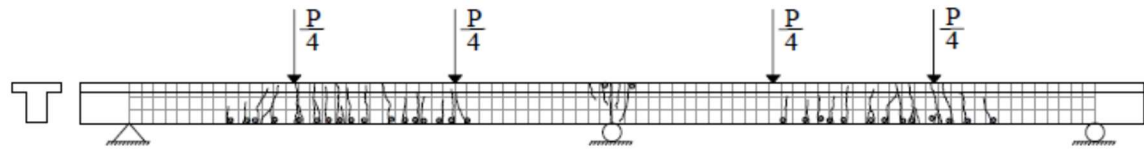
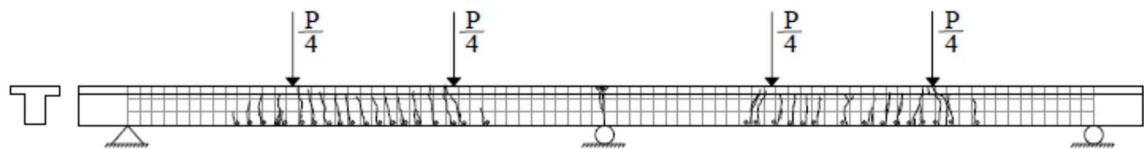
**Fig. 4.4 Plastic Hinge Locations for Single Point Loading at Midspan**

Crack occurs when the stress in the extreme fiber of concrete in tension zone exceeds the modulus of rupture  $f_r$ . Once the concrete cracked, the stresses have been transferred to nearest adjacent reinforcing rebar, the bonded (grouted) and unbonded tendons. Concurrently, cracks keep propagating and deflection increasing with the load increases until the tendon has yielded, then drastically increasing jump occur in tendon stresses as shown later in this chapter.

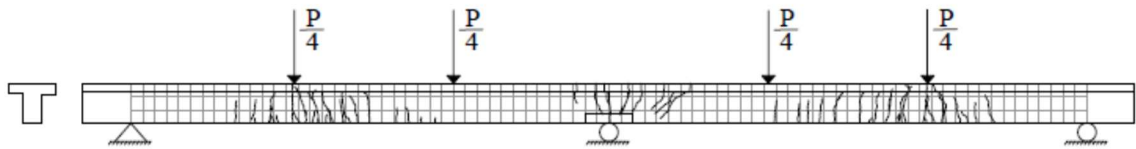
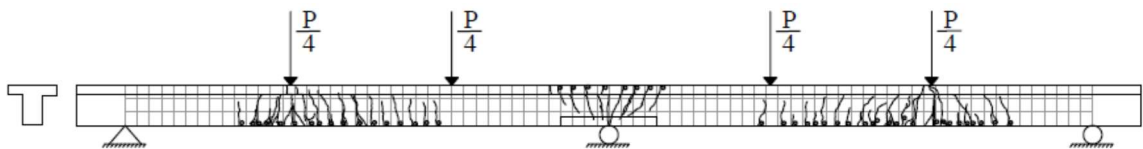
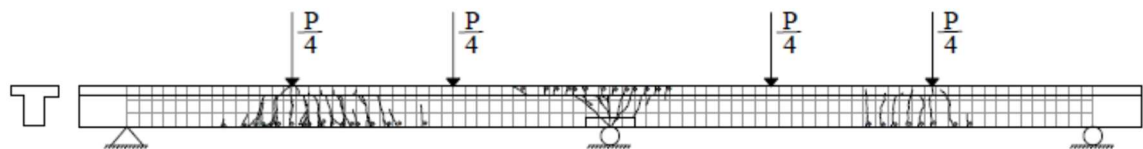
The observations showed that no. of cracks depends on the partial prestressing ratio (PPR) since all test specimens have the same prestressing steel area. Thus the no. of cracks mainly is relevant to non-prestressed reinforcement index ( $\omega$ ) as mentioned in the previous chapter. The no. of cracks and the maximum crack width for all beams at the right, left span and middle support are shown in Table 4.1.

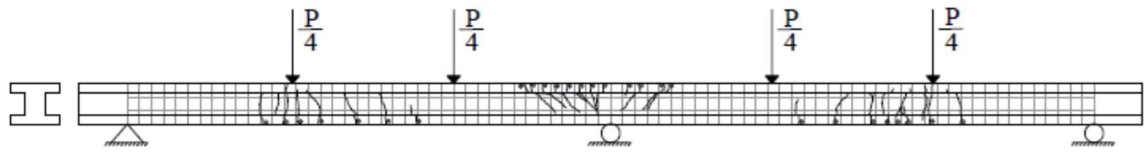
Crack patterns at failure with varying parameters such as effective prestressing stress and area of non-prestressing steel are shown in Fig. 4.5.



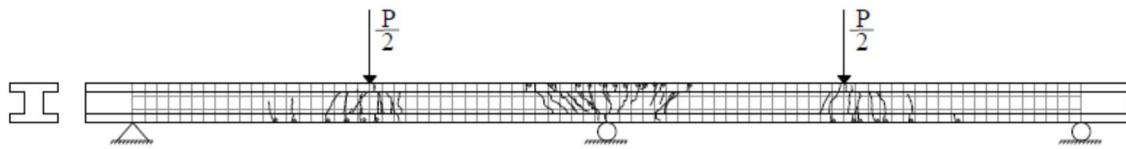
**Test 1****Test 2****Test 3**



**Test 4****Test 5****Test 6**



**Test 7**



**Test 8**

**Fig 4.5 Crack Patterns at Failure for All Test Specimens**

**Table 4.1 Summary of Results for Crack Width and no. of Cracks**

Beam no.	Crack Location	no. of cracks	Max. Crack Width	
			in	mm
<b>1</b>	Right Span	15	0.060	1.52
	Left Span	12	0.067	1.70
	Middle Support	1	0.757	22.53
<b>2</b>	Right Span	13	0.117	2.97
	Left Span	18	0.124	3.15
	Middle Support	5	0.299	7.60
<b>3</b>	Right Span	16	0.134	3.41
	Left Span	19	0.114	2.88
	Middle Support	1	0.837	19.23
<b>4</b>	Right Span	15	0.072	1.82
	Left Span	19	0.054	1.37
	Middle Support	7	0.264	6.70
<b>5</b>	Right Span	25	0.153	3.88
	Left Span	21	0.140	3.56
	Middle Support	9	0.200	5.08
<b>6</b>	Right Span	14	0.070	1.79
	Left Span	16	0.077	1.95
	Middle Support	13	0.325	8.25
<b>7</b>	Right Span	8	0.232	5.90
	Left Span	7	0.220	5.60
	Middle Support	12	0.338	8.59
<b>8</b>	Right Span	7	0.233	5.91
	Left Span	8	0.245	6.23
	Middle Support	12	0.231	5.88

### 4.3 Modes of Failure and Plastic Hinge Formation

It can be noticed from the crack patterns for all tests that the non-prestressing steel ratio significantly affect the distribution and width of the cracks. This study mainly focused on the effect of tensile non-prestressing reinforcement at the middle support location and at the maximum positive moment location as well. It is observed that non-prestressing reinforcement at the middle support location affect the shape of the curvature diagram under certain applied loading can change the cracking load and cracks spreading at both middle, and maximum positive moment locations. According to the bending moment diagram for a two-span continuous beam with third-points loading, the positive moment at the exterior third-points load location is equal to two thirds ( $2/3$ ) of the negative moment at the middle support location. Thus, the formation of the first crack usually occurs earlier at the middle support when the applied moment exceeds the modulus of rupture. Then with the load increases, the crack at the middle support location propagate while the first crack just occurs at the maximum positive moment location when the applied moment exceeds the modulus of rupture at this location. However, this scenario changes if the non-prestressing reinforcement ratio at the middle support increases, which can delay the formation of cracks to be beyond crack formation at the positive moment location. The first crack location and the cracking loads are summarized in Table 4.2.

**Table 4.2 Summary of Location of First Crack and Cracking Load**

<b>Beam no.</b>	<b>First Crack Location</b>	<b>P<sub>cr</sub> (kips)</b>
<b>1</b>	Right Span	26.0
	Left Span	26.0
	Middle Support	19.8
<b>2</b>	Right Span	25.4
	Left Span	25.0
	Middle Support	23.0
<b>3</b>	Right Span	29.0
	Left Span	29.0
	Middle Support	20.0
<b>4</b>	Right Span	32.0
	Left Span	31.7
	Middle Support	33.5
<b>5</b>	Right Span	27.6
	Left Span	28.0
	Middle Support	28.0
<b>6</b>	Right Span	26.5
	Left Span	26.5
	Middle Support	28.5
<b>7</b>	Right Span	30.0
	Left Span	29.0
	Middle Support	42.0
<b>8</b>	Right Span	22.5
	Left Span	20.0
	Middle Support	25.0

#### 4.4 Load-Deformation Behavior

Several deformations for all beam specimens were observed during the test that includes; load vs. deflection at different beam length, load vs. strain in the concrete extreme compressive fiber and tensile non-prestressing steel, the moment-curvature relationship at different load levels, the stress increase in the unbonded tendon and prestressing force in the tendon as well. Different instruments devices were used to observe these deformations as mentioned in chapter three, such as Linear Voltage Differential Transducers (LVDTs), foil strain gauges and 50-kips load cell to measure the prestressing force in the unbonded tendon and 100-kips load cell for the total applied load.

##### 4.4.1 Load-Deflection Relationship

In order to understand the flexural behavior and the failure modes of the test beams, deflections at different beam lengths were measured. The deflection at both spans at  $L/3$ , midspan, and  $2L/3$  from the exterior support were observed using Linear Voltage Differential Transducers (LVDTs). The load-deflection relationships of the right span at three locations for all beam tests are shown in Figs. 4.6 to 4.13. However, the relationship between the applied load and the deflection at the maximum positive moment location for both spans are shown in Figs. 4.14 to 4.21. It can be noticed from the figures that deflections at midspan and  $2L/3$  did not continue reading up to failure, and that is because the actual deflection at these locations exceeded the LVDTs limit.

There are three stages can be recognized from the load-deflection relationships, the first stage is the uncracked (elastic) which starts from application of the load until first crack appearance, the second stage takes place after cracking up to yielding of non-

prestressed reinforcement, and the third stage occurs from yielding of non-prestressed steel to failure of the beam. Different parameters were studied by fixing the other parameters to show the effectiveness of that parameter in one plot. For beams 1 to 7, there are two locations that beam can produce cracks, the first location is in middle support and the second is near the point load next to the exterior support. When the applied load increases, the moment at the middle support section increases and reaches the modulus of the rupture, the middle support crack occurs, and the deflection starts to increase rapidly and the stress in the tensile non-prestressed steel at the middle support location increases as well.

To study the influence of the investigated design parameters such as effective stress in the bonded and unbonded tendons, area of reinforcing tensile steel at the maximum negative and positive locations and cross-section shape, the relationship between the total applied load and deflection are presented in Figs. 4.22, 4.23, 4.24 and 4.25, respectively.

**Table 4.3 Summary of Beam Camber due to Bonded and Unbonded Tendons**

Beam No.	Camber from Bonded Tendon (in)	Camber from Unbonded Tendon (in)	Total Camber (in)
1	-0.014	-0.010	-0.024
2	-0.011	-0.010	-0.021
3	-0.010	-0.012	-0.022
4	-0.020	-0.010	-0.030
5	-0.015	-0.010	-0.025
6	-0.015	-0.011	-0.026
7	-0.012	-0.005	-0.017
8	-0.008	-0.001	-0.009

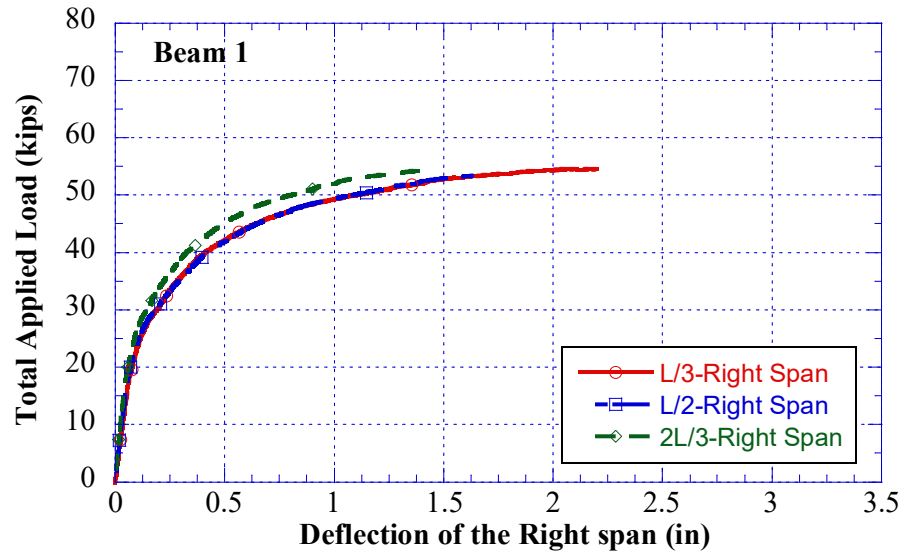


**Fig. 4.6 Relationship between Applied Load and Deflection at Different locations for Beam 1**

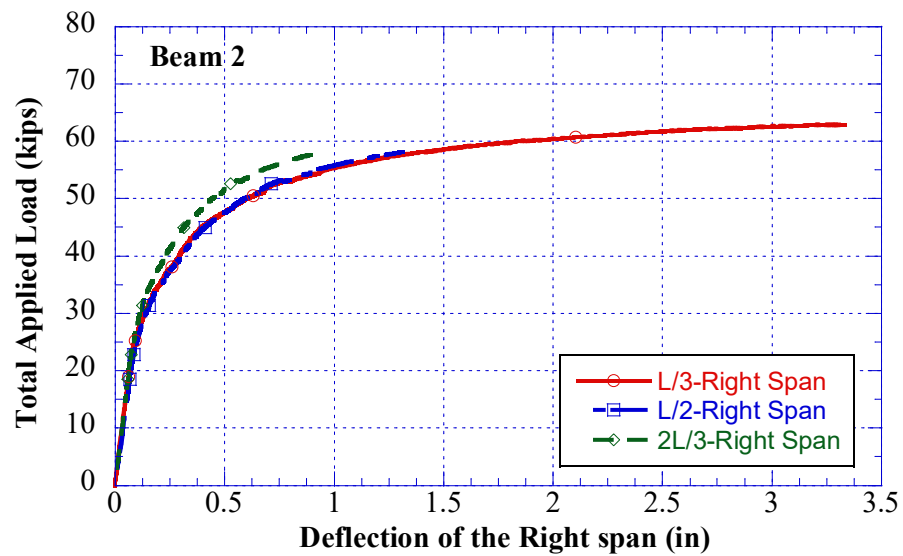


**Fig. 4.7 Relationship between Applied Load and Deflection at Different locations for Beam 2**



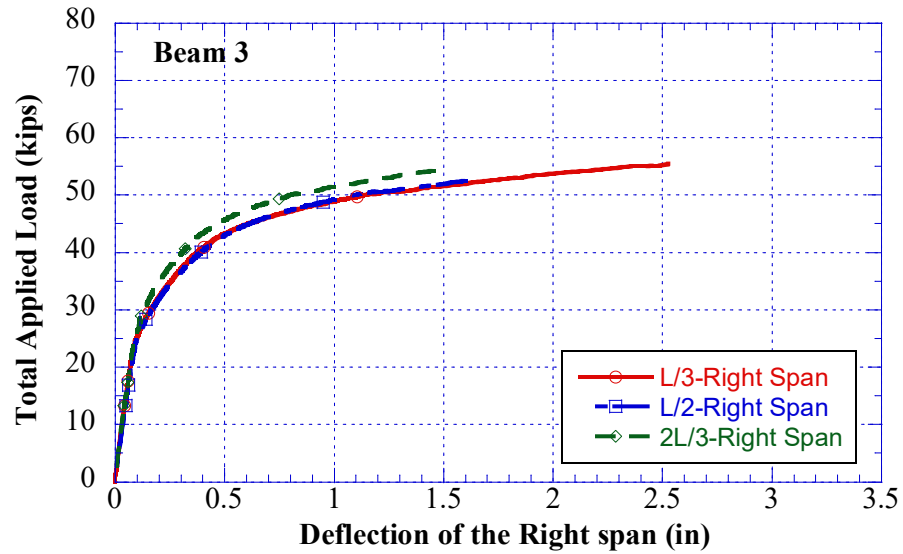


**Fig. 4.8 Relationship between Applied Load and Deflection at Different locations for Beam 3**

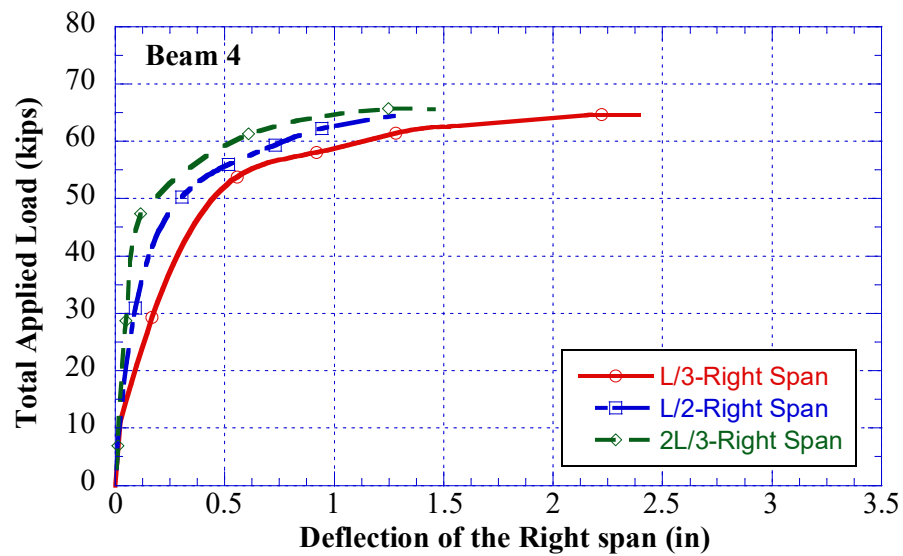


**Fig. 4.9 Relationship between Applied Load and Deflection at Different locations for Beam 4**

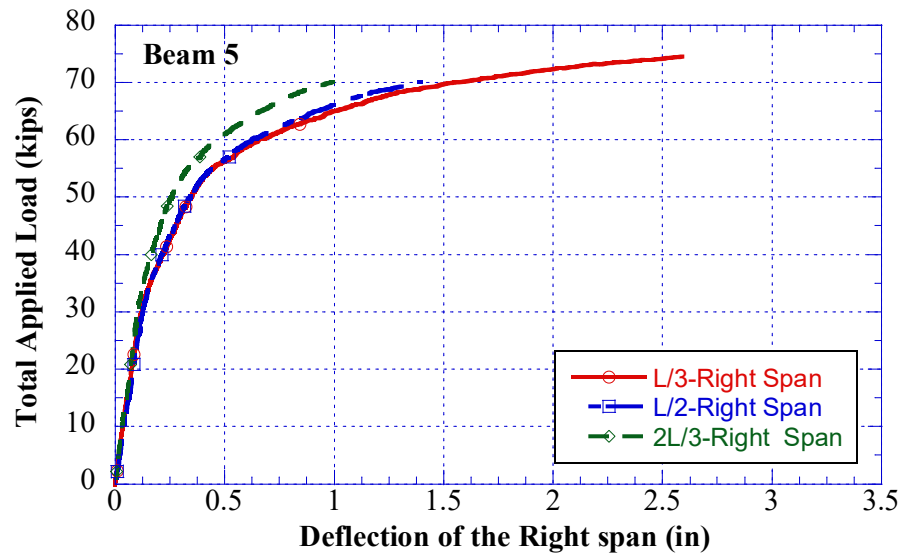


**Fig. 4.10 Relationship between Applied Load and Deflection at Different locations  
for Beam 5**

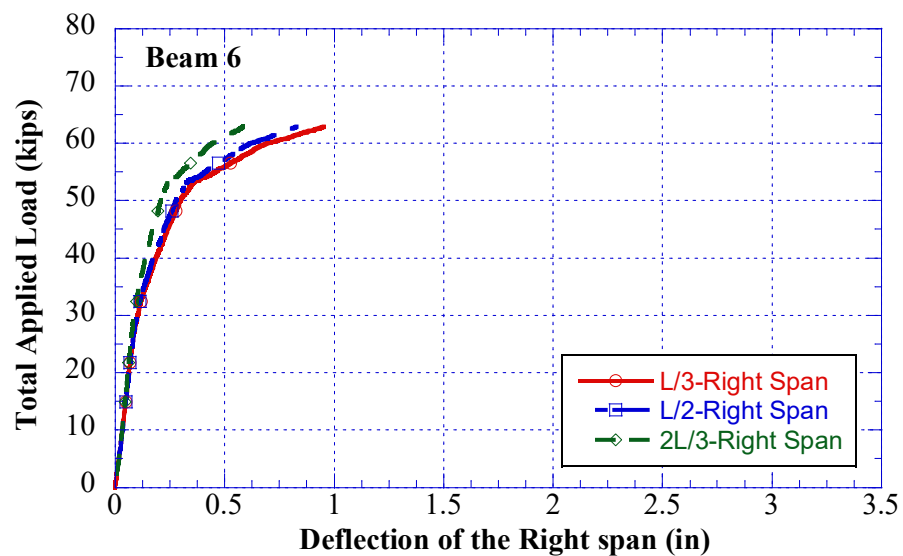


**Fig. 4.11 Relationship between Applied Load and Deflection at Different locations  
for Beam 6**

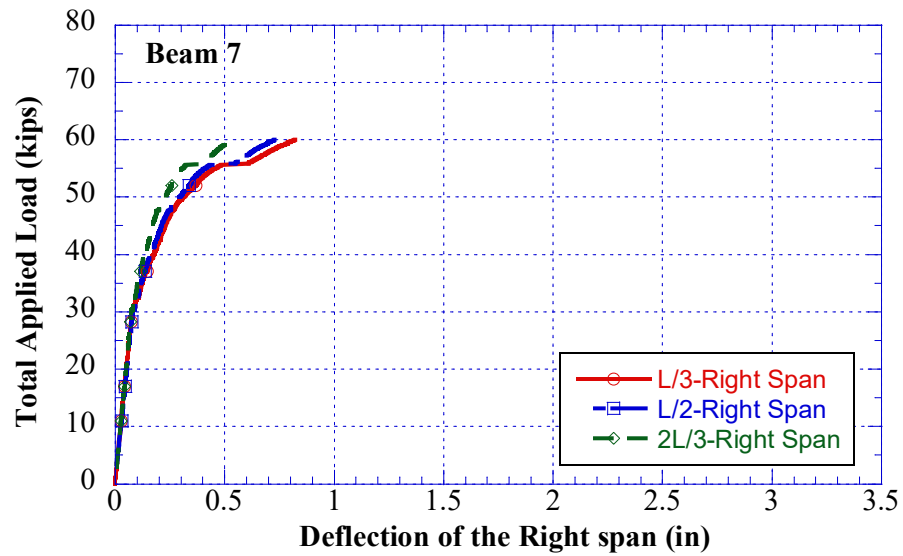


**Fig. 4.12 Relationship between Applied Load and Deflection at Different locations  
for Beam 7**

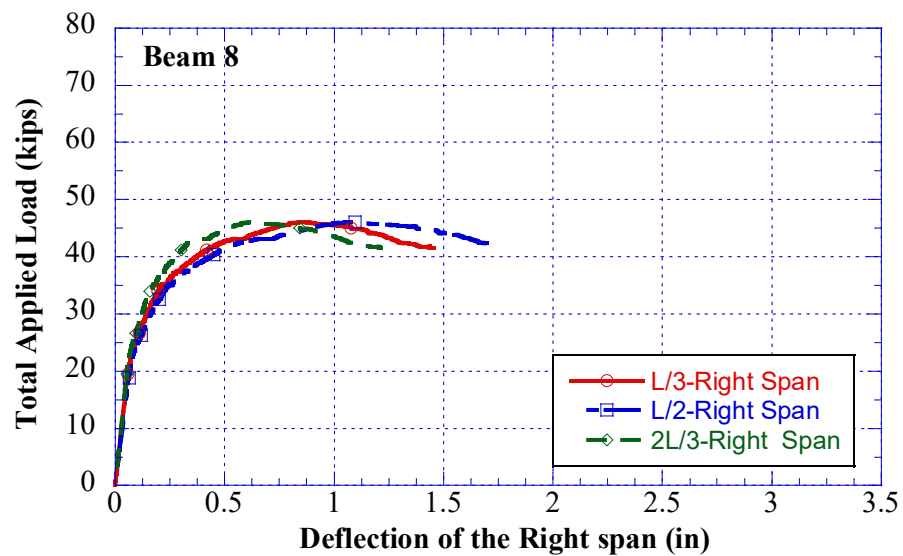


**Fig. 4.13 Relationship between Applied Load and Deflection at Different locations  
for Beam 8**

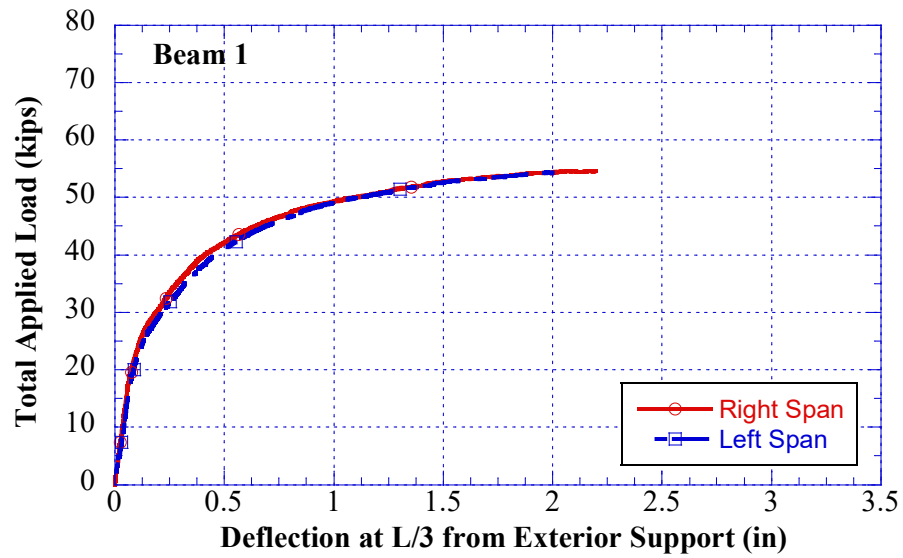


**Fig. 4.14 Relationship between Applied Load and Deflection at Maximum Positive Moment in both Spans for Beam 1**

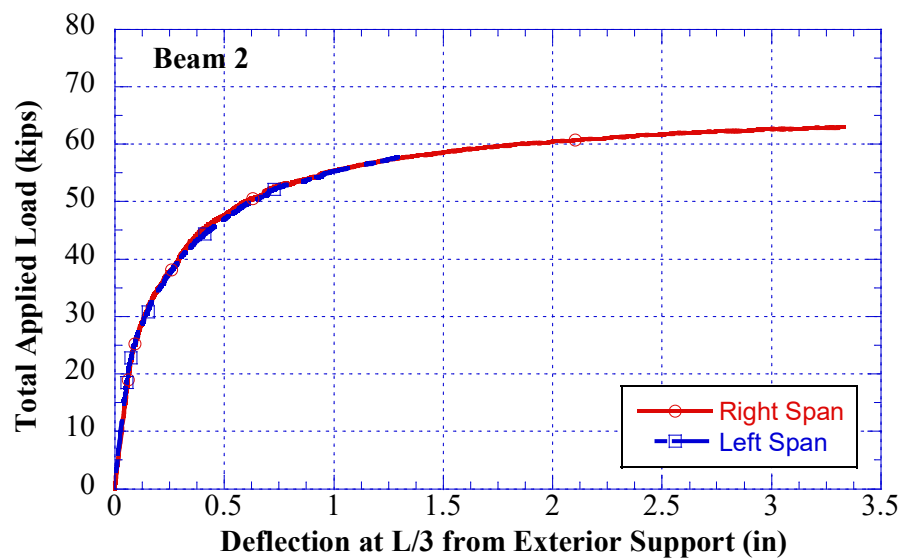


**Fig. 4.15 Relationship between Applied Load and Deflection at Maximum Positive Moment in both Spans for Beam 2**

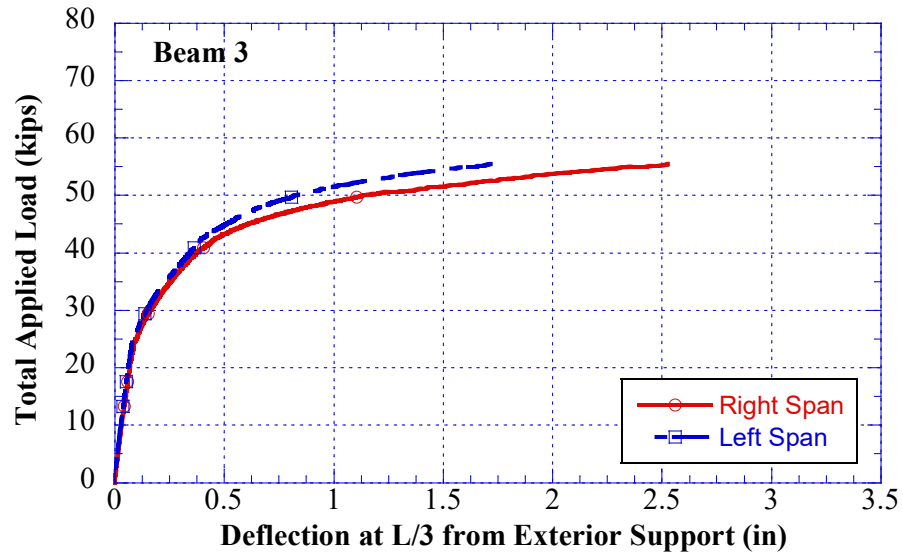


**Fig. 4.16 Relationship between Applied Load and Deflection at Maximum Positive Moment in both Spans for Beam 3**

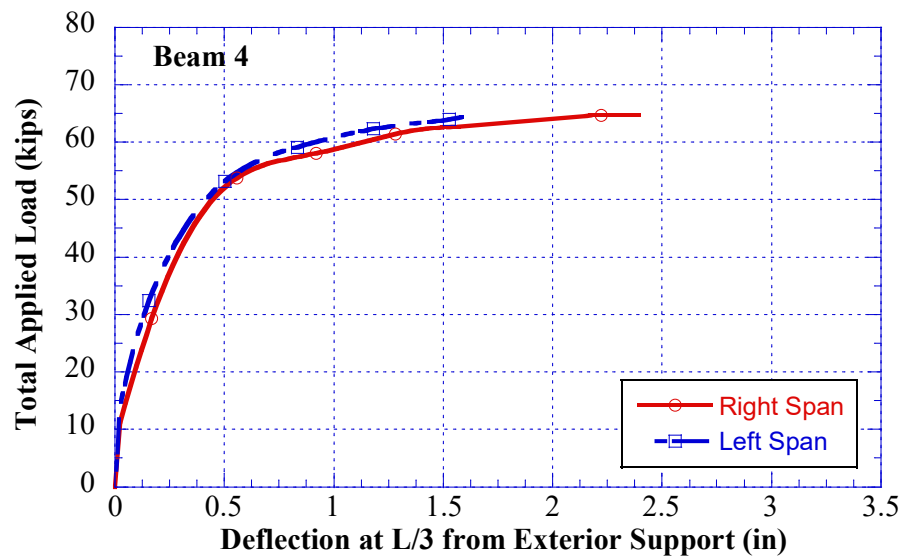


**Fig. 4.17 Relationship between Applied Load and Deflection at Maximum Positive Moment in both Spans for Beam 4**

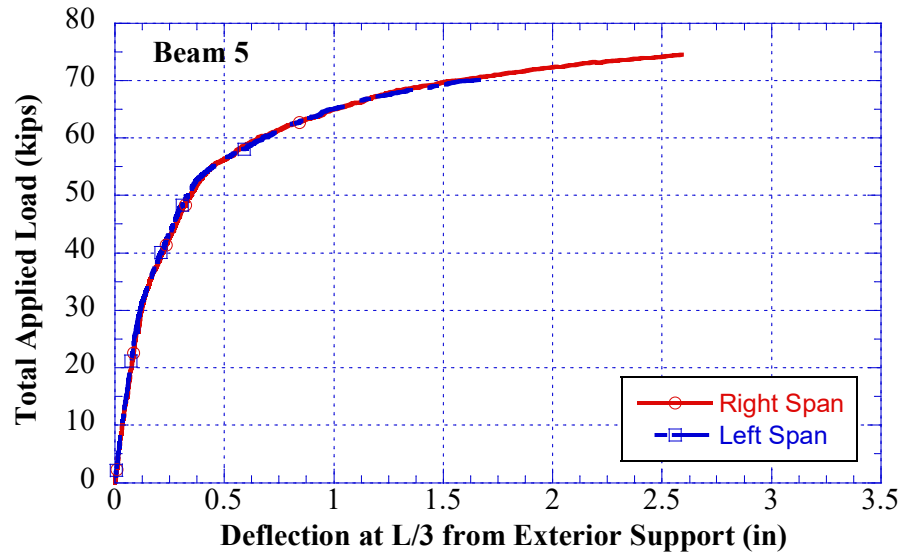


**Fig. 4.18 Relationship between Applied Load and Deflection at Maximum Positive Moment in both Spans for Beam 5**

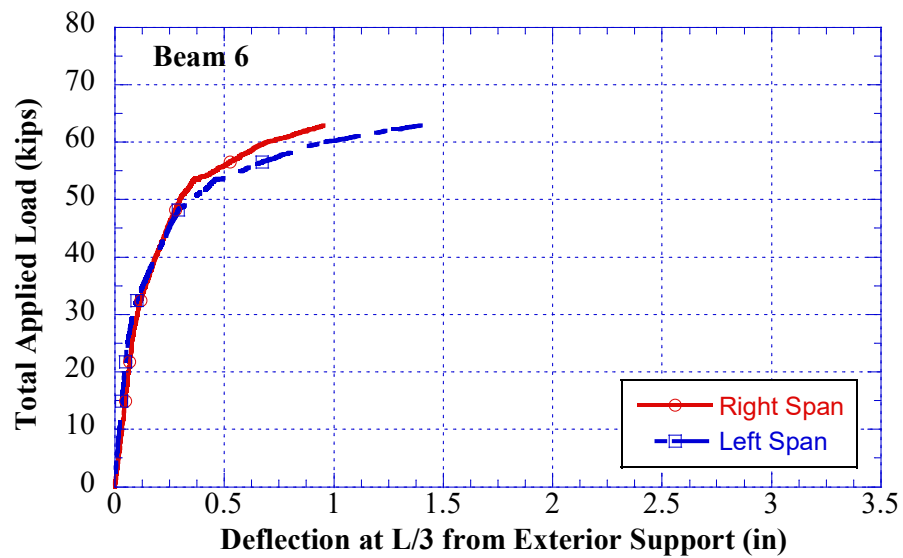


**Fig. 4.19 Relationship between Applied Load and Deflection at Maximum Positive Moment in both Spans for Beam 6**

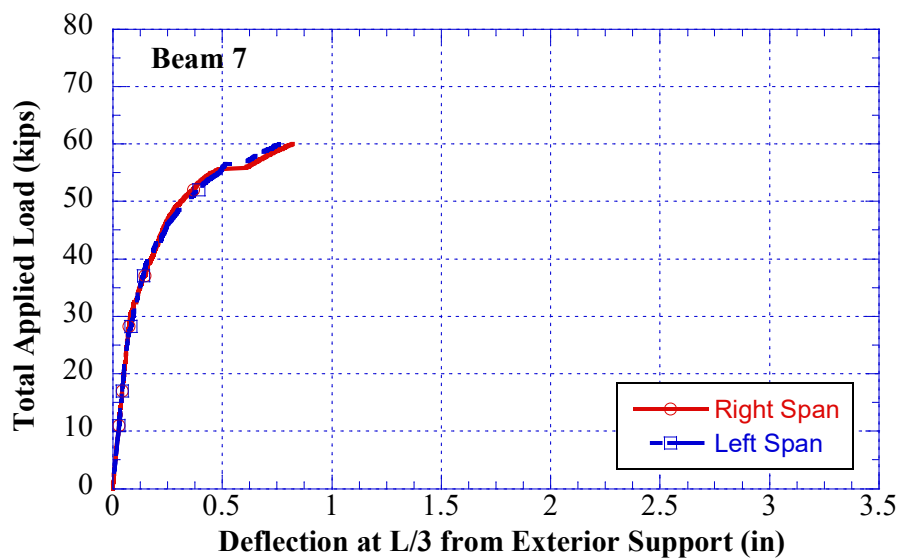


**Fig. 4.20 Relationship between Applied Load and Deflection at Maximum Positive Moment in both Spans for Beam 7**

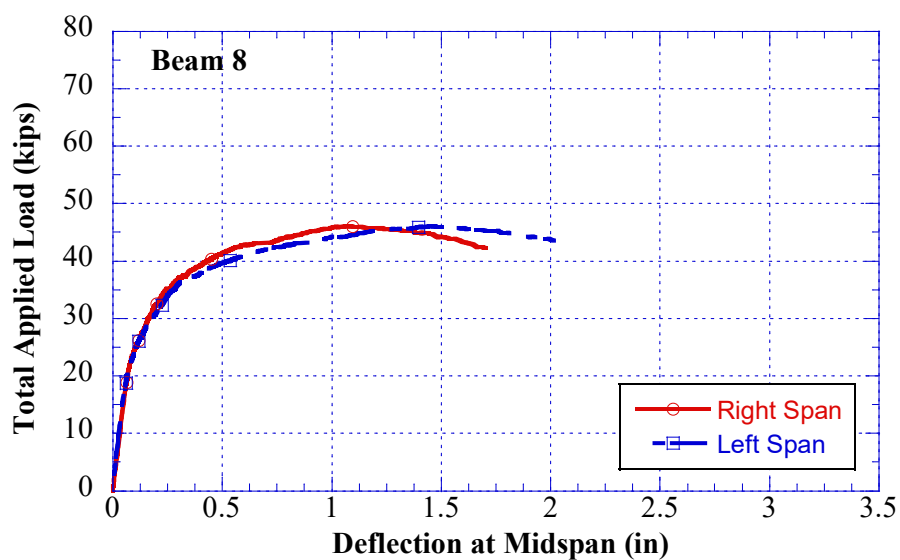


**Fig. 4.21 Relationship between Applied Load and Deflection at Maximum Positive Moment in both Spans for Beam 8**

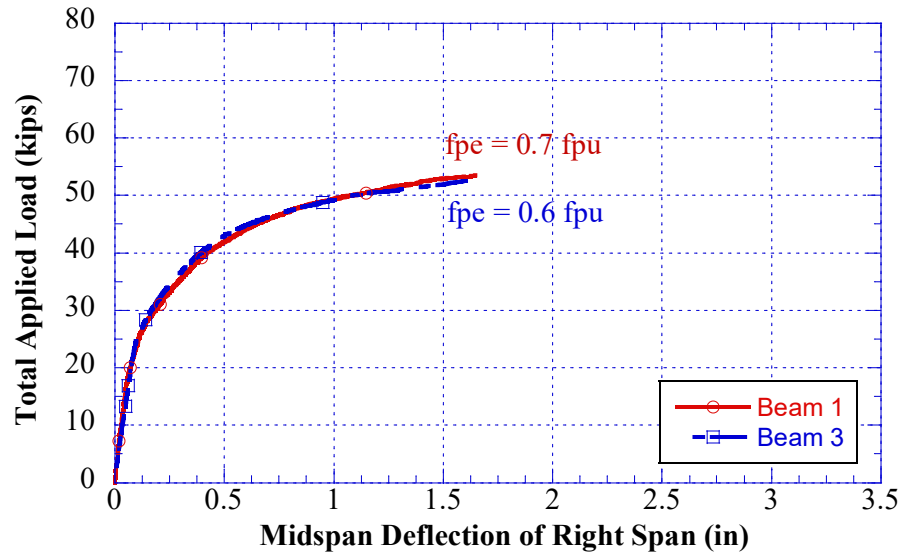


Fig. 4.22 Relationship between Applied Load and Deflection for varying  $f_{pe}$

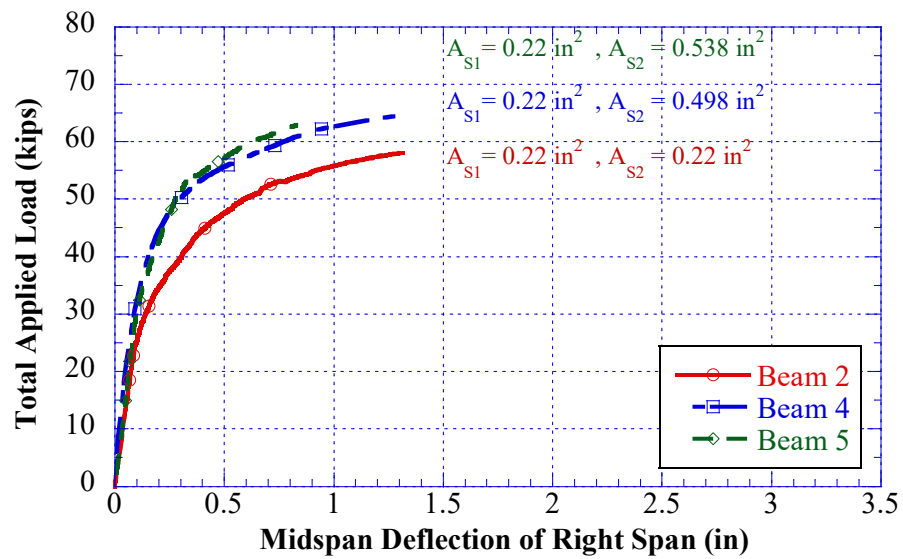


Fig. 4.23 Relationship between Applied Load and Deflection for varying  $A_{s2}$



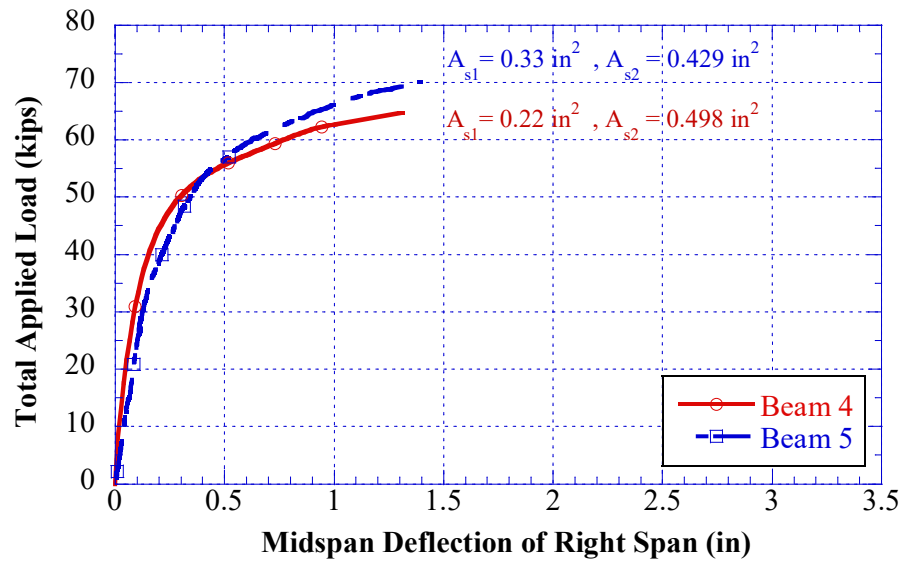


Fig. 4.24 Relationship between Applied Load and Deflection for varying  $A_{SI}$

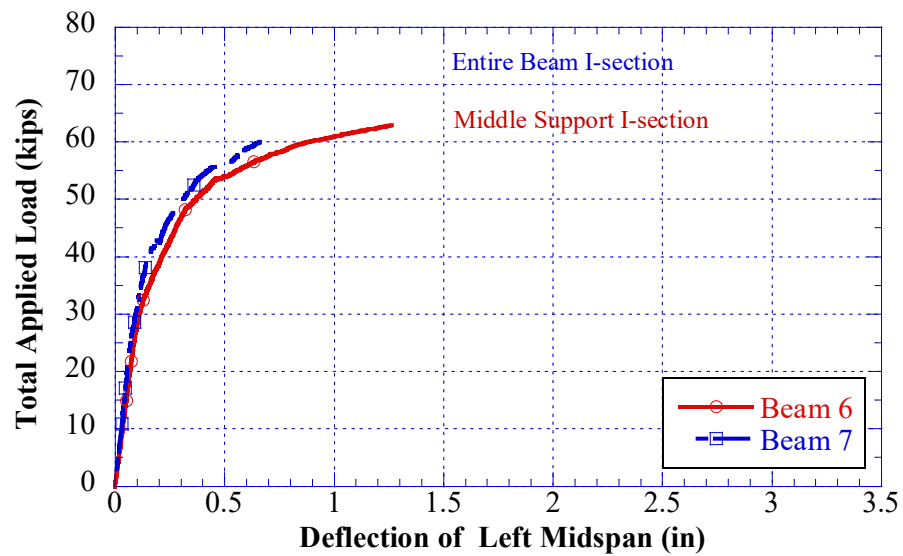


Fig. 4.25 Relationship between Applied Load and Deflection

for varying *cross-section*

#### **4.4.2 Load - Strain Relationship**

To observe the strain in non-prestressing steel at the maximum positive moment location, foil strain gauges were installed at steel in tension and compression zones. Relationships between the total applied load and strain in reinforcing steel in the right and left span for all beam tests are presented in Figs. 4.26 to 4.41. The figures show that the strain in steel rebar that in compression increases in compression then decreases to the be in tension just before and at ultimate. This behavior occurs because the depth of the neutral axis keeps decreasing until it becomes less than the depth of steel rebar that in compression, thus, all top and bottom reinforcing steel are in tension zone.

In addition, relationships between applied load and strain in tensile reinforcing steel are presented for different studied design parameters such as effective stress in the strands, reinforcing steel in tensions and cross-section shape as shown in Figs 4.42 to 4.45. The plots show that varying the effective stress in the prestressing tendons and changing the cross-section area of the beam at the interior support show a very small change in the strain which can be ignored.

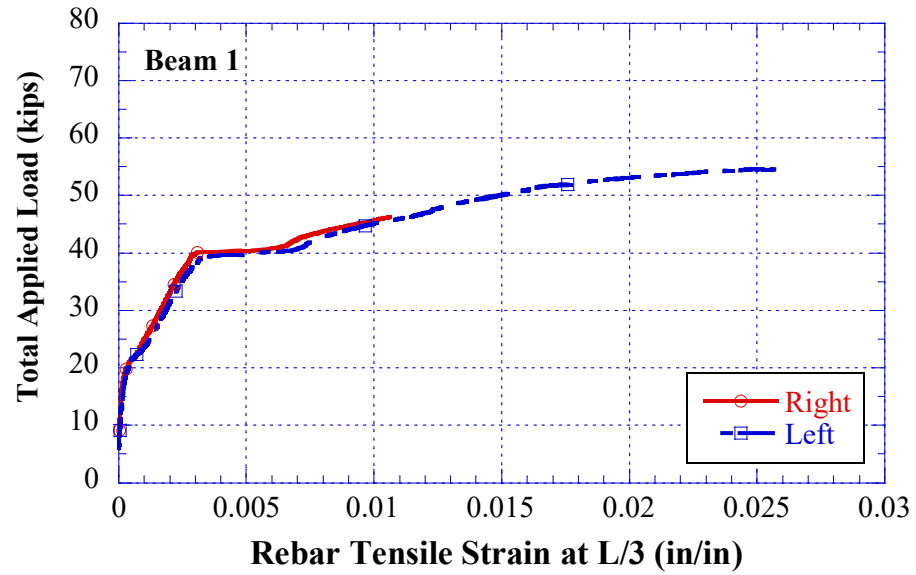


**Fig. 4.26 Relationship between Applied Load and Rebar Tensile Strain for Beam 1**

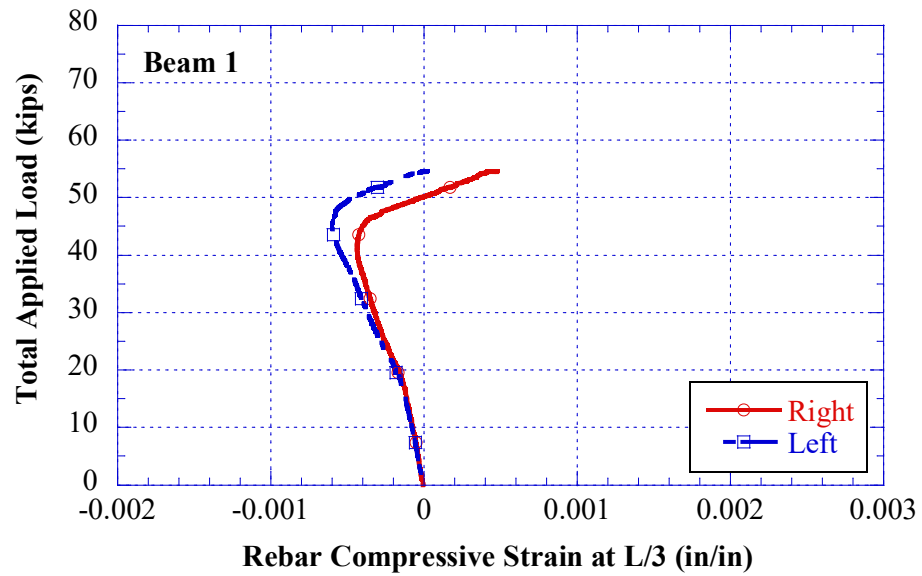


**Fig. 4.27 Relationship between Applied Load and Rebar Compressive Strain for**

**Beam 1**

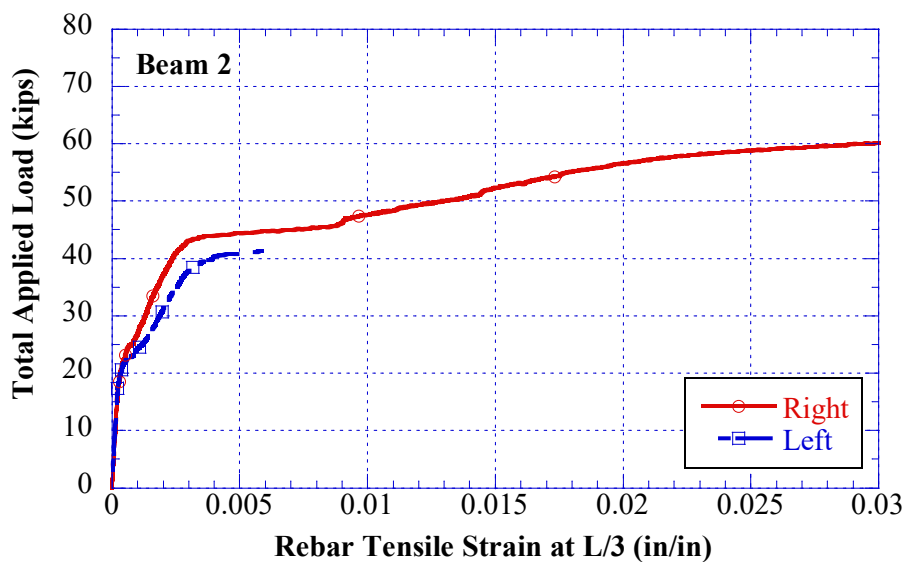


Fig. 4.28 Relationship between Applied Load and Rebar Tensile Strain for Beam 2

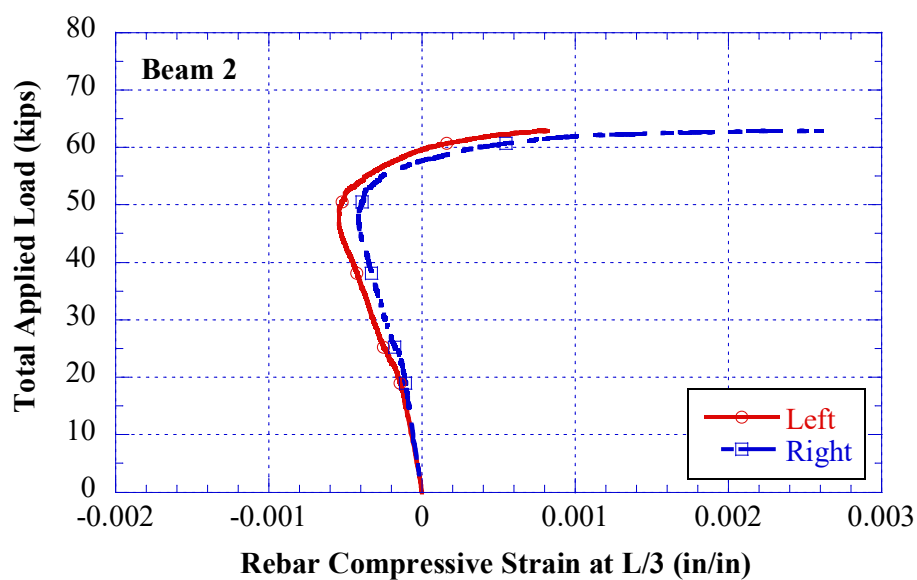


Fig. 4.29 Relationship between Applied Load and Rebar Compressive Strain for  
Beam 2

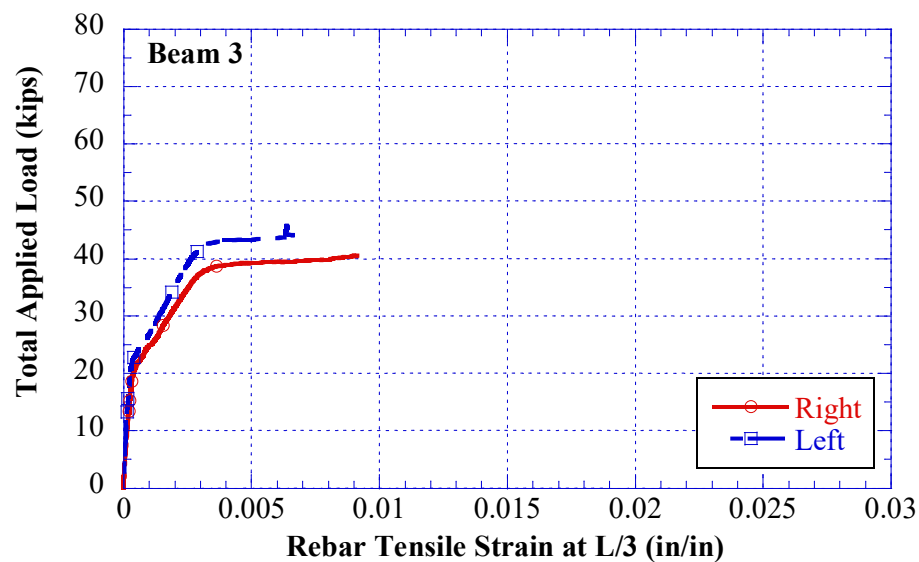


Fig. 4.30 Relationship between Applied Load and Rebar Tensile Strain for Beam 3

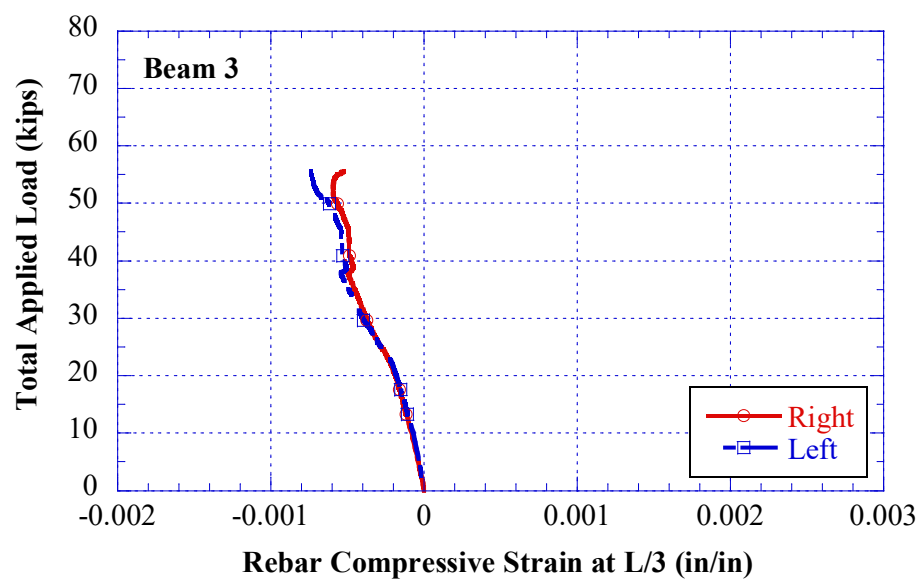


Fig. 4.31 Relationship between Applied Load and Rebar Compressive Strain for  
Beam 3

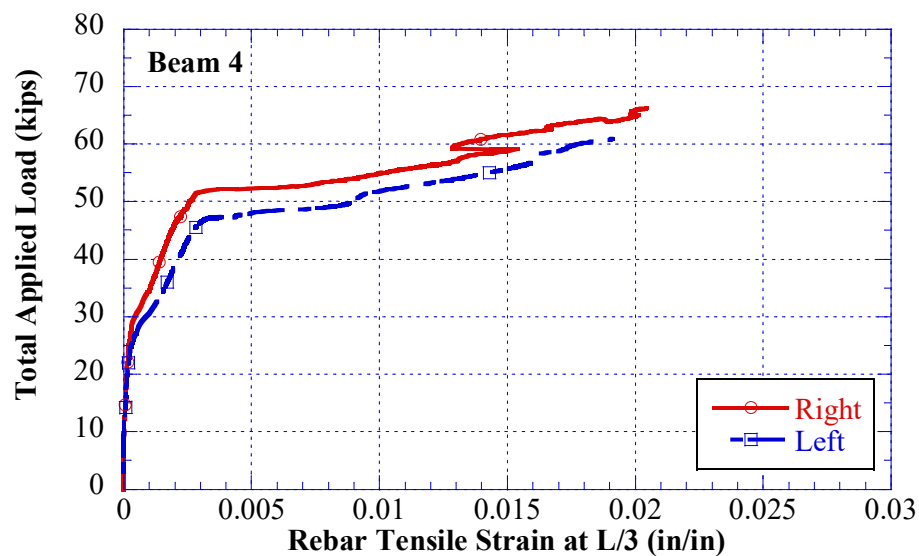


Fig. 4.32 Relationship between Applied Load and Rebar Tensile Strain for Beam 4

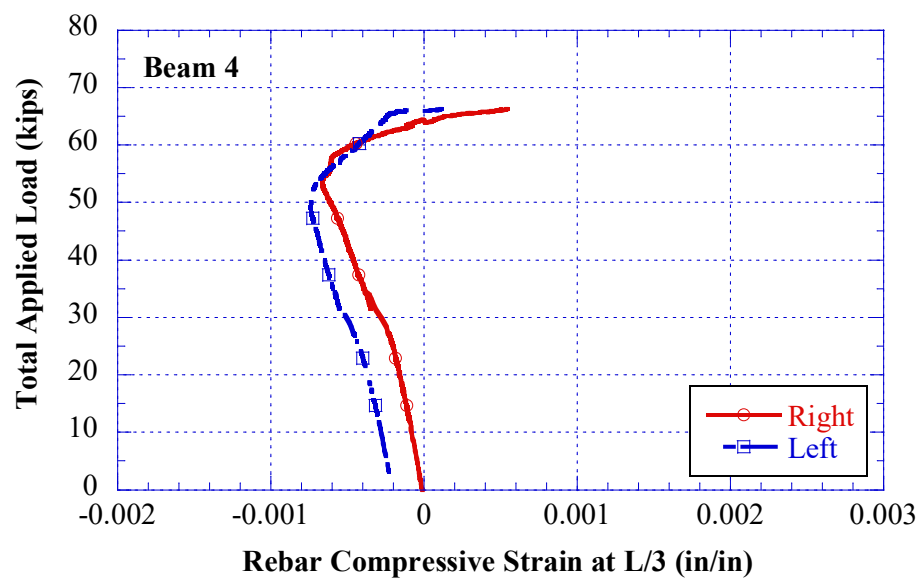
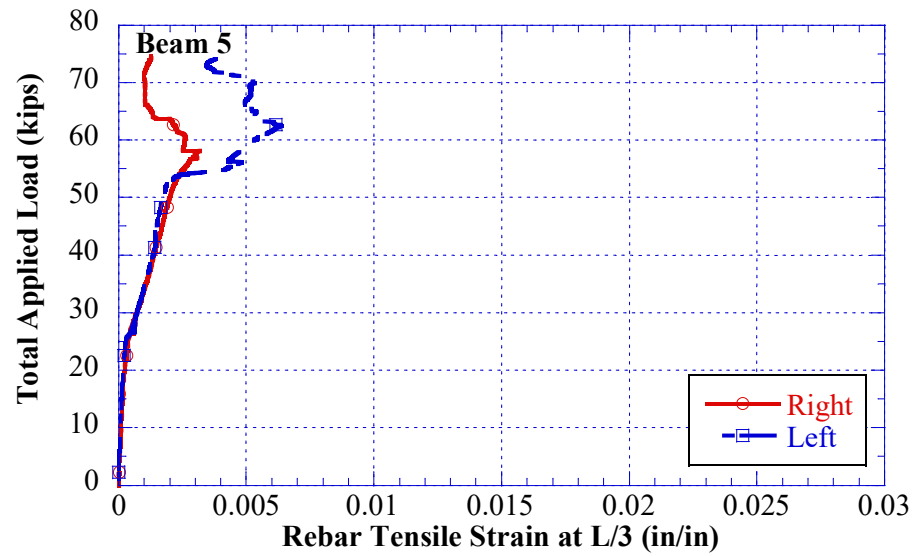
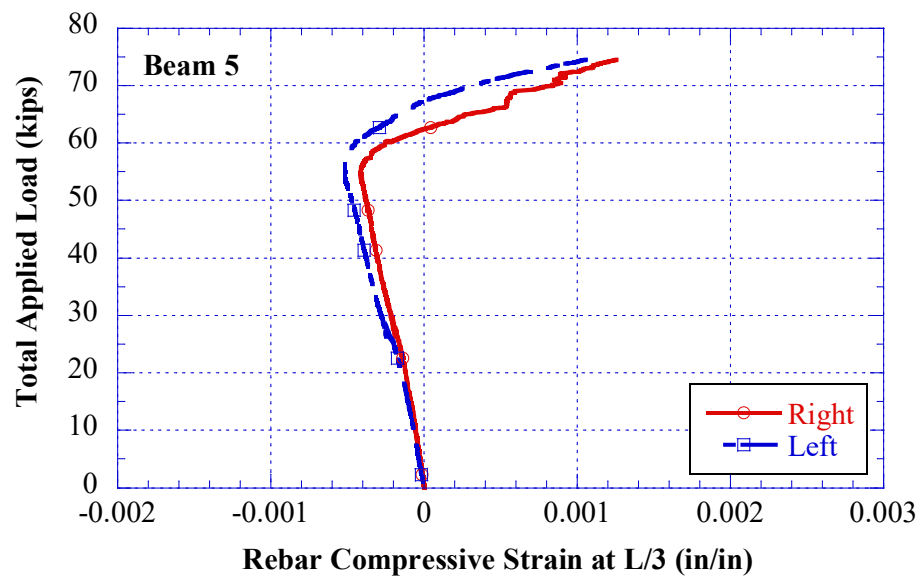


Fig. 4.33 Relationship between Applied Load and Rebar Compressive Strain for  
Beam 4



**Fig. 4.34 Relationship between Applied Load and Rebar Tensile Strain for Beam 5**



**Fig. 4.35 Relationship between Applied Load and Rebar Compressive Strain for  
Beam 5**

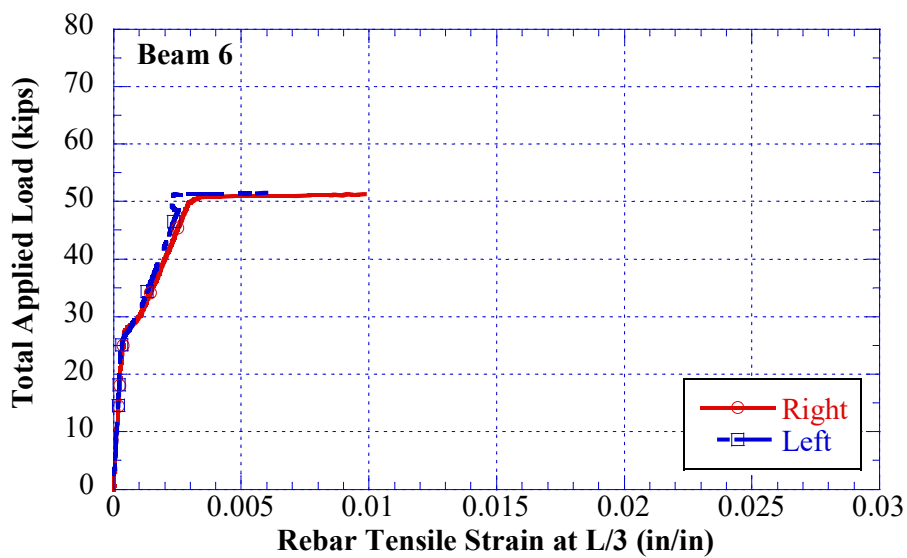


Fig. 4.36 Relationship between Applied Load and Rebar Tensile Strain for Beam 6

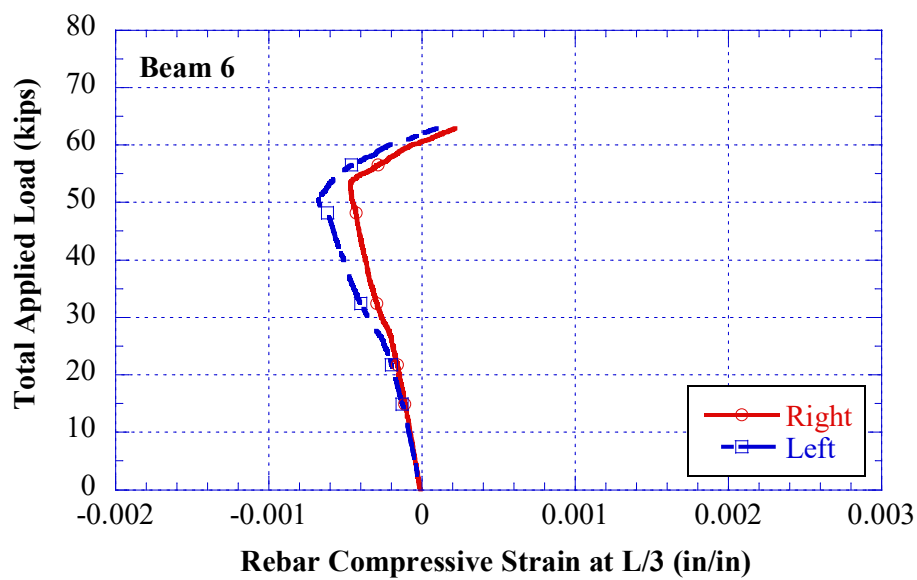


Fig. 4.37 Relationship between Applied Load and Rebar Compressive Strain for  
Beam 6



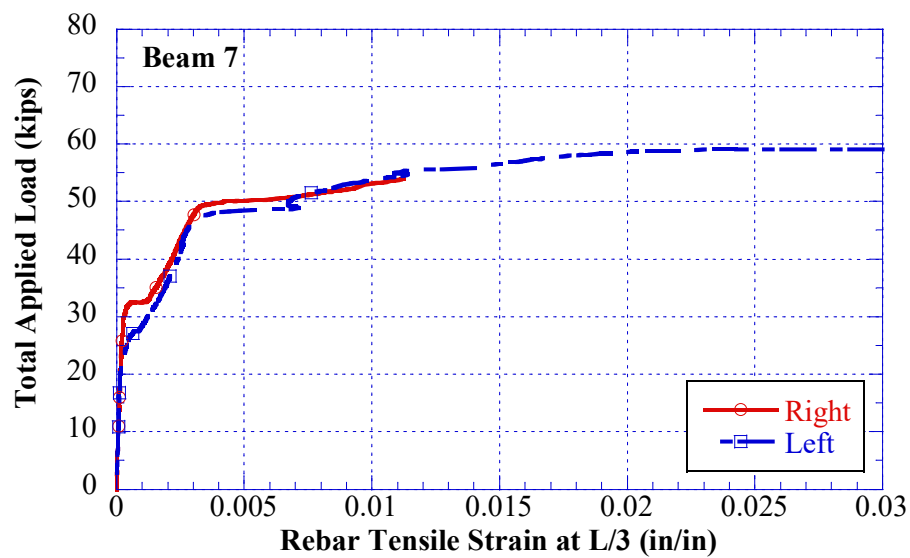
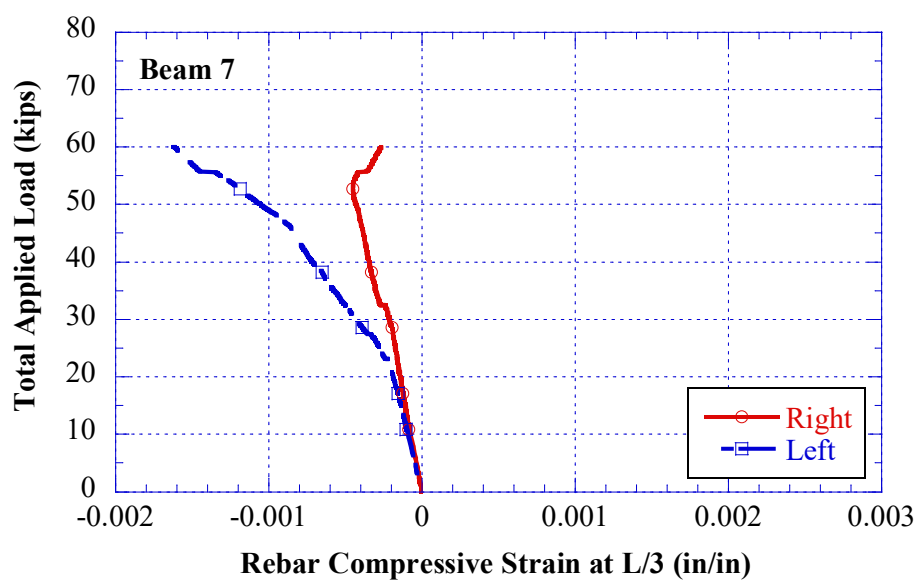


Fig. 4.38 Relationship between Applied Load and Rebar Tensile Strain for Beam 7



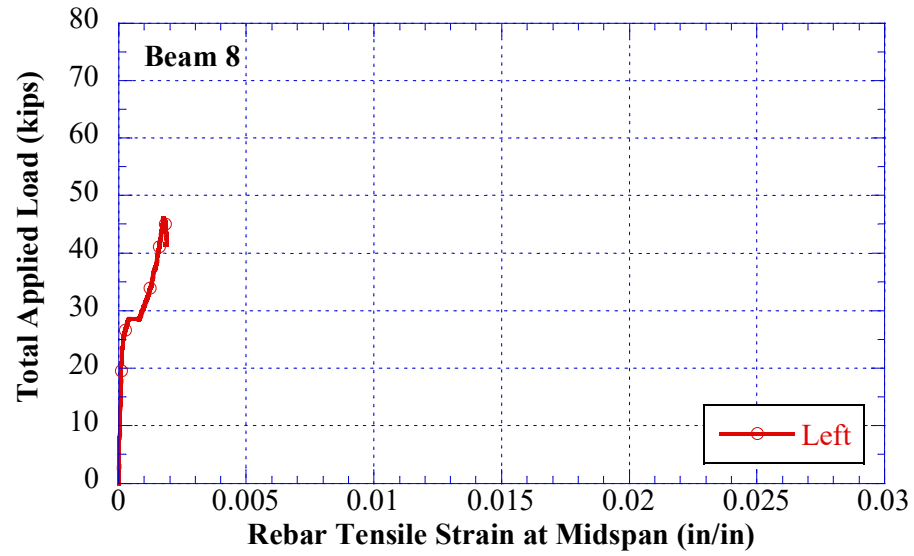


Fig. 4.40 Relationship between Applied Load and Rebar Tensile Strain for Beam 8

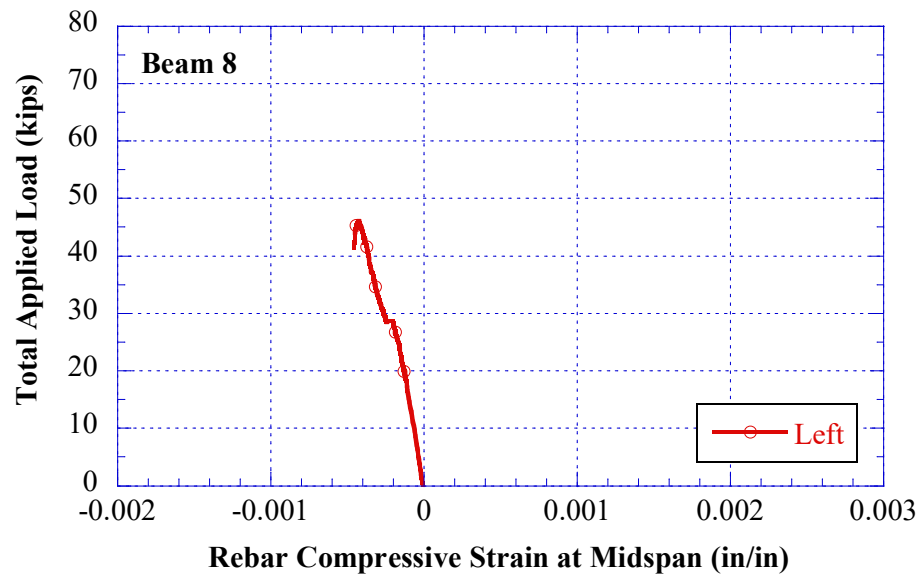
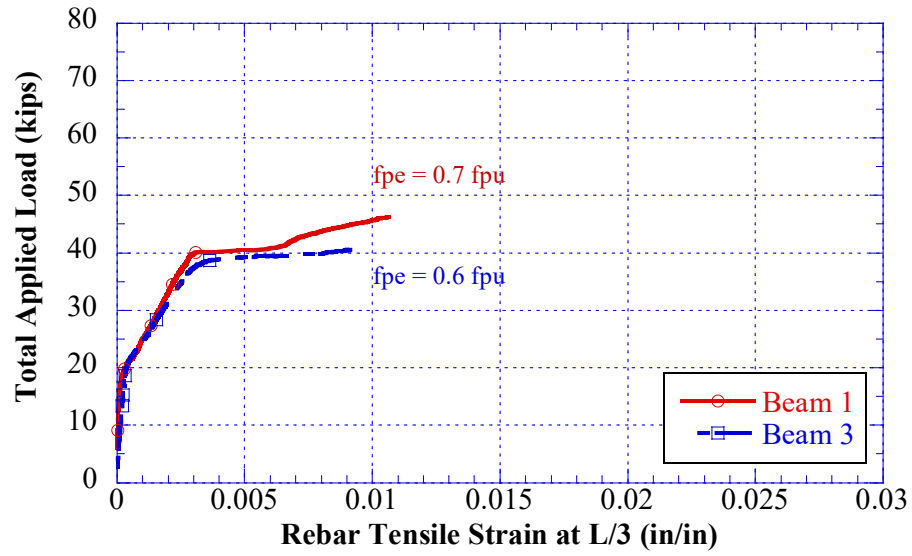
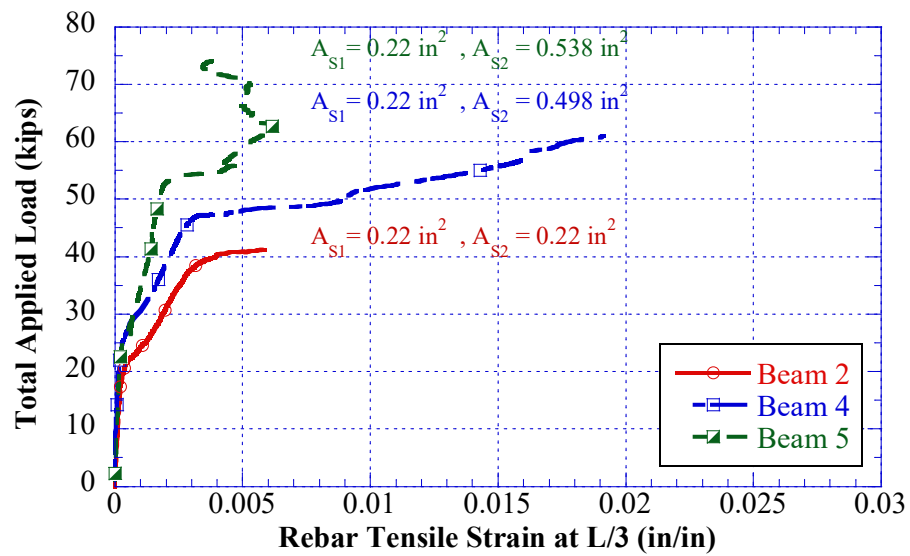


Fig. 4.41 Relationship between Applied Load and Rebar Compressive Strain for  
Beam 8



**Fig. 4.42 Relationship between Applied Load and Rebar Tensile Strain  
for varying  $f_{pe}$**



**Fig. 4.43 Relationship between Applied Load and Rebar Tensile Strain  
for varying  $A_{s2}$**

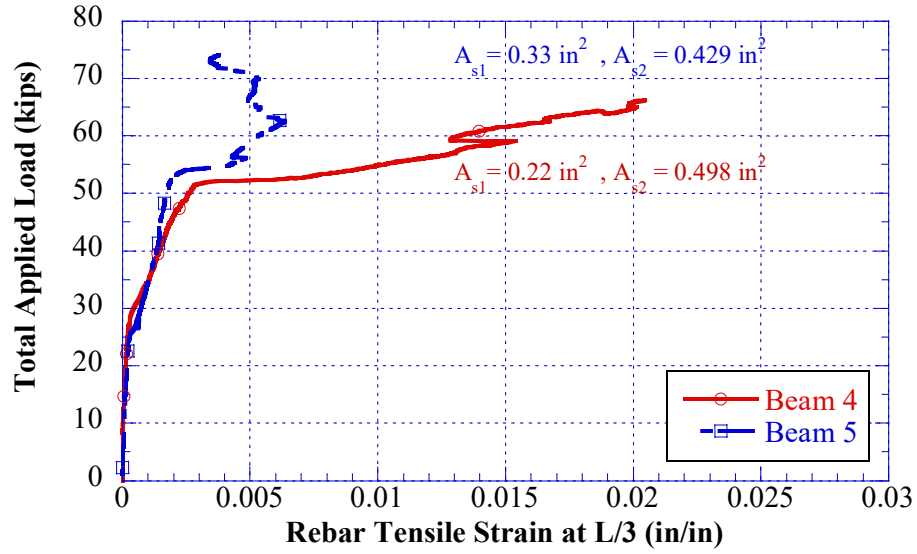


**Fig. 4.44 Relationship between Applied Load and Rebar Tensile Strain  
for varying  $A_{sI}$**

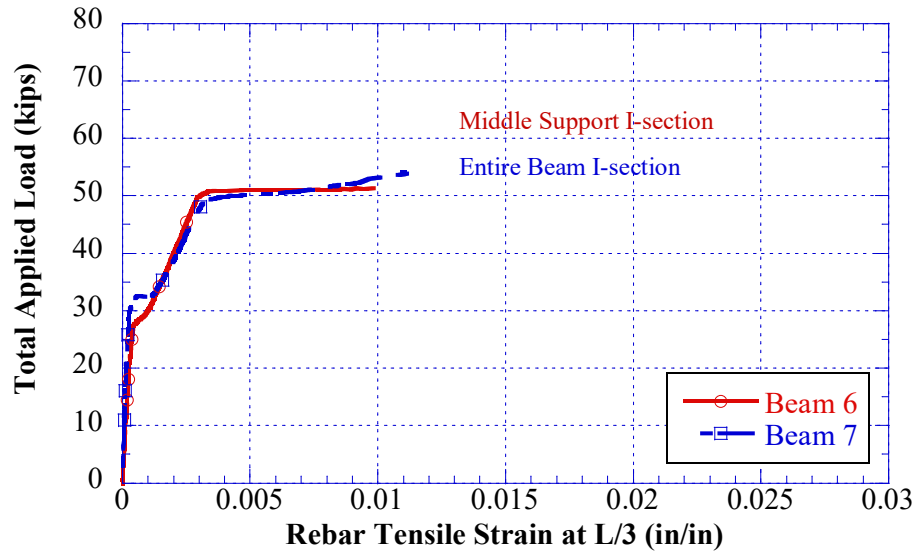


**Fig. 4.45 Relationship between Applied Load and Rebar Tensile Strain  
for varying *cross-section***

#### 4.4.3 Stress in Prestressing Steel

Each test beam has two strands one is bonded using cable grout and the second strand is unbonded strand. Due to the limited capacity of the testing machine setup, 5/16-inch diameter was used for both tendons in all specimens. Two 50-kip capacity load cells were installed at the beam dead end and placed between two rigid steel plates to provide uniformly distributed pressure against the load cells as mentioned in chapter three. The increase in the unbonded tendon stress from the externally applied load until the failure is defined as  $\Delta f_{psU}$ . The load cell for the unbonded tendon measured the increase in the tendon stress due to the deformation along the whole beam. However, the load cell for the grouted tendon was installed for two reasons; the first one is to measure the prestressing stress during the post-tensioning, and the second reason is to satisfy that this stress does not increase with applied load. Therefore, there is no slipping between the strand and surrounded cable grout.

The relationships between the stress increase in unbonded tendon and the total applied load for all test beams are shown in Figs 4.46 to 4.53. It can be noticed from the graphs that there is no significant increase in the stress in the unbonded tendon within the elastic stage. However, the stress in the unbonded tendon drastically increases when the cracks occur and propagate until failure. In addition, that is rational behavior, where within the elastic stage there is no cracks appear in the beam, which means no elongation in the unbonded tendon, but when cracks occur and develop the stresses transfer from concrete to non-prestressed reinforcement and finally to the unbonded tendon.

Moreover, the relationships between the stress increase and applied load with different parameter changed to study the effects of these factors on the stress in the unbonded tendon as shown in Figs. 4.54 to 4.57. The stress increase  $\Delta f_{psU}$  and stress at failure  $f_{psU}$  in the unbonded tendon are summarized in Table 4.4.

**Table 4.4 Summary of Stress Increase  $\Delta f_{psU}$  and Stress  $f_{psU}$  in the Unbonded Tendon at Failure**

<b>Beam No.</b>	<b><math>\Delta f_{psU}</math> (ksi)</b>	<b><math>f_{psU}</math> (ksi)</b>
1	91.75	264.97
2	85.43	270.85
3	87.06	274.57
4	58.14	261.92
5	57.36	266.71
6	46.50	251.50
7	40.34	246.85
8	52.90	259.90

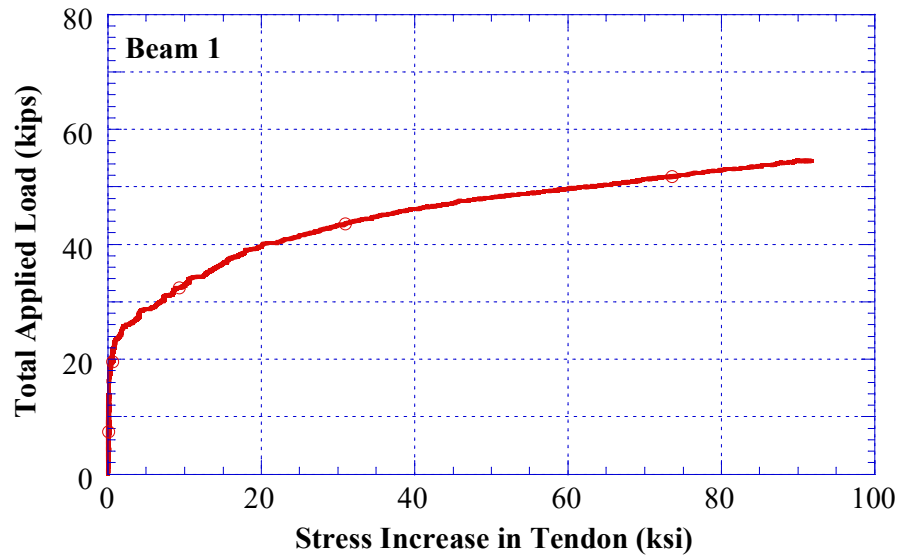


**Fig. 4.46 Relationship between Applied Load and Stress Increase in Unbonded Tendon for Beam 1**

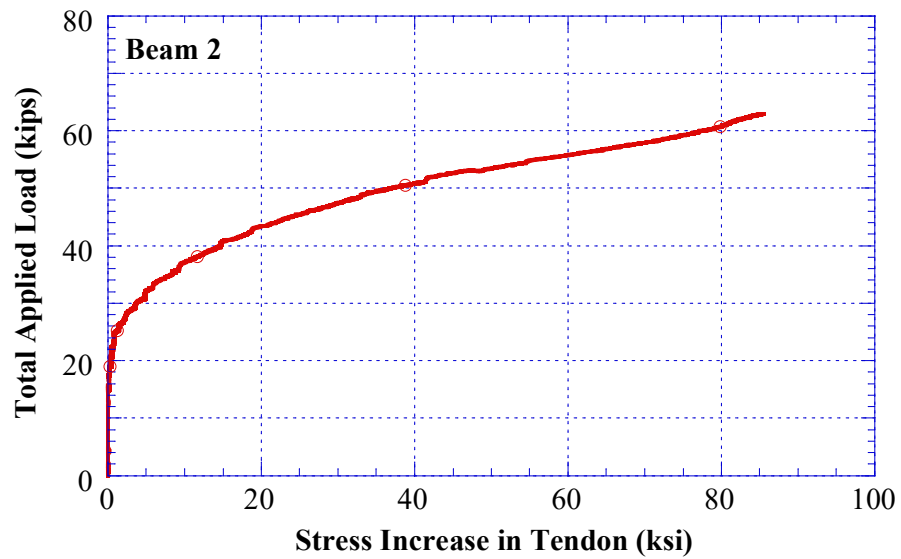


**Fig. 4.47 Relationship between Applied Load and Stress Increase in Unbonded Tendon for Beam 2**

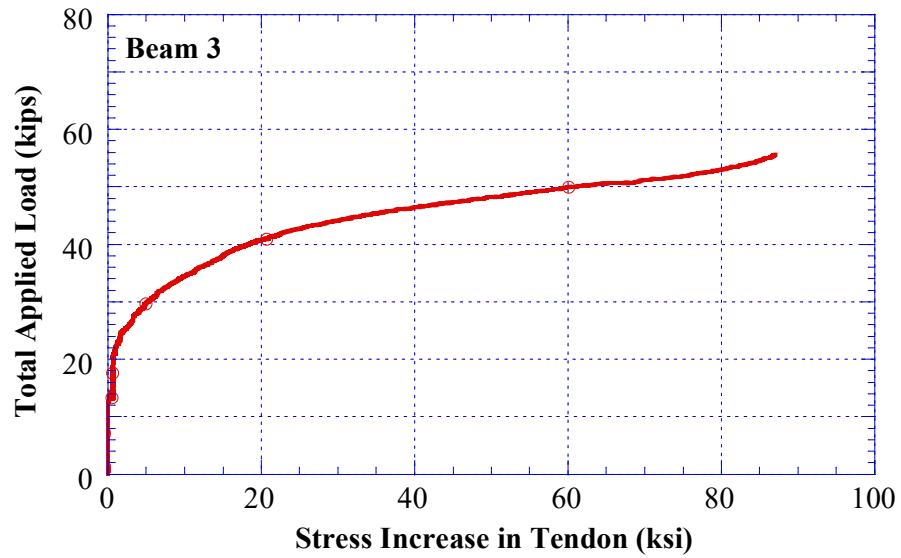


**Fig. 4.48 Relationship between Applied Load and Stress Increase in Unbonded Tendon for Beam 3**

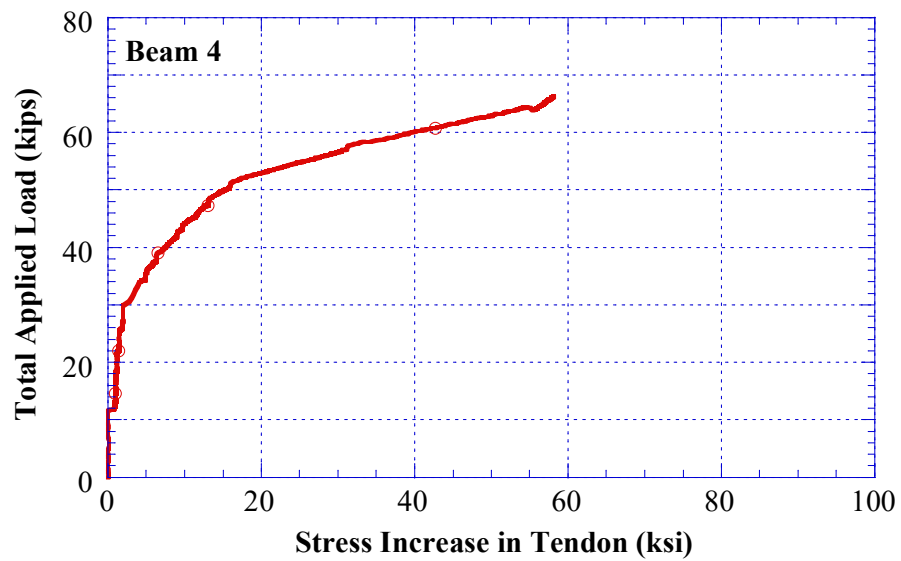


**Fig. 4.49 Relationship between Applied Load and Stress Increase in Unbonded Tendon for Beam 4**



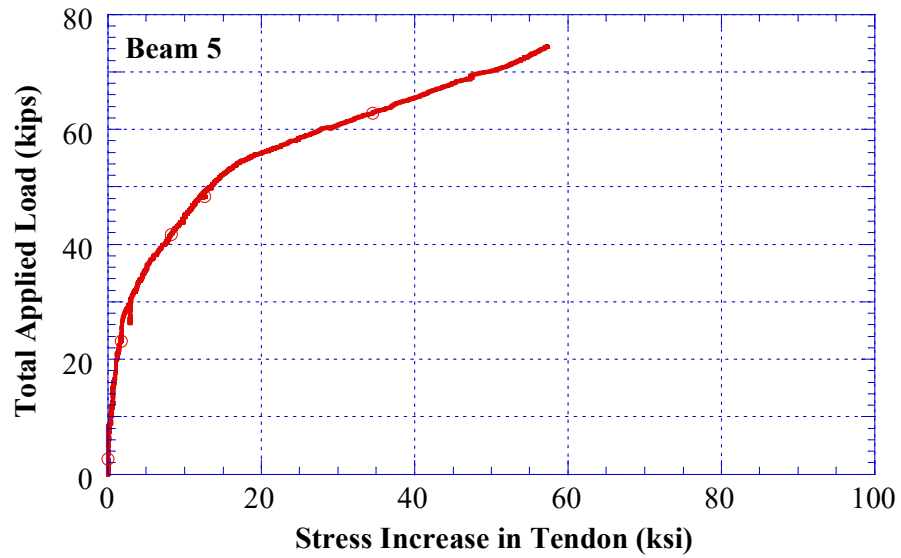


**Fig. 4.50 Relationship between Applied Load and Stress Increase in Unbonded Tendon for Beam 5**

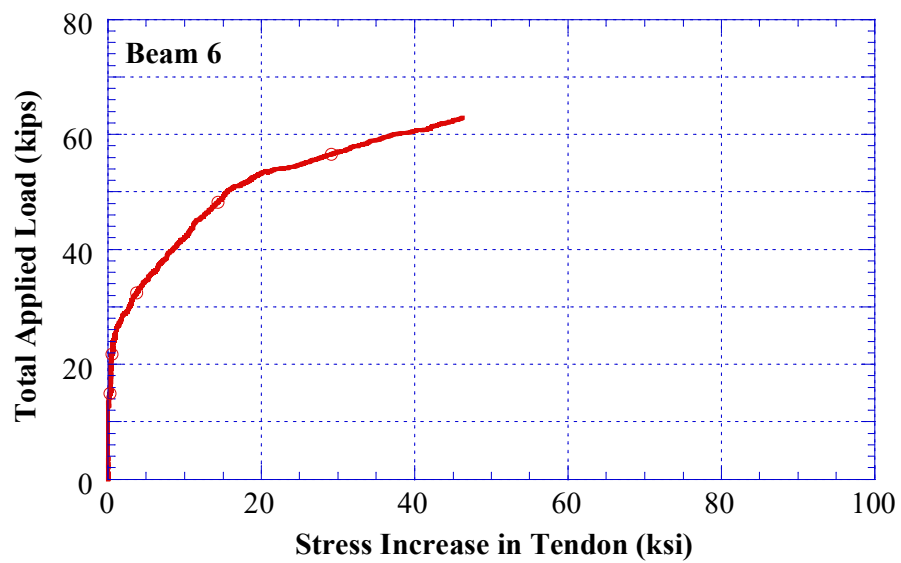


**Fig. 4.51 Relationship between Applied Load and Stress Increase in Unbonded Tendon for Beam 6**

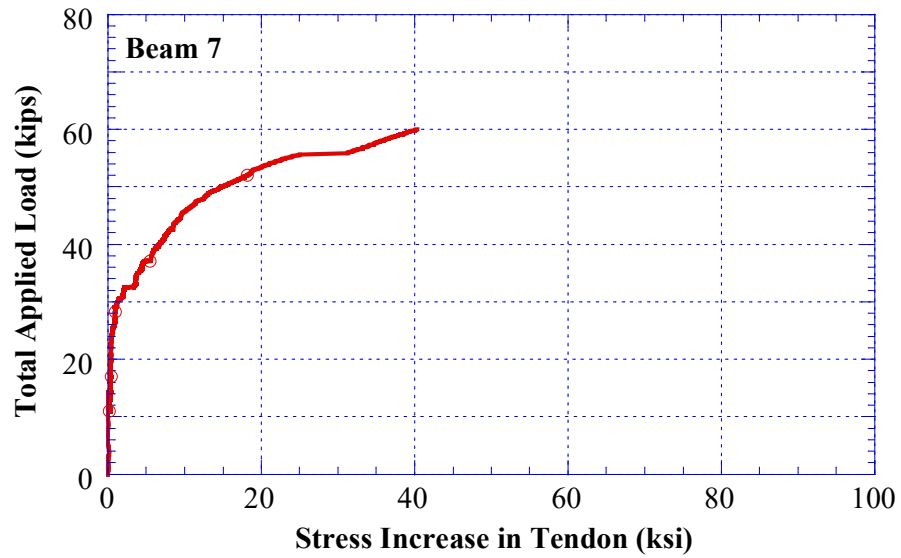


**Fig. 4.52 Relationship between Applied Load and Stress Increase in Unbonded Tendon for Beam 7**

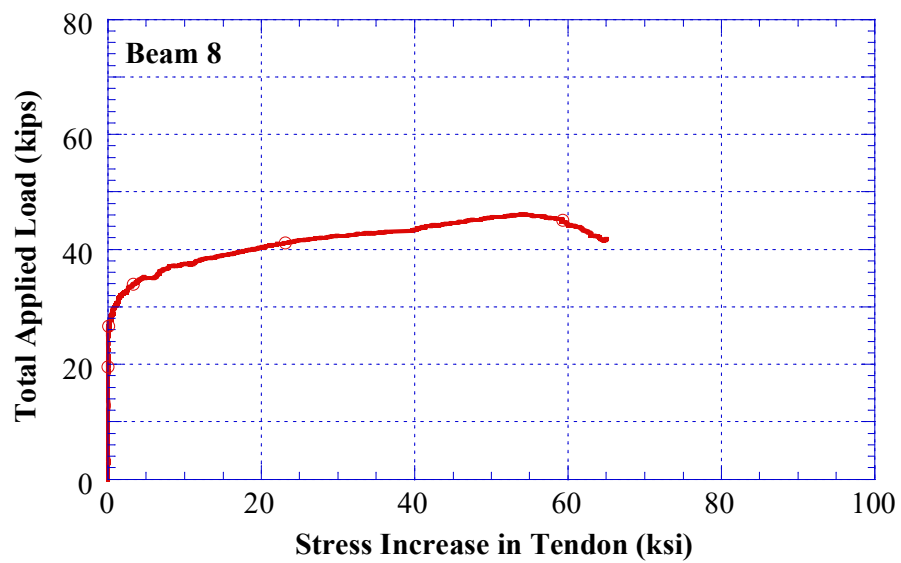


**Fig. 4.53 Relationship between Applied Load and Stress Increase in Unbonded Tendon for Beam 8**

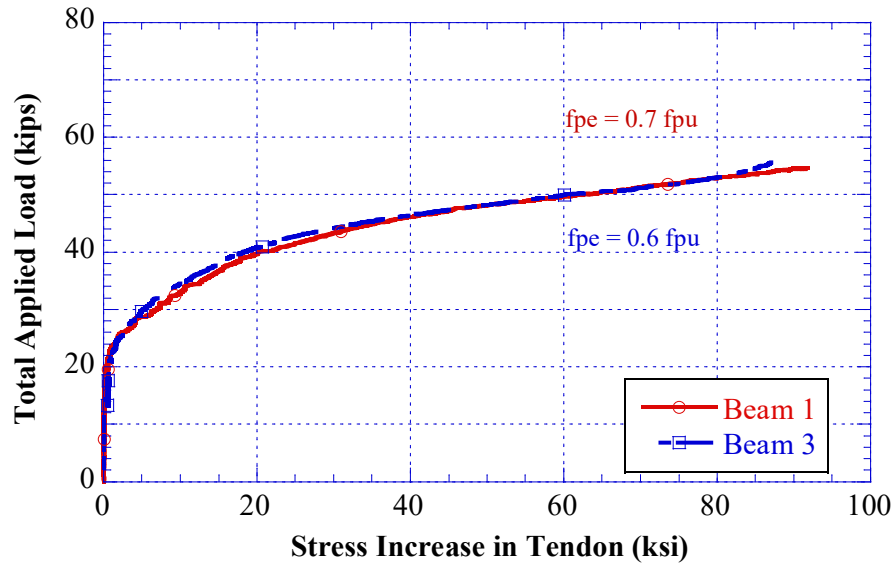


**Fig. 4.54 Relationship between Applied Load and Stress Increase in Unbonded Tendon for varying  $f_{pe}$**

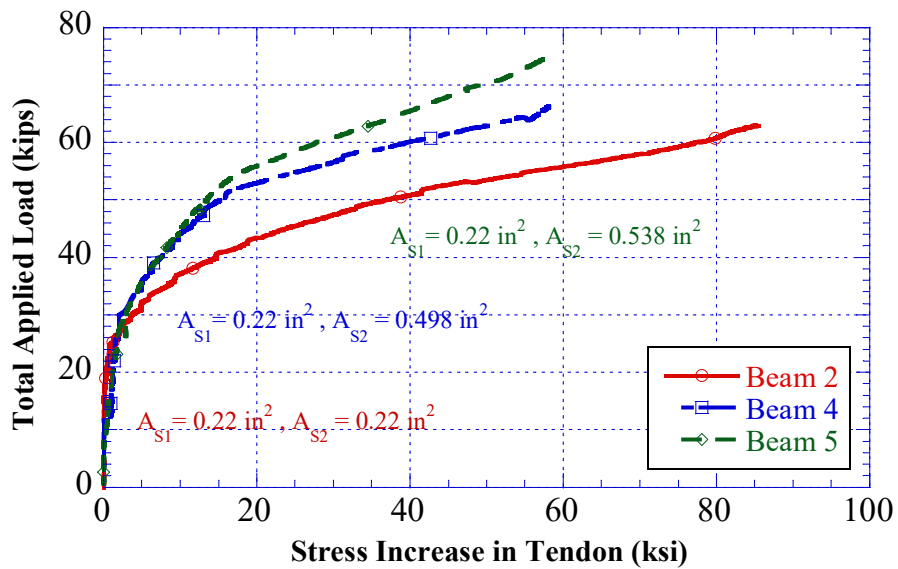


**Fig. 4.55 Relationship between Applied Load and Stress Increase in Unbonded Tendon for varying  $A_{s2}$**

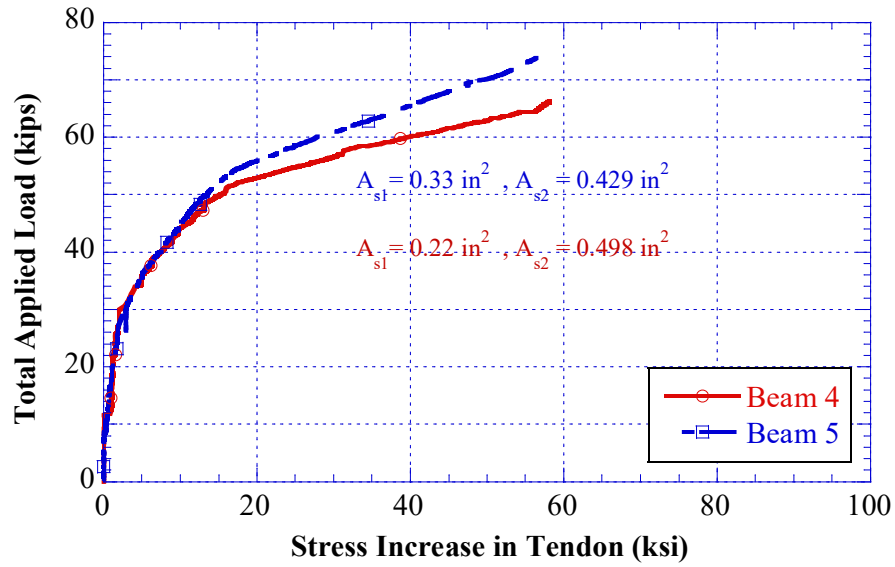


**Fig. 4.56 Relationship between Applied Load and Stress Increase in Unbonded Tendon for varying  $A_{sl}$**

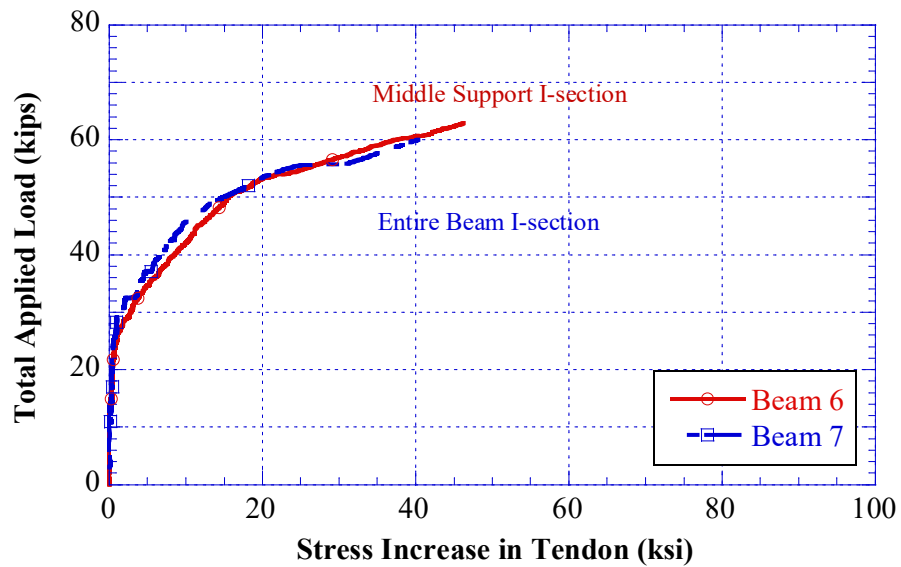


**Fig. 4.57 Relationship between Applied Load and Stress Increase in Unbonded Tendon for varying Cross-Section**

## CHAPTER V

### ANALYTICAL INVESTIGATION

#### 5.1 Introduction

The main objective of this study is to propose an analytical model approach to study the flexural behavior of two-span continuous concrete members prestressed with bonded and unbonded tendons. The flexural analysis of reinforced concrete beams is based on existing the bond interaction between the concrete and reinforcing steel. However, a different scenario is applied in concrete beams prestressed with bonded and unbonded tendon. The bonded tendon works similarly to the non-prestressed reinforcement where the grout surrounding the bonded tendon provides a full bond between tendon and sheathing duct pipe which transfer this bond to the adjacent concrete. In contrast, the unbonded tendon elongates independently with the surrounding concrete, which means strain the unbonded tendon is not same as in concrete. This means that there is no strain compatibility between these components which arise the analysis problem. Moreover, it can be noticed from the applied load and force in the unbonded tendons relationships in the previous chapter, that the force in the tendon significantly increases when cracks are propagating which indicate to a relevant between the stress in the unbonded tendon and the deformation of the entire beam.

Therefore, the main problem is to estimate the increase in the stress in the unbonded tendon  $\Delta f_{ps}$ , many researchers have investigated this aspect, but still, there is no rational, simple and accurate methodology adopted by ACI-318 revisions.

In this chapter, a new approach is presented to calculate the stress in the bonded and unbonded tendons for two-span continuous high strength concrete beams. The study is based on beam analysis rather than section analysis developed the method that proposed by Ozkul (2007) which was applied for simple span beams prestressed with the unbonded tendon.

This chapter presents a detailed procedure with equations for calculating the elongation, strain, and stress in the unbonded tendon for beams with various tendon profiles under single point load at midspan and third-point load as well.

## **5.2 Methodology Background**

Trussed-Beam model was used for calculating the stress in the unbonded for the simply supported beam. The model was adopted by Tanchan (2001); Nassif and Ozkul (2002); Nassif, Ozkul, and Harajli (2003); Nassif, Ozkul, Hwang, and Han (2004); Ozkul, Nassif, and Malhas (2005), Ozkul (2007); and Unal (2011).

## **5.3 Trussed-Beam Model for Continuous Beams**

The stress increase in the unbonded tendon  $\Delta f_{ps}$  is affected by the flexural deformation of the whole beam for the reasons mentioned above. Similar basic concepts of the trussed-beam model for simple span beam are explored herein to develop a model for two-span continuous concrete beams prestressed with bonded and unbonded tendon. Consider a two-span continuous beam with a rectangular cross-section prestressed with bonded and unbonded tendons. Third-point load at each span is considered in the analysis, two-harped point's tendon profile under the applied loads is adopted. The beam is divided into two main structural elements; the first element is the reinforced concrete beam element

which includes the non-prestressed steel and the bonded tendon, and the second element is the unbonded prestressing tendon. Both elements work independently, but they are connected at the ends only. To keep the eccentricity between the center of the concrete beam and the unbonded elements constant, deviators under the point loads and at the middle support location are placed. These deviators prevent the unbonded tendon vertical movement but allow the axial movement so tendon can elongate freely. When the load applies, and the section is cracked at the middle support location, the tensile stresses are transferred to the reinforcement until the section at  $L/3$  from the exterior support is cracked, then the tensile stresses are transferred to the unbonded tendon. As the load and deflection keep increase, beam ends and middle support start rotating until the failure occurs due concrete crushing in compression.

### **5.3.1 Main Assumptions**

Several basic assumptions are made to proceed with this method and simplify the procedure. These assumptions are based on a rational behavior of the potential deformation in the model. The assumptions can be summarized as follow:

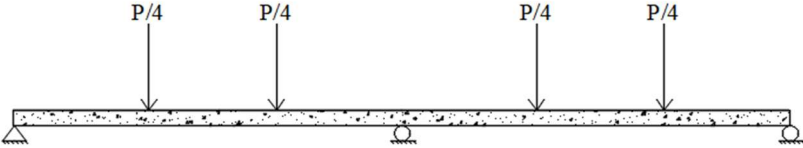
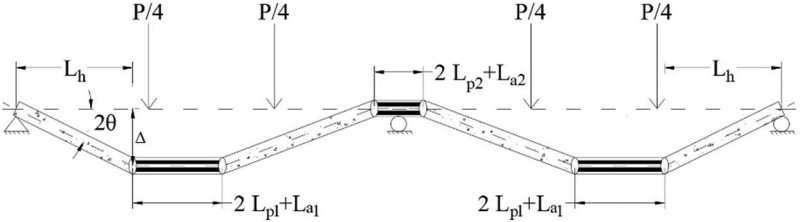
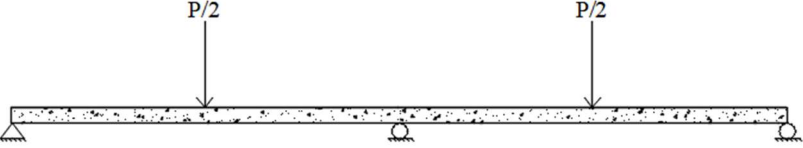
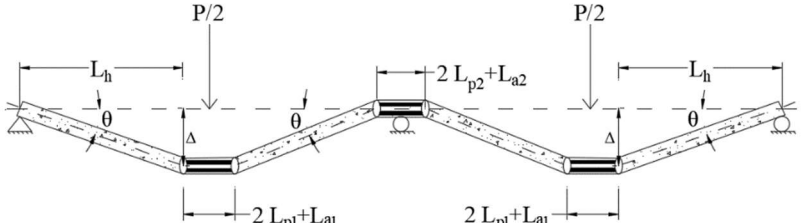
1. Friction losses between the unbonded tendon and the adjacent material are negligible.
2. Fully bond is assumed between the bonded (grouted) tendon and the concrete, etc. no slip occurs.
3. The material properties for concrete, steel, and/or FRP tendons are known.
4. The force in the unbonded tendon is constant for the entire tendon length. This assumption is made based on the observation of the stress change in the unbonded tendon in both spans in the test specimens. Where two strain gauges were installed in

the unbonded tendon one in each span and during the post-tensioning, it was noticed that the difference in the stress in the tendon between the two spans was about 300 microstrain when the prestressing force reaches to 12 kips. Furthermore, the prestressing force in the tendon at failure was about 15.8 kips. Therefore the difference between the stress in the unbonded tendon between the two spans is very small and can be ignored.

5. Plane sections remain plane before and after deformation. In another word, a linear relationship between strains in a section according to the neutral axis depth (Park and Paulay, 1975).
6. Shear deformations are negligible.
7. The beam is considered cracked when the applied stresses exceed the modulus of rupture of concrete,  $f_r$ .
8. Plastic hinges forms at maximum negative and positive moment locations, i.e., the first plastic hinge forms at the middle support location and the second plastic hinge forms at mid-span or under  $L/3$  from the exterior support for the single and third-point load respectively as shown in Table 5.1.
9. The plastic hinge deformations are the main cause for the unbonded tendon elongation as shown in Table 5.1.



**Table 5.1 Failure Mechanisms of Two-Span Continuous Beam due to Loading Type**

<b>Loading Type</b>	
<b>Mechanism at Failure</b>	
<b>Loading Type</b>	
<b>Mechanism at Failure</b>	

### 5.3.2 Mathematical Formulation for Two-Span Continuous Beam with Third-Point Loading

This methodology is modified analysis that adopted in the literature on the simple span for analyzing simply supported beams prestressed with unbonded tendons. The method that explained herein is explored to be applicable on analysis two-span continuous beams prestressed with bonded and unbonded steel or FRP strands. As mentioned before, the regular section analysis which includes force and moment equilibrium is not enough to find the stress in the unbonded tendon due to the bond lack between the tendon and the adjacent concrete, etc. there is no strains compatibility at the section. Therefore, additional relationships are required to provide equations to find the unknowns. Thus, this method is based on equilibrium equations, deflection compatibility and the conservation of energy principle. All unknowns' parameters and the provided relationships are listed in Table 5.2.

**Table 5.2 Summary of Unknowns and Provided Relationships**

No.	Unknowns Parameters	Provided Relationships
1	Neutral axis depth, $c$	Force equilibrium
2	Strain at one point, $\varepsilon$	Moment equilibrium
3	Deflection at L/3 from exterior support, $\Delta_L$	Moment-Area Integration
4	Stress in the unbonded tendon, $f_{ps}$	Energy Conservation

The behavior of the two-span continuous beams prestressed with bonded and unbonded tendons mainly consists of two stages; the first stage is the linear analysis which starts from the applying load until the first crack occurs. The second stage starts beyond the cracking up to failure occurs when all plastic hinges are formed. In order to solve these equations, a computational software is required. In this study MATLAB R2017b was used

to perform the analysis, the analysis steps and the flowchart is explained in section 5.4 of this chapter.

The MATLAB program starts with the input of the following information:

1. Section properties
  - flange width  $b_f$ .
  - web width  $b$ .
  - beam height  $h$ .
  - flange height  $h_f$ .
2. Areas of all reinforcement which includes
  - Non-prestressed steels at top and bottom of the beam,  $A_s$  and  $A_s'$ .
  - Bonded tendon,  $A_{psB}$ .
  - Unbonded tendons,  $A_{psU}$ .
3. Depths of all reinforcement which include depth of the tensile steel  $d_s$ , compressive steel  $d_s'$ , bonded tendon  $d_{psB}$ , and unbonded tendon  $d_{psU}$  at both positive and negative moment locations.
4. Mechanical material properties, i.e., all stress-strain relationship for prestressing and non-prestressing reinforcement, concrete compressive strength  $f_c'$ .

The program is based on an increment of the concrete compressive strain of the extreme fiber in the maximum positive moment location, which takes place at  $L/3$  from the exterior support and under the first point load. Then, the first iteration of the program can proceed to calculate the depth of the neutral axis  $c_{(i)}$  as shown in Eq. (5.1), which is required to calculate the strains in non-prestressed steel and bonded tendon. It can be noticed that the

stress in the unbonded tendon  $f_{psU}$  is required to calculate  $c_{(i)}$ , therefore for the first iteration, it is assumed that  $f_{psU} = f_{pe}$ .

$$c_{(i)} = \frac{A_{psU}f_{psU(i)} + A_{psB}f_{psB(i)} + A_s f_{s(i)} \pm A_s f'_{s(i)}}{\alpha_{(i)} \bar{f}_c b} \quad (5.1)$$

Where:

$f_{psU(i)}$  the stress in the unbonded tendon, it is assumed equals to the effective prestressing stress  $f_{pe}$  for the first iteration. Otherwise, it could be calculated from the stress-strain relationship of the prestressing tendon as shown in Fig. 5.4.

$f_{psB(i)}$  the stress in the bonded tendon at L/3 from the exterior support.

$f_{psB(i)}$  the stress in the bonded tendon.

$\alpha_{(i)}$  the concrete compressive force position identifier, the mean stress factor can be computed from the following formula (Park and Paulay, 1975).

$$\alpha_{(i)} = \frac{\varepsilon_{c(i)}}{\varepsilon'_c} - \frac{\varepsilon_{c(i)}^2}{3\varepsilon'^2_c} \quad (5.2)$$

And

$\varepsilon'_c$  the concrete strain corresponding to the ultimate compressive strength  $f'_c$  as shown in Fig. 5.1. Nawy (2010).

$\varepsilon_{c(i)}$  the concrete strain corresponding to the compressive strength  $f_c$ .

Where

$f_{c(i)}$  the stress in the extreme compression fiber at the corresponding concrete strain  $\varepsilon_{c(i)}$ ,

It can be calculated using Hognestad's stress-strain formula as follows:

$$f_{c(i)} = f'_c \left[ 2 \frac{\varepsilon_{c(i)}}{\varepsilon'_c} - \left( \frac{\varepsilon_{c(i)}}{\varepsilon'_c} \right)^2 \right] \quad (5.3)$$

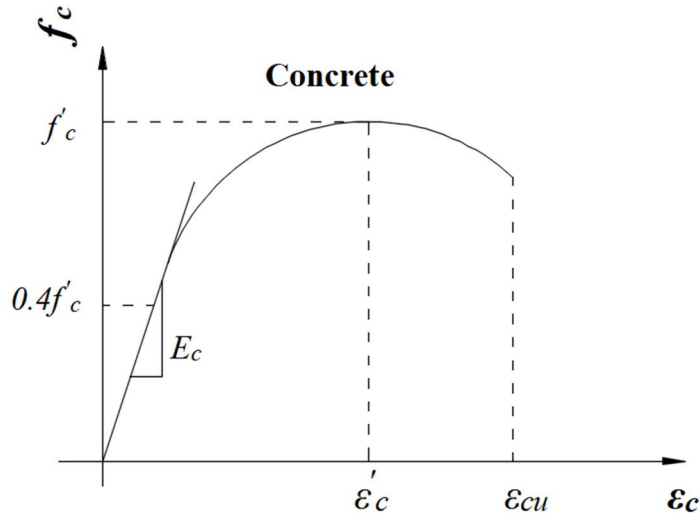


**Fig. 5.1 Concrete Stress-Strain Curve**

Strains, forces and reinforcement depths are illustrated in Fig. 5.2 which represents the typical section which used in the analysis. Since the beam specimens have T and I cross-section shapes, some of the parameters shown in the typical section are changed accordingly. For instance, the section width  $b$ , can be used as the flange width  $b_f$ , also the compressive force of concrete  $C$ , may split into two forces according to the comparison between the neutral axis depth,  $c_{(i)}$  and the flange height,  $h_f$ ; one from the flange contribution  $C_f$ , and the other from the web contribution  $C_w$ .

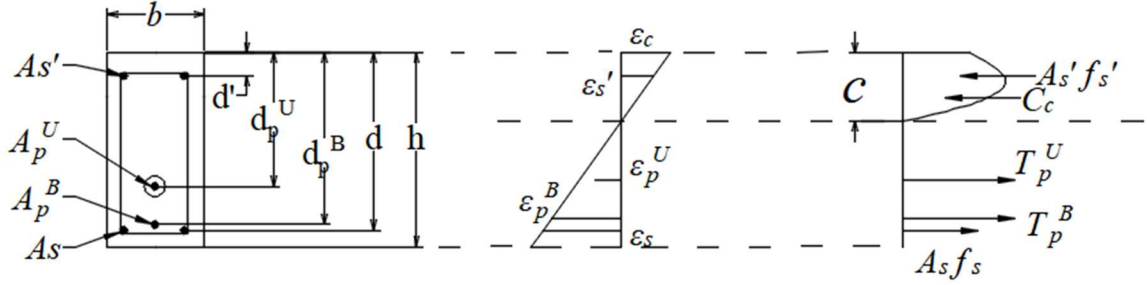


**Fig. 5.2 Typical Cross Section Used in the Analysis**

Once the neutral axis depth is known, the strains of all non-prestressed steel and bonded tendon can be calculated from the strain compatibility of the section as follows:

Non-prestressed steel in tension,

$$\varepsilon_{s(i)} = \varepsilon_{c(i)} \left[ \frac{d_s - c_{(i)}}{c_{(i)}} \right] \quad (5.4)$$

Non-prestressed steel in compression,

$$\varepsilon'_s = \varepsilon_{c(i)} \left[ \frac{d'_s - c_{(i)}}{c_{(i)}} \right] \quad (5.5)$$

Prestressed bonded tendon,

$$\varepsilon_{psB(i)} = \varepsilon_{peB} + \varepsilon_{c(i)} \left[ \frac{d_{psB} - c_{(i)}}{c_{(i)}} \right] \quad (5.6)$$

Once all strains are known, stresses are calculated accordingly using a stress-strain relationship. Elastic-fully plastic stress-strain relationship is used in the model to calculate the stress of the non-prestressed steel as shown in Fig. 5.3.

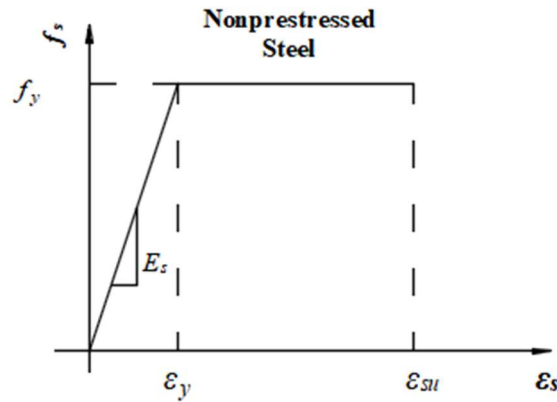


**Fig. 5.3 Typical Stress-Strain Relationship for Non-prestressed Steel**

To calculate the stress in the prestressed tendon, the stress-strain relationship is used as shown in Fig. 5.4, where Fig. 5.4a is used for prestressed steel tendon which consists of two stages; linear and nonlinear stages. However, Fig. 5.4b is used for Fiber Reinforced Polymer tendon which has an elastic range only up to stress at failure  $f_{fpu}$ .

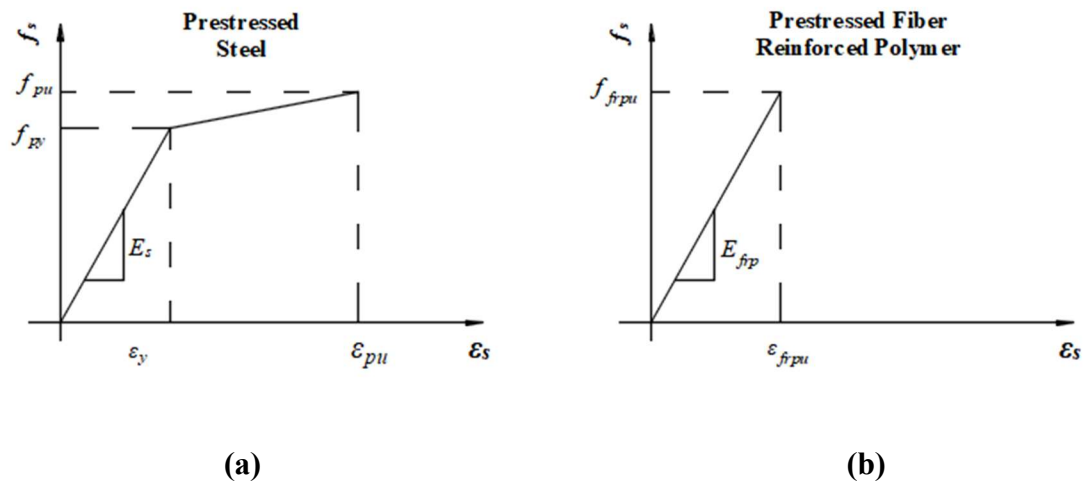


**Fig. 5.4 Stress-Strain Relationships for; (a) Prestressed Steel Tendon,  
(b) Prestressed FRP Tendon**

To calculate the concrete modulus of elasticity  $E_c$ , ACI 318-14 Eq. (19.2.2.1.b) is used for normal weight concrete as follows:

$$E_c = 57,000\sqrt{f'_c} \text{ (in psi)} \quad (5.7)$$

However, ACI 363R-10 committee recommended using an empirical equation based on Myers and Carrasquillo (1998) for high-strength concrete as follows:

$$E_c = 39,900\sqrt{f'_c} + 1,730,000 \text{ (in psi)} \quad (5.8)$$

Then, the stress in the unbonded tendon can be calculated by applying the force equilibrium equation at L/3 from the exterior support where the maximum moment takes place.

$$f_{psU(i)}^F = \frac{\alpha_{(i)}\hat{f}_c b c_{(i)} - A_s f_{s(i)} + \hat{A}_s \hat{f}_{s(i)} - A_{psB} f_{psB(i)}}{A_{psU}} \quad (5.9)$$

Since all tension and compression forces are known, the moment capacity of the section could be expressed as shown in Eq. (5.10) below:

$$\begin{aligned} M_{n(i)} = & A_s f_{s(i)} (d_s - \gamma_{(i)} c_{(i)}) - \hat{A}_s \hat{f}_{s(i)} (\gamma_{(i)} c_{(i)} - \hat{d}) \\ & + A_{psB} f_{psB(i)} (d_{psB} - \gamma_{(i)} c_{(i)}) \\ & + A_{psU} f_{psU(i)}^F (d_{psU} - \gamma_{(i)} c_{(i)}) \end{aligned} \quad (5.10)$$

This nominal moment capacity from Eq. (5.10) is compared with the modulus of rupture  $M_r$ , if  $M_{n(i)} < M_r$  that means the section is uncracked and within the elastic stage, vice versa when  $M_{n(i)} \geq M_r$  lead to cracked section and nonlinear analysis is required until failure.

At this point, the strain in the unbonded tendon stills unknown and beam analysis is required. Therefore, the concept of energy conservation is adopted to relevant the applied



work with the internal energy stored mainly in the unbonded tendon. The full derivation is illustrated below.

### 5.3.2.1 Derivation of Calculating the Strain in Unbonded Tendon Using Energy Conservation with Third-Point Loading

Since the stress-strain relationship of prestressing steel reinforcement is assumed elastic-perfectly plastic, the continuous beam collapses after formation of plastic hinges in both spans at the maximum positive moment location ( $L/3$  from the exterior support) and maximum negative moment location at interior support as shown in Fig. 5.5.

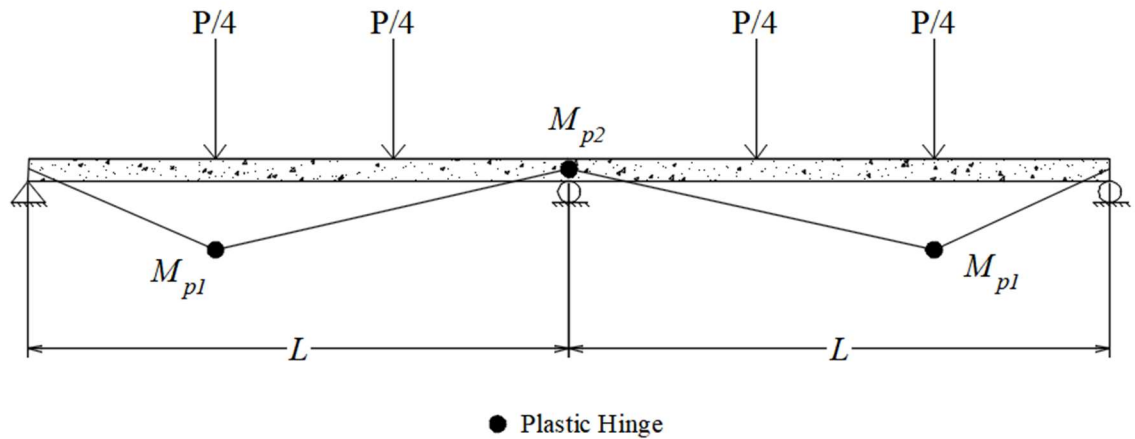


**Fig. 5.5 Failure Mechanism of Two-Span Continuous Beam with Third-Point Loading**

When the load applied increases until the applied moment at the locations of the maximum positive and negative moment exceeds the modulus of rupture  $M_r$ , then the section becomes cracked at that location. The amount of non-prestressed reinforcement in

the tension zone mostly affects the cracking load at both locations. Usually, the first visible crack takes place at the location of the interior support according to the experimental program observations. Simultaneously, the applied moment at the maximum positive moment location increases until it exceeds the modulus of rupture  $M_r$ , then the section at this location is cracked. The cracks at both locations are developing and propagating and stresses in the concrete transferring to the non-prestressed steel, bonded and unbonded tendons. The failure occurs when the moment capacity of the section at the ultimate positive and negative locations reaches the plastic moment capacity  $M_p$ . This moment  $M_p$  achieved when the strain in the extreme tension fiber reaches 0.003, the stress of the non-prestressed steel in tension and the bonded tendon is yield as  $f_y$  and  $f_{py}$  respectively. In addition, the stress in the unbonded tendon sometimes yields according to the Partial Prestressing Ratio  $PPR$ .

To apply the concept of conservation energy on two-span continuous beams with bonded and unbonded tendon, the calculation of both the external work was done by applied load and the internal energy in the beam components are calculated. Consider one span with third-point load type as follows:

#### 1) External Work:

The definition of external work is the multiplication of the applied force times the deformation due to that force. Therefore, the only external work can be calculated in the beam is the applied point loads multiplying the deflection under that point load, by assuming the maximum deflection  $\Delta$  at failure takes place at location  $L/3$  from the exterior support as shown in Fig. 5.6b.

Thus, the work done by external loads can be expressed as follows:

$$\frac{P}{4}\Delta_L + \frac{P}{4}\frac{\Delta_L}{2} = \frac{3}{8}P\Delta_L \quad (5.11)$$

## 2) Internal Work:

According to the concept of conservation energy, this means that the external work done calculated in Eq. (5.11) must be resisted by the beam to satisfy both sides of the equation. Thus, the components which resist the external load can be summarized as follow:

- Internal work was done by plastic moment  $M_p$ ,

For a two-span continuous beam with third-point load, three plastic hinges must be formed to achieve failure mechanism. Different scenarios of failure mechanisms were tried, but the rational scenario is the failure mechanism that requires less energy to perform plastic hinges. This mechanism is when three plastic hinges formed one at the middle support location where the maximum negative moment takes place and one in each span at  $L/3$  from the exterior support at the location of the maximum positive moment as shown in

The following equation represents calculating the internal work done by plastic moments multiplying by the rotations:

$$M_{pl1}3\theta + M_{pl2}\theta \quad (5.12)$$

Where

$M_{pl1}$  the maximum positive moment at location  $L/3$  from the exterior support,

$M_{pl2}$  the maximum negative moment at middle support location,

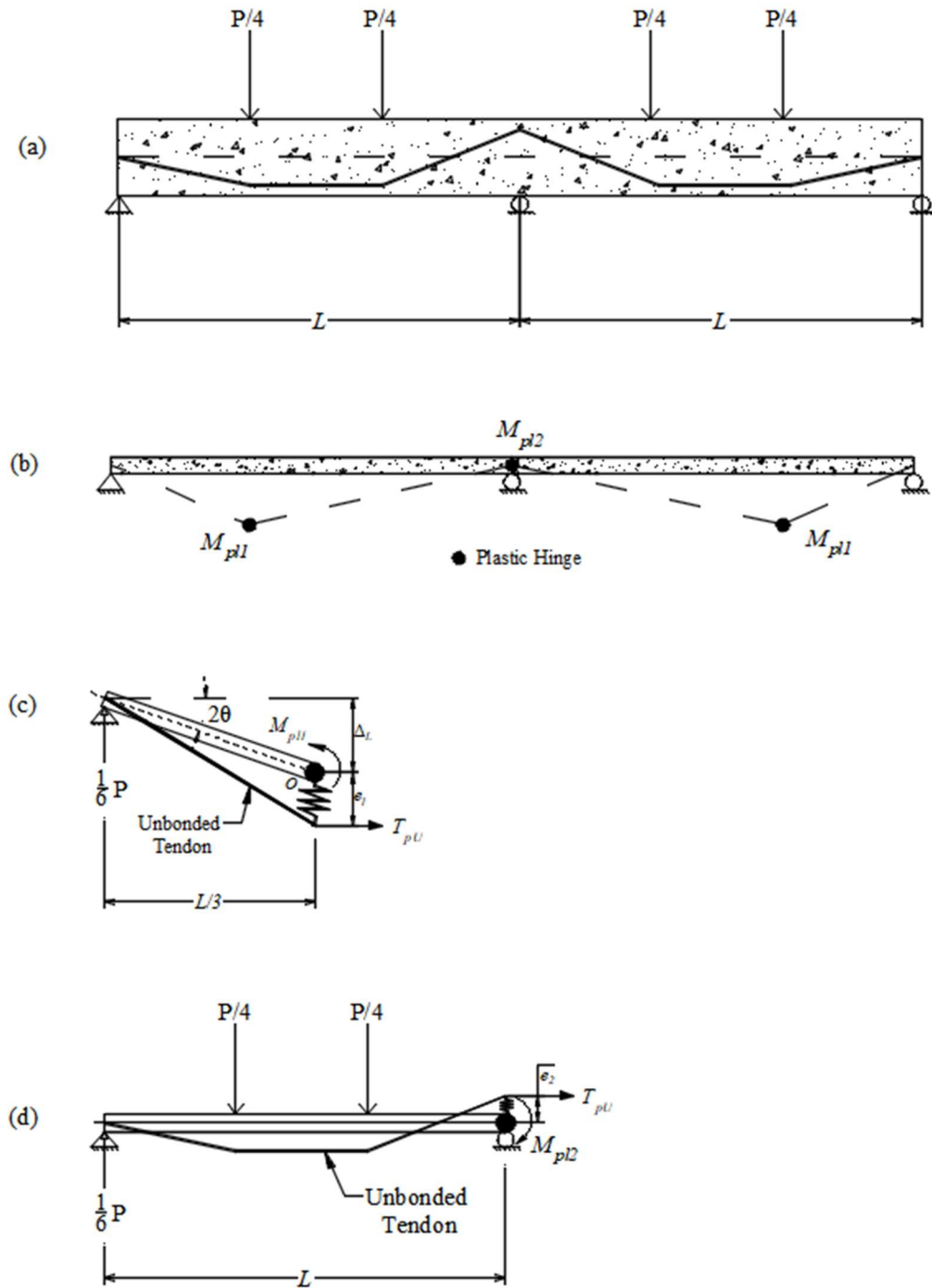


**Fig. 5.6 Beam Tendon Profile and Collapse Mechanism under Third-Point Loading:**

**(a) Beam Unbonded Tendon Profile; (b) Collapse Mechanism, (c) Plastic Hinge at Positive Moment at Ultimate; and (d) Plastic Hinge at Negative Moment at Ultimate.**

This plastic moment at the maximum positive location  $M_{pl1}$  can be calculated by taking a section at  $L/3$  from the exterior support and take the first moment about point  $o$  (neutral axis location) as shown in Fig. 5.6c. There are two components which generate the moment, the reaction at the exterior support and the force in the unbonded tendon as follows:

$$M_{pl1} = \frac{1}{6}PL_L - T_{pU}e_1 \quad (5.13)$$

The same procedure can be applied to find the plastic moment at the middle support location  $M_{pl2}$ , but the section is in middle support as explained in Fig. 5.6d. Both forces are involved; the reaction at the exterior support and the single point load applied at midspan in addition to the force in the unbonded tendon. The plastic moment  $M_{pl2}$  yields:

$$M_{pl2} = \frac{1}{4}PL_L - T_{pU}e_2 \quad (5.14)$$

- The internal work done by elongating of the unbonded tendon

When the load increases, the beam deflects due to the applied load. This deflection causes the unbonded tendon to elongate simultaneously. The force in the unbonded tendon  $T_{pU}$  generates a work due to this elongation. The work can be calculated as follows:

$$\frac{T_{pU}\delta_U}{2} \quad (5.15)$$

Where

$\delta_U$  the elongation of the unbonded tendon,

By equating the external work with the internal strain energy, the equation becomes

$$\frac{3}{8}P\Delta_L = M_{pl1}3\theta + M_{pl2}\theta + \frac{T_{pU}\delta_U}{2} \quad (5.16)$$

Where

$T_{pU}$  the prestressing force in the unbonded tendon which equals to the multiplication of the area of prestressing tendon times the stress in the tendon  $A_{psU}f_{psU}$ ,

$e_1$  the eccentricity of the unbonded tendon at the location of the maximum positive moment,

$e_2$  the eccentricity of the unbonded tendon at the location of the maximum negative moment,

where

$$\theta = \frac{\Delta_L}{2L_L} \quad (5.17)$$

By substituting Eq. (5.13) and (5.14) into Eq. (5.16), the elongation in the prestressing tendon can be obtained:

$$\delta_U = \frac{\Delta_L}{L_L} [3e_1 + e_2] \quad (5.18)$$

Then, the strain in the unbonded tendon can be calculated:

$$\varepsilon_{psU} = \varepsilon_{peU} + \frac{\delta_U}{2L} \quad (5.19)$$

where

$\varepsilon_{peU}$  the strain in the unbonded prestressed tendon at  $f_{peU}$ .

Finally, the stress-strain relationship is used to obtain the stress in the unbonded prestressing tendon corresponding to the strain  $\varepsilon_{psU}$ . Once the strain in the tendon is known, then the stress in the bonded and unbonded prestressing tendon can be calculated using the following expressions:

- $\varepsilon_{ps} < \varepsilon_{py}$

$$f_{ps} = \varepsilon_{ps} E_{ps} \quad (5.20)$$

- otherwise

$$f_{ps} = f_{py} + (\varepsilon_{ps} - \varepsilon_{py}) \frac{(f_{pu} - f_{py})}{\left(\varepsilon_{pu} - \frac{f_{py}}{E_{ps}}\right)} \quad (5.21)$$

The typical stress-strain relationship for prestressing tendon used in the proposed model is shown in Fig. 5.7.

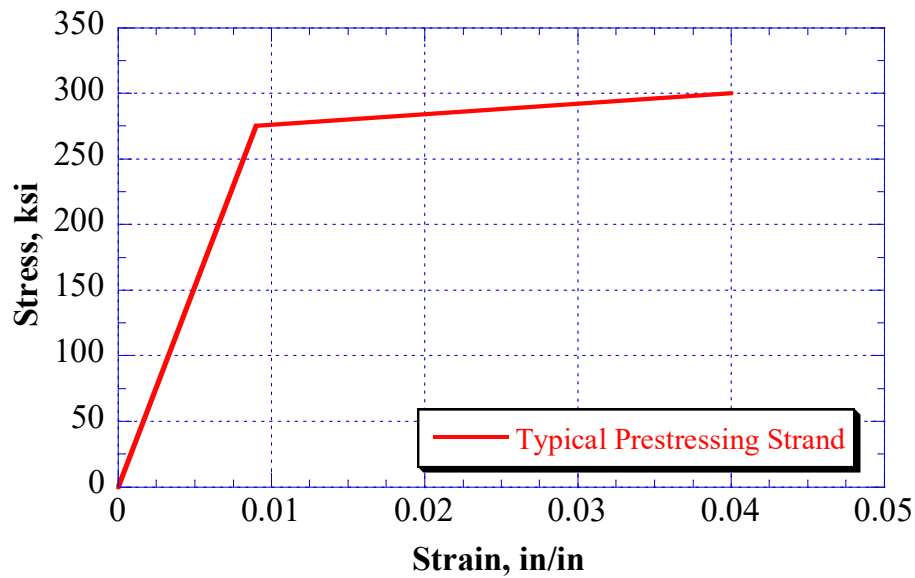


**Fig. 5.7 Typical Stress-Strain Relationship for Prestressing Tendon**

### **5.3.2.2 Deflection Calculation from Curvature Diagram using Moment-Area Integration with Third-Point Loading**

Since the increase in the tendon stress is a member-dependent, calculating the deflection of the member is based on integrating the curvature for the entire beam. Also, the strain at the extreme fiber of concrete in compression varies along the beam. Therefore the curvature distribution can be best describing the average values.

The curvature distribution is assumed taking as similar of the bending moment diagram in the elastic analysis, thus two peak points on the curvature diagram are assumed, the first one takes place around the first load that is close to the exterior support (the maximum positive moment), and the second is at the interior support (negative moment).

Four modes are investigated to calculate the deflection of the beam; these modes include; cracking of concrete, yielding of non-prestressing steel, yielding of prestressing tendon and concrete crushing.

#### **Mode 1: Cracking of concrete in tension**

A prestressed concrete beam with hybrid tendons behaves elastically prior to cracking. At this stage, the deformation of the member stills within the elastic range until the stress of the extreme concrete fiber in compression reaches the modulus of rupture  $f_r$ . once the section is cracked; the non-prestressed steel reinforcement starts to resist most of the additional applied load. Only one span is considered to calculate the curvature for the continuous beam,. As mentioned before, two plastic hinges are assumed to form to satisfy the failure mechanism (one under the first exterior load and the second at the interior support). Therefore, the curvature at those locations is assumed equal. However, it is



assumed that the curvature at the second applied load is half of the maximum curvature in the beam according to the bending moment diagram in the elastic range as shown in Fig.

5.8.

$$\sum M_{@a} = 0$$

$$Ay_{cr(i)} = \frac{1}{L} \left[ \frac{665}{1728} \Phi_{cr(i)} L^2 \right] \quad (5.22)$$

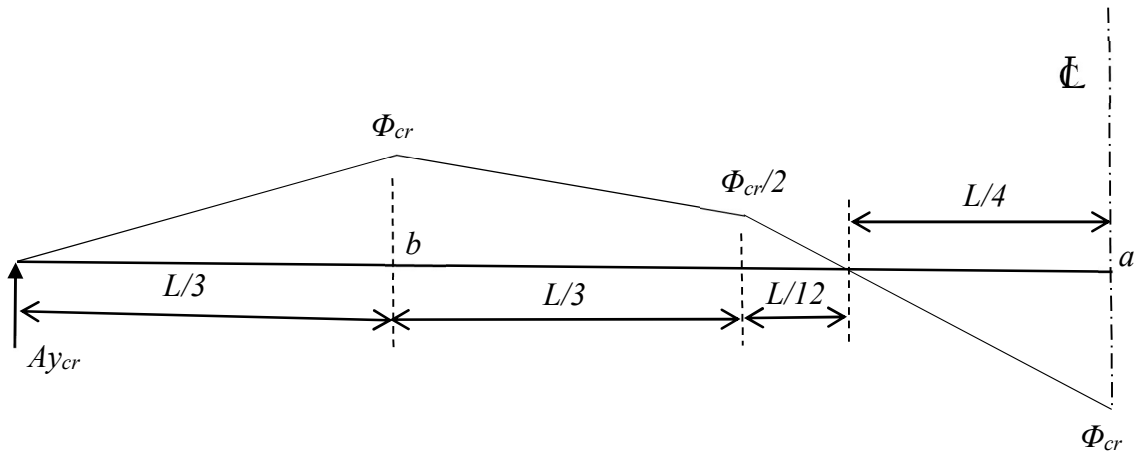


**Fig. 5.8 Curvature Distribution of Continuous Beam at Cracking Concrete in Tension**

Then the deflection under the first applied load can be calculated from the following expression:

$$\sum M_{@b} = 0$$

$$\Delta_{cr(i)} = Ay_{cr(i)} \frac{L}{3} - \left[ \frac{1}{54} \Phi_{cr(i)} L^2 \right] \quad (5.22)$$

## Mode 2: Yielding of Non Pre-stressed steel

With load increase beyond cracking, the non-prestressing steel  $A_s$  starts yielding and beam rotates at hinges, but the section at the hinges not fully plastic yet because of the presence of prestressing tendon. As mentioned in the previous section, the plastic hinges regions are having the maximum curvature at this state as shown in Fig. 5.9.

The exterior reaction of the curvature diagram is calculated by taking the first moment for all the area under the curvature for one span about the interior support location as follows:

$$Ay_{y(i)} = \frac{1}{L} \left[ \begin{aligned} &\frac{1}{2} \Phi_{cr(i)} L_g \left( L - \frac{2}{3} L_{g(i)} \right) + \Phi_{cr(i)} (Z - L_{g(i)}) \\ &\quad \left( L - L_{g(i)} - \frac{1}{2} (Z - L_{g(i)}) \right) \\ &+ \frac{1}{2} (\Phi_{y(i)} - \Phi_{cr(i)}) (Z - L_{g(i)}) \\ &\quad \left( L - L_{g(i)} - \frac{2}{3} (Z - L_{g(i)}) \right) + \frac{53}{432} \Phi_{y(i)} L^2 \end{aligned} \right] \quad (5.23)$$

Then, the deflection at the exterior applied load is computed by taking the first moment of the curvature area of one span about the interior support point, this yield:

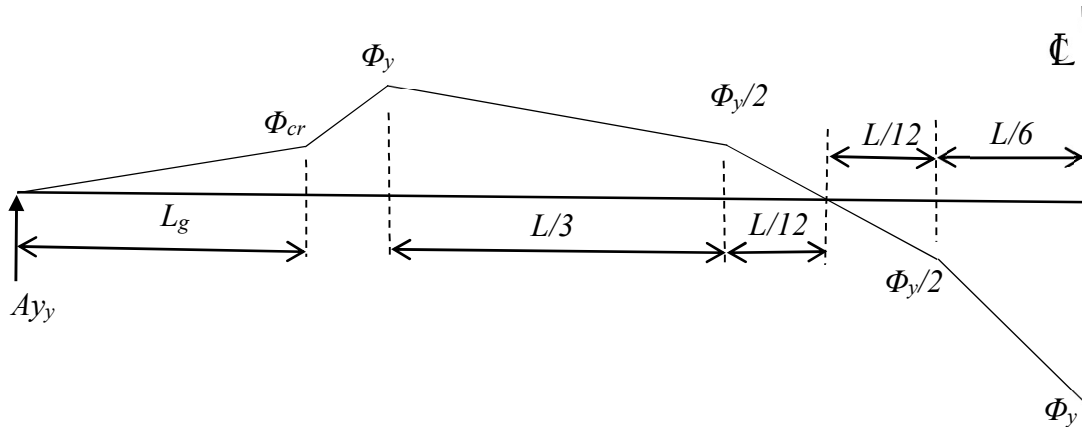


**Fig. 5.9 Curvature Distribution of Continuous Beam at Yielding of Non-Prestressed Steel**

$$\Delta_{y(i)} = Ay_{y(i)} \frac{L}{3} - \left[ \begin{aligned} & \frac{1}{2} \Phi_{cr(i)} L_g(i) \left( Z - \frac{2L_g(i)}{3} \right) + \frac{1}{2} \Phi_{cr(i)} (L_{y(i)} - L_g(i))^2 \\ & + \frac{1}{2} (\Phi_{y(i)} - \Phi_{cr(i)}) (L_{y(i)} - L_g(i)) \\ & \left( \frac{1}{3} (L_{y(i)} - L_g(i)) \right) \end{aligned} \right] \quad (5.24)$$

### Mode 3: Yielding of prestressed tendon

At this limit state, the prestressing steel  $A_{ps}$  starts yields, and the beams fail simultaneously at the plastic hinges. The curvature increases rapidly in this state because of the yielding of the tendon. The potential curvature diagram is explained in Fig. 5.10, which shows all the components of the curvature distribution diagram. Obviously, it can be noticed that the inflection point is kept at the same position for all limit states.

$$Ay_{py(i)} = \frac{1}{L} \left[ \begin{aligned} & \frac{1}{2} \Phi_{cr(i)} L_g \left( L - \frac{2}{3} L_g(i) \right) + \Phi_{cr(i)} (L_{y(i)} - L_g(i)) \\ & \left( L - L_g(i) - \frac{1}{2} (L_{y(i)} - L_g(i)) \right) \\ & + \frac{1}{2} (\Phi_{y(i)} - \Phi_{cr(i)}) (L_{y(i)} - L_g(i)) \\ & \left( L - L_g(i) - \frac{2}{3} (L_{y(i)} - L_g(i)) \right) + \Phi_{y(i)} (L_{py(i)} - L_{y(i)}) \\ & \left( L - L_{y(i)} - \frac{1}{2} (L_{py(i)} - L_{y(i)}) \right) + \frac{1}{2} (\Phi_{py(i)} - \Phi_{y(i)}) \\ & (L_{py(i)} - L_{y(i)}) \\ & \left( L - L_{y(i)} - \frac{2}{3} (L_{py(i)} - L_{y(i)}) \right) + \frac{53}{432} \Phi_{py(i)} L^2 \end{aligned} \right] \quad (5.25)$$

The actual deflection at the maximum positive moment can be calculated as follows:

$$\Delta_{py(i)} = Ay_{py(i)} \frac{L}{3} - \left[ \begin{aligned} & \frac{1}{2} \Phi_{cr(i)} L_{g(i)} \left( Z - \frac{2}{3} L_{g(i)} \right) \\ & + \frac{1}{2} \Phi_{cr(i)} (L_{y(i)} - L_{g(i)})^2 \\ & + \frac{1}{2} (\Phi_{y(i)} - \Phi_{cr(i)}) (L_{y(i)} - L_{g(i)}) \\ & \left( \frac{1}{3} (L_{y(i)} - L_{g(i)}) \right) \\ & + \frac{1}{2} \Phi_{y(i)} (L_{py(i)} - L_{y(i)})^2 + \frac{1}{2} (\Phi_{py(i)} - \Phi_{y(i)}) \\ & (L_{py(i)} - L_{y(i)}) \left( \frac{1}{3} (L_{py(i)} - L_{y(i)}) \right) \end{aligned} \right] \quad (5.26)$$

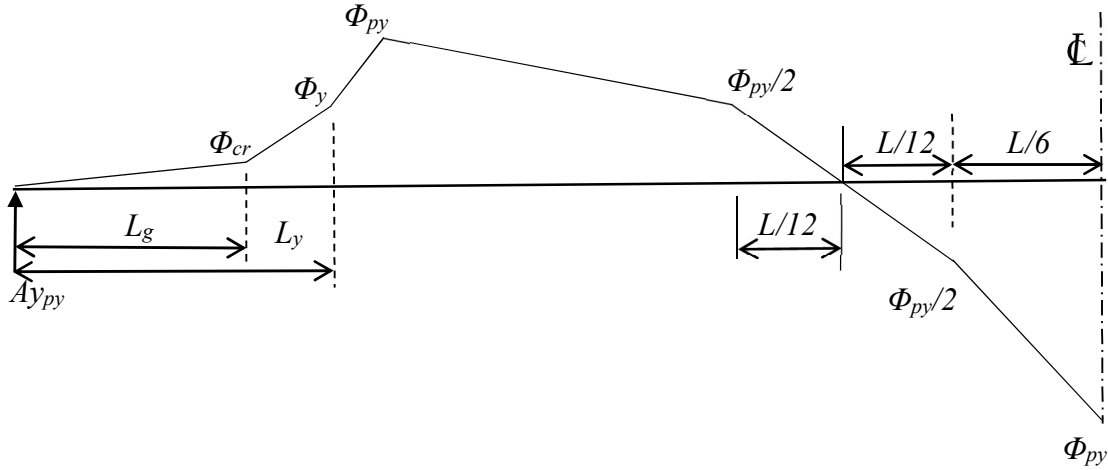


**Fig. 5.10 Curvature Distribution of Continuous Beam at Yielding of Prestressing Tendon**

Another way to simplify the above curvature calculation, by assuming the curvature diagram takes shape as shown in Fig. 5.11. It can be noticed that change in the area of the curvature due to the contribution of curvature of yielding non-prestressing steel is small and can be negligible.

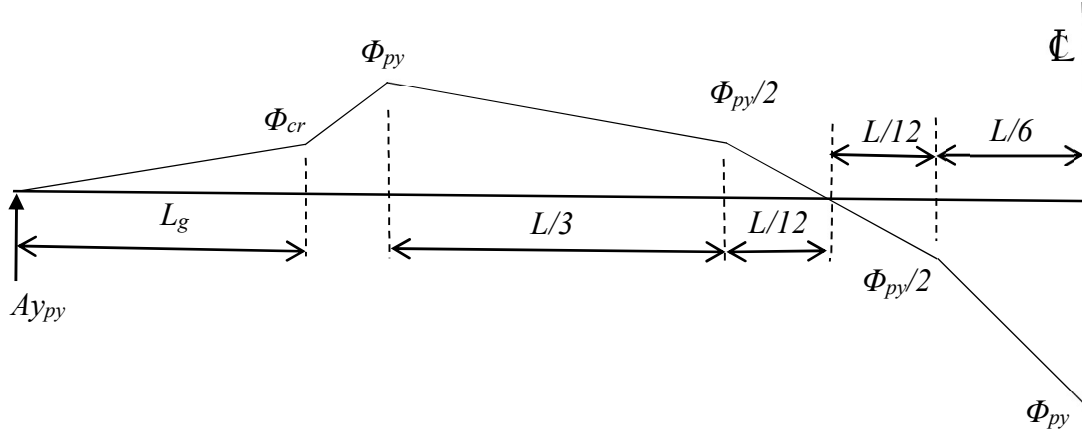


**Fig. 5.11 Simplified Curvature Distribution of Continuous Beam at Yielding of prestressing Steel**

Then, Eq. (5.25) and (5.26) can be rewritten based on the curvature distribution in Fig. 5.11 as follows:

$$Ay_{py(i)} = \frac{1}{L} \left[ \begin{array}{l} \frac{1}{2} \Phi_{cr(i)} L_g \left( L - \frac{2}{3} L_{g(i)} \right) + \Phi_{cr(i)} (Z - L_{g(i)}) \\ \left( L - L_{g(i)} - \frac{1}{2} (Z - L_{g(i)}) \right) + \frac{1}{2} (\Phi_{py(i)} - \Phi_{cr(i)}) \\ (Z - L_{g(i)}) \\ \left( L - L_{g(i)} - \frac{2}{3} (Z - L_{g(i)}) \right) + \frac{53}{432} \Phi_{py(i)} L^2 \end{array} \right] \quad (5.27)$$

And

$$\Delta_{py(i)} = Ay_{py(i)} \frac{L}{3} - \left[ \begin{array}{l} \frac{1}{2} \Phi_{cr(i)} L_{g(i)} \left( Z - \frac{L_{g(i)}}{3} \right) + \frac{1}{2} \Phi_{cr(i)} (Z - L_{g(i)})^2 \\ + \frac{1}{2} (\Phi_{py(i)} - \Phi_{cr(i)}) (Z - L_{g(i)}) \left( \frac{1}{3} (Z - L_{g(i)}) \right) \end{array} \right] \quad (5.28)$$

#### Mode 4: Crushing of concrete in compression

At the ultimate limit state, the plastic hinges are fully formed, where the strain in concrete at the extreme compressive fiber reaches the ultimate value and starts crushing. The beam completely fails at this limit state. Fig. 5.12 illustrates the actual curvature distribution along one span of the continuous beam at the ultimate limit state. It shows that the regions reach the ultimate curvature  $\Phi_u$  are at the plastic hinges only to satisfy the failure mechanism.

$$Ay_{u(i)} = \frac{1}{L} \left[ \begin{array}{l} \frac{1}{2} \Phi_{cr(i)} L_g \left( L - \frac{2}{3} L_{g(i)} \right) + \Phi_{cr(i)} (L_{y(i)} - L_{g(i)}) \\ \left( L - L_{g(i)} - \frac{1}{2} (L_{y(i)} - L_{g(i)}) \right) + \frac{1}{2} (\Phi_{y(i)} - \Phi_{cr(i)}) \\ (L_{y(i)} - L_{g(i)}) \\ \left( L - L_{g(i)} - \frac{2}{3} (L_{y(i)} - L_{g(i)}) \right) + \Phi_{y(i)} (L_{py(i)} - L_{y(i)}) \\ \left( L - L_{y(i)} - \frac{1}{2} (L_{py(i)} - L_{y(i)}) \right) + \frac{1}{2} (\Phi_{py(i)} - \Phi_{y(i)}) \\ (L_{py(i)} - L_{y(i)}) \\ \left( L - L_{y(i)} - \frac{2}{3} (L_{py(i)} - L_{y(i)}) \right) + \frac{2}{3} \Phi_{u(i)} L_a L + \frac{1}{2} \Phi_{u(i)} \\ \left( \frac{L}{3} - \frac{L_a}{2} \right) \\ \left( \frac{L}{2} - \frac{L_a}{4} \right) + \frac{11}{1728} \Phi_{u(i)} L^2 - \frac{1}{4} \Phi_{u(i)} \left( \frac{L}{4} - \frac{L_a}{2} \right) \\ \left( \frac{L}{12} - \frac{L_a}{3} \right) - \frac{1}{8} \Phi_{u(i)} L_a^2 \end{array} \right] \quad (5.30)$$

Where

$$L_{g(i)} = \frac{6M_{cr(i)}}{P_{(i)}} \quad (5.29)$$

$$L_{y(i)} = \frac{6M_{y(i)}}{P_{(i)}} \quad (5.30)$$

$$L_{py(i)} = \frac{6M_{py(i)}}{P_{(i)}} \quad (5.31)$$

Then, the deflection of the beam at the ultimate limit state can be calculated by integrating the curvature diagram as follows:

$$\Delta_{u(i)} = Ay_{u(i)} \frac{L}{3} - \left[ \begin{aligned} & \frac{1}{2} \Phi_{cr(i)} L_{g(i)} \left( Z - \frac{2}{3} L_{g(i)} \right) + \frac{1}{2} \Phi_{cr(i)} (L_{y(i)} - L_{g(i)})^2 \\ & + \frac{1}{2} (\Phi_{y(i)} - \Phi_{cr(i)}) (L_{y(i)} - L_{g(i)}) \\ & \left( \frac{1}{3} (L_{y(i)} - L_{g(i)}) \right) \\ & + \frac{1}{2} \Phi_{y(i)} (L_{py(i)} - L_{y(i)})^2 + \frac{1}{2} (\Phi_{py(i)} - \Phi_{y(i)}) \\ & (L_{py(i)} - L_{y(i)}) \left( \frac{L}{3} - L_{y(i)} - \frac{2}{3} (L_{py(i)} - L_{y(i)}) \right) \\ & + \frac{1}{8} \Phi_{u(i)} L_a^2 \end{aligned} \right] \quad (5.32)$$

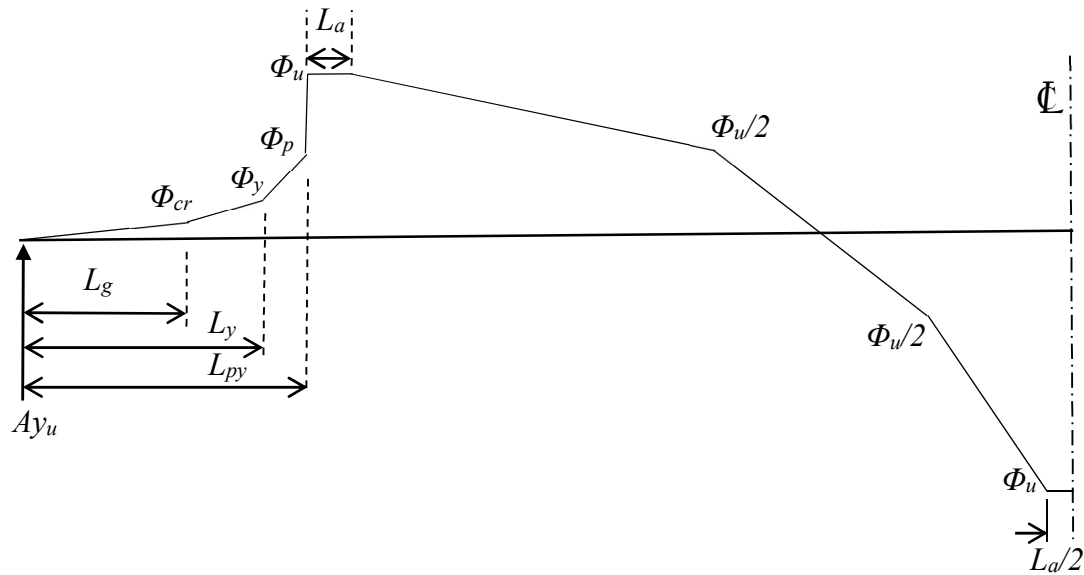


**Fig. 5.12 Curvature Distribution of Continuous Beam at crushing of Concrete in Compression**

Fig. 3.37 represents the exact curvature distribution at ultimate limit state. It can be seen that calculation the areas under the curve is sophisticated, therefore, the curvature diagram can be simplified as shown in Fig. 5.13 below:

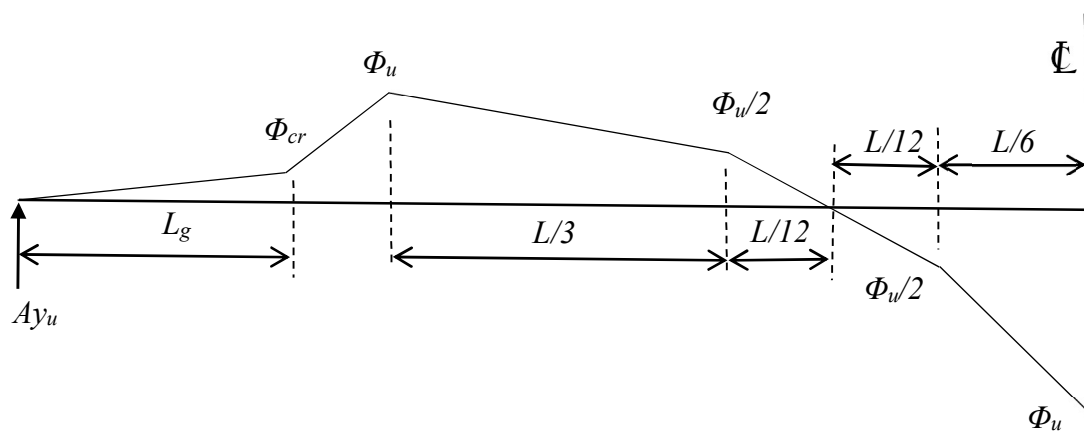


**Fig. 5.13 Simplified Curvature Distribution of Continuous Beam at crushing of Concrete in Compression**



Accordingly, the deflection calculation for the simple approach at ultimate limit state yield:

$$Ay_{u(i)} = \frac{1}{L} \left[ \begin{array}{l} \frac{1}{2} \Phi_{cr(i)} L_g \left( L - \frac{2}{3} L_{g(i)} \right) + \Phi_{cr(i)} (Z - L_{g(i)}) \\ \left( L - L_{g(i)} - \frac{1}{2} (Z - L_{g(i)}) \right) + \frac{1}{2} (\Phi_{u(i)} - \Phi_{cr(i)}) \\ (Z - L_{g(i)}) \\ \left( L - L_{g(i)} - \frac{2}{3} (Z - L_{g(i)}) \right) + \frac{53}{432} \Phi_{u(i)} L^2 \end{array} \right] \quad (5.33)$$

And

$$\Delta_{u(i)} = Ay_{u(i)} \frac{L}{3} - \left[ \begin{array}{l} \frac{1}{2} \Phi_{cr(i)} L_{g(i)} \left( Z - \frac{L_{g(i)}}{3} \right) + \frac{1}{2} \Phi_{cr(i)} (Z - L_{g(i)})^2 \\ + \frac{1}{2} (\Phi_{u(i)} - \Phi_{cr(i)}) (Z - L_{g(i)}) \left( \frac{1}{3} (Z - L_{g(i)}) \right) \end{array} \right] \quad (5.34)$$

### 5.3.3 Mathematical Formulation for Two-Span Continuous Beam with Single-Point Loading at Midspan

To extend the proposed method illustrated in the previous sections to a different type of loading, two-span continuous beam prestressed with both bonded and unbonded tendon under a single-point load applied at midspan is presented herein. To apply basic concepts which used with beam under third-point loading, two-span continuous beam with rectangular cross-sectional area and one-point harped tendon profile for bonded and

unbonded tendons is considered, moreover, the applied loads are a single point load at midspan is used as shown in Fig. 5.14.

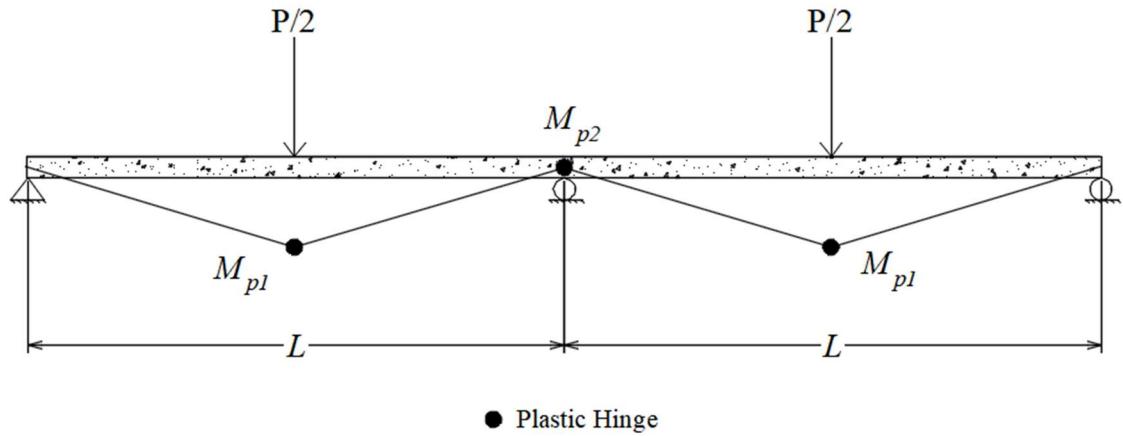


**Fig. 5.14 Failure Mechanism of Two-Span Continuous Beam with Single-Point Load at Midspan**

All basic concept assumptions are still valid in this model. Also, Eqs. (5.1) to (5.10) for calculating concrete stress  $f_c$ , neutral axis depth  $c$ , stress in the unbonded tendon  $f_{psU}$  and the moment capacity of the section  $M_n$  are used herein.

There are two differences must be derived and calculated in this section; the first one is applying the conservation energy and the second thing is the calculation the deflection at midspan from the curvature diagram using the moment-area integration.

### 5.3.3.1 Derivation of Calculating the Strain in Unbonded Tendon Using Energy Conservation with Single-Point Loading

In order to apply the concept of energy conservation, the failure mechanism of the beam under a single-point load at mid-span must be known. Rationally, a plastic hinge forms at the locations of maximum positive and negative moments, this concept is confirmed in beam 8 from the experimental program. Therefore, three plastic hinges must be formed to satisfy the failure mechanism, one at the middle support location and one at the midspan for each span as shown in Fig. 5.14.

As explained in the previous sections, external and internal works must be calculated in order to find a relationship between the deflection in the beam and the elongation in the unbonded tendon. Consider one span has  $L$  in length with single-point load applied at midspan  $P/2$  and the maximum deflection  $\Delta_L$  takes place at midspan. Therefore, the external work done by the applied load can be calculated as follows:

$$\text{External Work} = \frac{P}{2} \Delta_L \quad (5.35)$$

Where

$\Delta_L$       maximum deflection at midspan

Then, the internal energy required to resist the external work done by applied load must be calculated herein. There are three components participated in performing the internal work; these are the work done by plastic hinges, the secondary moment due to prestressing and the elongation of the unbonded tendon. The relationships of calculating the internal work by different components can be described as follow:

- Internal work was done by plastic moment  $M_{pl}$ ,

Assuming the maximum moment at midspan location is  $M_{pl1}$  and the rotation done caused by this moment is  $\theta$ , and the maximum moment at middle support location is  $M_{pl2}$ , and the rotation is  $2\theta$ . Thus, the internal work done by plastic hinges can be expressed as follow:

$$M_{pl1}2\theta + M_{pl2}\theta \quad (5.36)$$

Where the plastic moment at midspan  $M_{pl1}$  can be calculated by taking a section at midspan and consider the segment next to the exterior support as shown in Fig. 5.15c. By taking a moment at the neutral axis position at the point  $o$ , then plastic moment  $M_{pl1}$  yields:

$$M_{pl1} = \frac{5}{32}PL_L - T_{pU}e_1 \quad (5.37)$$

where

$e_1$  the eccentricity of the unbonded tendon at midspan.

Now, to find the plastic moment at the middle support  $M_{pl2}$ , consider one span as shown in Fig. 5.15d. Then, apply the moment equilibrium equation at the middle support location, the plastic moment can be calculated as follows:

$$M_{pl2} = \frac{1}{2}PL_L - \frac{5}{32}P(2L_L) - T_{pU}e_2 \quad (5.38)$$

Eq. (5.38) can be re-written as follows:

$$M_{pl2} = \frac{3}{16}PL_L - T_{pU}e_2 \quad (5.39)$$

$e_2$  the eccentricity of the unbonded tendon at middle support location.

it can be noticed from Eqs. (5.37) and (5.39) that the force in the unbonded tendon  $T_{pU}$ , is the same at both locations because it is assumed that there is no friction and bond between the tendon and the surrounding concrete.

- Internal work was done by the unbonded prestressing force

The prestressing force in the unbonded tendon can cause an internal work in the beam. This work can be calculated by multiply the prestressing force by the axial elongation of the tendon as expressed in Eq. (5.40):

$$\frac{T_{pU}\delta_U}{2} \quad (5.40)$$

Considering that:

$$\theta = \frac{\Delta_L}{L_L} \quad (5.41)$$

Where

$$L_L = \frac{L}{2} \quad (5.42)$$

Therefore, By equating the external work done by the applied load with the internal work done by plastic moment, prestressing moment and prestressing force, the elongation of the unbonded tendon can be expressed as shown in the following formula:

$$\delta_U = \frac{2\Delta_L}{L_L} [2e_1 + e_2] \quad (5.43)$$

Once the elongation in the unbonded tendon became known, then the same procedure is still applicable for calculating the strain and the stress as explained previously.

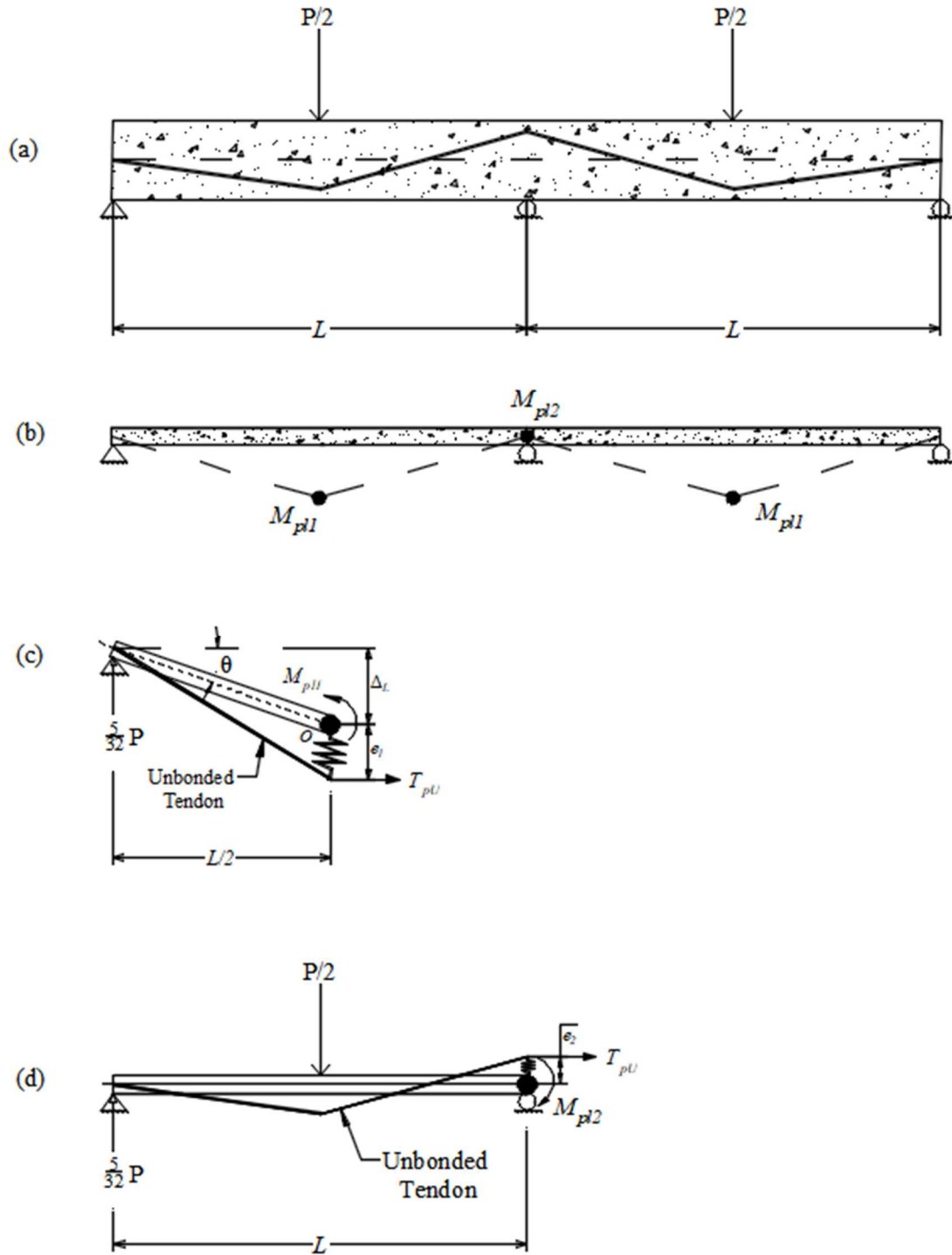


**Fig. 5.15 Beam Tendon Profile and Collapse Mechanism: (a) Beam Unbonded Tendon Profile; (b) Collapse Mechanism, (c) Plastic Hinge at Positive Moment at Ultimate; and (d) Plastic Hinge at Negative Moment at Ultimate.**

### 5.3.3.2 Deflection Calculation from Curvature Diagram using Moment-Area Integration with Single-Point Loading

After testing beam no. 8 which has two-span continuous beam post-tensioned using bonded and unbonded tendon under single concentrated load at midspan, the crack response was evaluated to understand the flexural behavior of the beam. The cracks distribution at and near the plastic hinge locations were observed to evaluate the curvature response on the beam. As mentioned previously in section 5.3.2.2 that the deflection in the beam can be calculated by taking the moment of the curvature diagram about the point in which the deflection be calculated. Since the maximum deflection and positive moment for beams tested under a single concentrated load take place at midspan, therefore the midspan section is considered herein.

When the applied load increases, the curvature in the beam increases accordingly until the first crack occurs  $\Phi_{cr}$ , then the load keeps increasing until the non-prestressed steel yields  $\Phi_y$ . Once the non-prestressed steel yielded and the stress transferred to the prestressed tendons until yielding, the curvature increases as well to  $\Phi_{py}$  then to  $\Phi_u$  at failure. The curvature along the span length varied in each section; it reaches a maximum at the location where the bending moment is high. Therefore, to simplify the calculation, the average curvature value can be used to represent the general curvature distribution at ultimate. The curvature distribution for two-span continuous beam under different load levels of the single concentrated load at midspan is shown in Fig. 5.16.

To calculate the area of the curvature diagram, the length of the plastic hinges must be known. Measuring the actual length of plastic hinge requires many strain gauges attached to non-prestressed and prestressed steel along the potential plastic hinge location.

To perform this test at Rutgers Laboratory requires a new acquisition system to connect all the strain gauges, also in this study, the time is manner so it can be conducted in the future research. Therefore, this study used the length of the plastic hinge from the literature. Harajli et al. (2002) proposed an expression to estimate the plastic hinge length based on load type and depth of non-prestressed steel as follows:

$$L_p = \frac{L}{f} + 1.5d \quad (5.44)$$

Where

$f$  load geometry factor= $\infty$ , 3, 6 for 1point, 2point and uniform loading

$d$  the depth of tension reinforcement

The term  $L/f$  in Eq. (5.44) is called  $L_a$  in other literature such as Mattock (1967) and Ozkul et al. (2008) which represents the constant moment region. Therefore the equation can be re-written as follows:

$$L_p = L_a + 1.5d_s \quad (5.45)$$

To calculate the reaction at exterior support  $A_y$  from the curvature diagram, the left span is considered then taking the first moment about the negative support location. Once the reaction is known, then half span is considered to find the deflection at midspan by taking the first moment about the midspan location as follows:

At Cracking:

$$A_{y_{cr}} = \frac{1}{L} \left[ \frac{5}{6} \Phi_{cr} L_L^2 \right] \quad (5.46)$$

$$\Delta_{L_{cr}} = A_{y_{cr}} \frac{L}{2} - \left[ \frac{1}{6} \Phi_{cr} L_L^2 \right] \quad (5.47)$$



After Cracking until Ultimate:

$$A_y = \frac{1}{L} \left[ \frac{1}{2} \Phi_{cr} L_g \left( L - \frac{2}{3} L_g \right) + 2 \Phi_{cr} L_L (L_\phi - L_g) + \frac{1}{2} (\Phi - \Phi_{cr}) L_L \right] \quad (5.48)$$

$$\left[ (L_\phi - L_g) + \Phi L_a \frac{L}{2} - \frac{1}{8} \Phi L_a^2 - \frac{1}{4} (\Phi - \Phi_{cr}) (L_{p2} + L_a) \right]$$

$$\Delta_L = A_y \frac{L}{2} - \left[ \frac{1}{2} \Phi_{cr} L_g \left( \frac{L}{2} - \frac{2L_g}{3} \right) + \frac{1}{2} (\Phi - \Phi_{cr}) (L_\phi - L_g) \right] \quad (5.49)$$

$$\left[ \left( \frac{L}{2} - L_g - \frac{2(L_\phi - L_g)}{3} \right) + \Phi_{cr} (L_\phi - L_g) \right]$$

$$\left[ \left( \frac{L}{2} - L_g - \frac{(L_\phi - L_g)}{2} \right) + \frac{1}{8} \Phi L_a^2 \right]$$

Where

$$L_{g(i)} = \frac{32M_{cr(i)}}{5P_{(i)}} \quad (5.50)$$

$$L_{\phi(i)} = \frac{32M_{(i)}}{5P_{(i)}} \quad (5.51)$$

Simplified Method at Ultimate:

Most of the design codes such ACI and AASHTO presented the design strength equation at ultimate limit state, i.e., the strength when the strain in the extreme fiber in concrete reaches 0.003. Therefore, some modification was made to the curvature diagram at ultimate to make simple to use by designers as shown in Fig. 5.16d. Thus, Eq. (5.48) and (5.49) can be re-written as follow:

$$A_{yu} = \frac{1}{L} \left[ \Phi_u L_{p1} \left( L - \frac{1}{2} L_{p1} - L_h \right) - \frac{1}{2} \Phi_u L_{p2} \left( \frac{1}{4} L_{p2} \right) \right] \quad (5.52)$$

$$\Delta_L = A_{yu} \frac{L}{2} - \left[ \frac{1}{8} \Phi_u L_{p1}^2 \right] \quad (5.53)$$

Where

$L_h$  the distance from the exterior support to the idealized curvature

$$L_h = \frac{L}{2} - L_{p1} - \frac{L_a}{2}$$

The plastic hinge lengths for positive and negative moment locations are  $L_{p1}$  and  $L_{p2}$  respectively

$$L_{p1} = 1.5d_{s1}$$

$$L_{p2} = 1.5d_{s2}$$

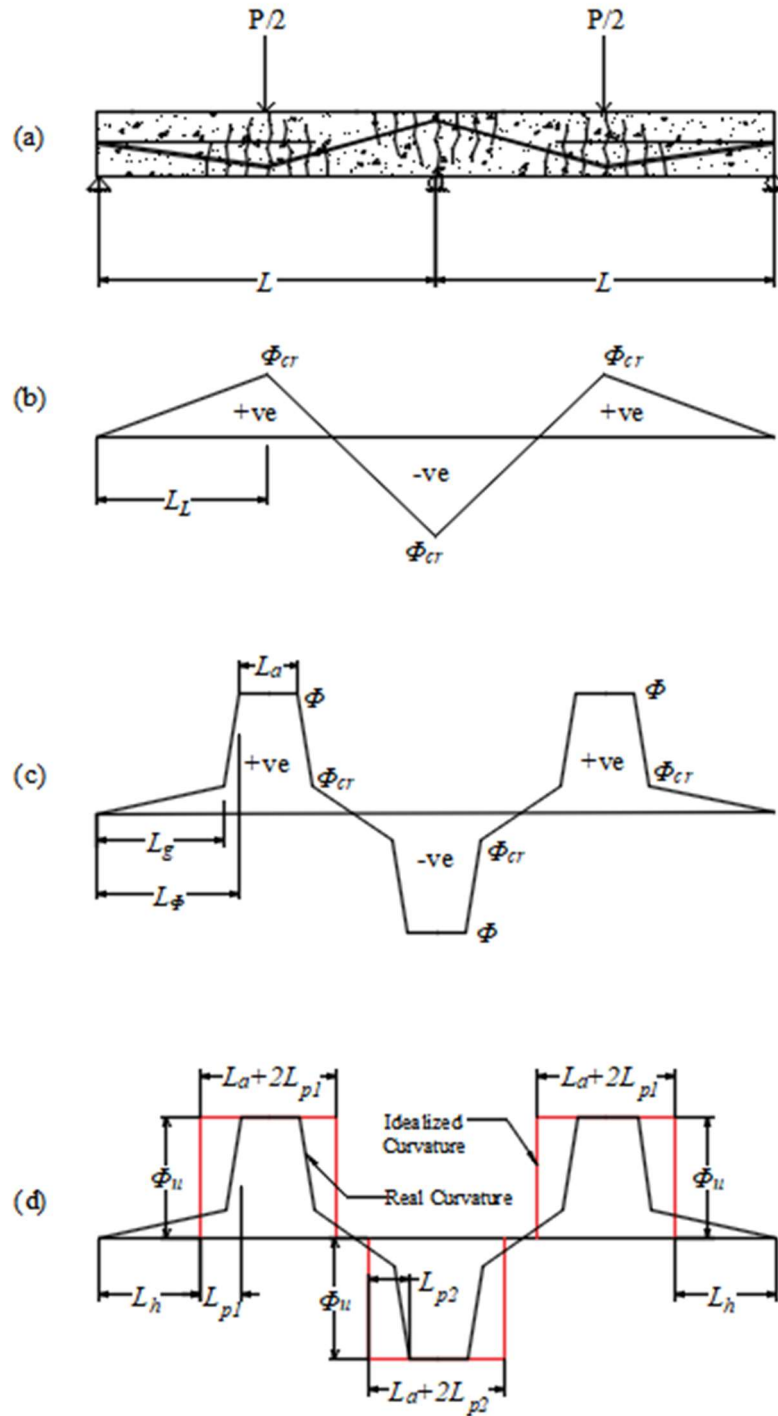


**Fig. 5.16 Curvature Distribution for a) Two-Span Beams under Single point Load, b) At Cracking, c) after Cracking until Ultimate, and d) Idealized Curvature at Ultimate.**

## 5.4 Flow Chart Analysis

The analytical formulations are based on the incremental analysis. The analysis uses small increments of the compressive strain in the extreme concrete fiber as an independent value. Then, stress in concrete is calculated using Hognestad's classical stress-strain parabola. Once, the concrete stress became known, the depth of the neutral axis  $c$  and stresses in the non-prestressed steel, bonded and the unbonded tendon is calculated. Since all stresses are known, the moment capacity of the section is computed as well. The curvature of the section can be calculated by the concrete strain on the neutral axis depth. The maximum deflection  $\Delta_L$  of the beam is calculated from the curvature diagram using the moment-area method. Once, the deflection became known, the elongation and strain of the unbonded tendon are calculated. The last unbonded stress is compared with the stress calculated from the second step if the difference between both stresses is less than the tolerance (0.1 ksi) that is mean this is the final stress. However, the difference is bigger than the tolerance, then substitutes the last stress in the neutral axis equation  $c$  and repeat all the following steps until meets the required tolerance. Then, the strain in concrete and unbonded tendon are compared with strains at failure 0.003 and 0.04, respectively.

To satisfy the required tolerance, all relationship equations above are re-written in MATLAB R2017b scripts. The program requires to input all section details, material properties, type of load and tolerance. The flow chart of all procedure steps is shown in Fig. 5.17.

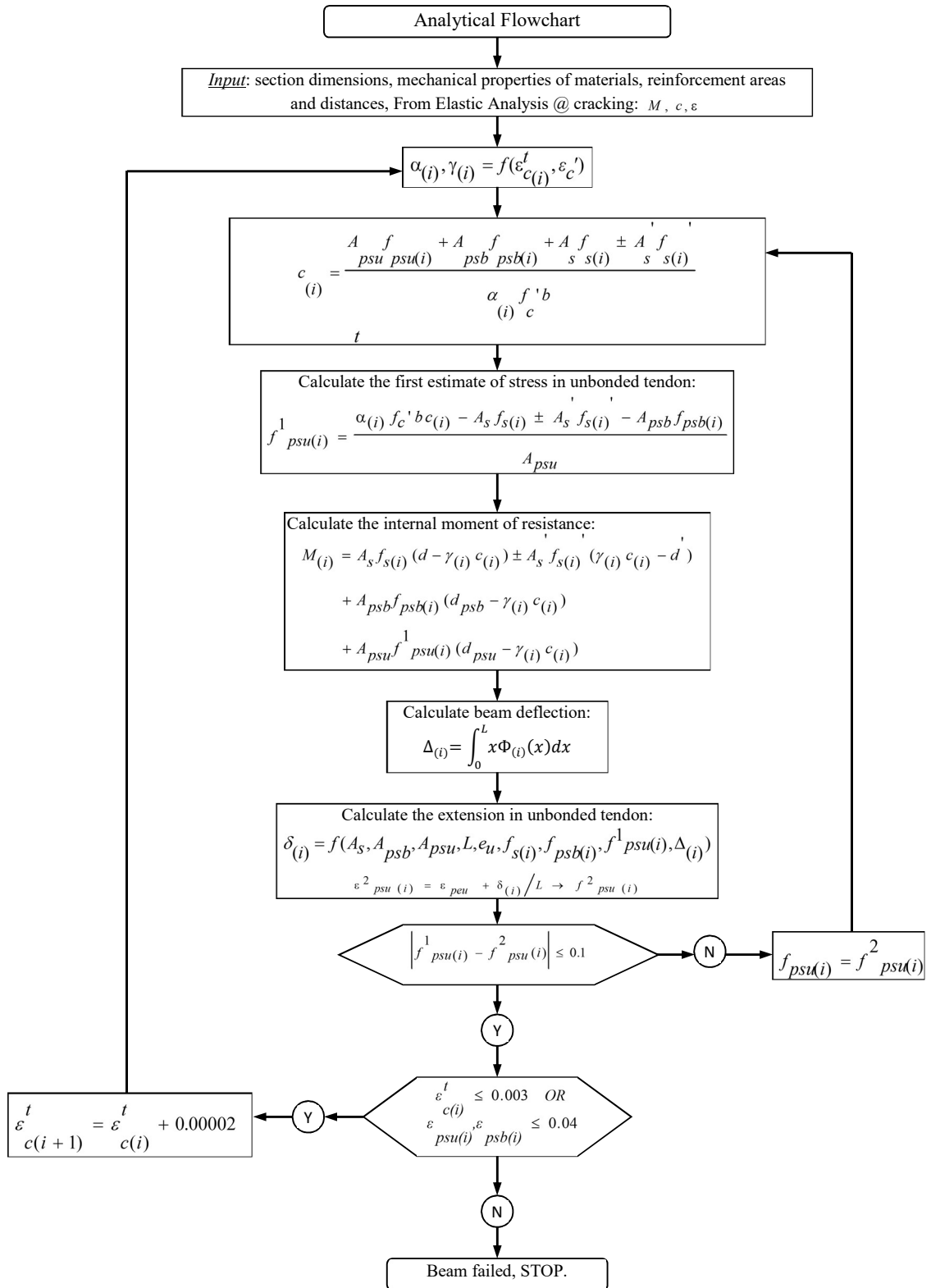


**Fig. 5.17 Flow Chart for Analysis of Two-Span Continuous Beam**

## 5.5 Moment-Deformation Relationship

From the observations for analysis of partially prestressed beams, it can be concluded that there are three stages in the moment-deflection relationship: uncracked elastic, cracked elastic and after yielding of non-prestressed steel.

After prestressing both tendons, the beam was cambered at both spans while it clamped at all supports to prevent any differential vertical movement. After the first crack occurs, the cracked state starts and ends when the concrete fails in compression.

The typical moment-deformation relationship at different stages is shown in Fig. 5.18.

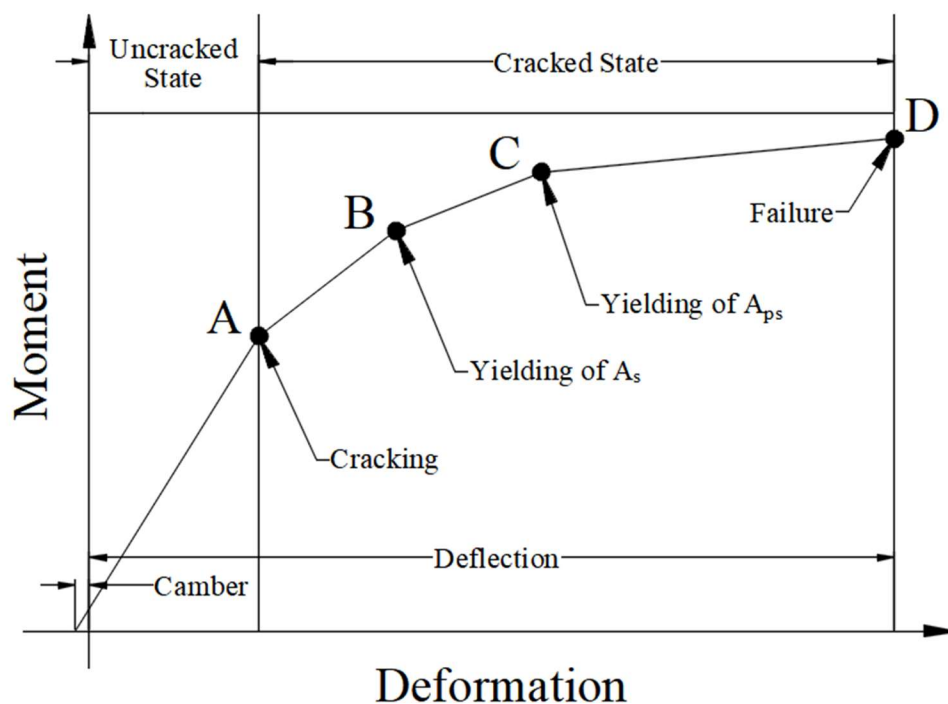


**Fig. 5.18 Moment versus Deformation Relationship of Beams Prestressed with Bonded and Unbonded Tendons**

## **CHAPTER VI**

### **MODEL VALIDATION AND COMPARISON OF RESULTS**

#### **6.1 Introduction**

This chapter carries out validating the proposed analytical models with the experimental results for two-span continuous concrete beams internally prestressed with bonded and unbonded tendons. The analysis results from the two models (third-point and single point load) which presented in chapter 5 of this study are validated with the results from experimental specimens that conducted in the civil engineering laboratory at Rutgers University herein. The accuracy and validity of the proposed models are discussed in this chapter.

The results produced by the beam specimens 1 to 7 which subjected to third-point load were used to validate the first model, while the second model was validated with the results of beam specimen 8 which was subjected to a single-point load at midspan. Moreover, beams tested by Tan and Tjandra (2007) and Loe et al. (2016) were included invalidating the proposed approach.

Furthermore, the effect of different design parameters on the flexural response and the stress in the unbonded tendon are studied in this chapter. The value of each design variable is varied without changing other parameters to clarify the effect of the studied variable on the beam response.

## 6.2 Validation of the Proposed Model using Load-Deformation Curves

The first analytical model presented in the previous chapter is applicable to analyze two-span continuous beams prestressed with bonded and unbonded tendon subjected to a third-point load. However, the second model is derived for two-span beams subjected to a single concentrated load at midspan. Therefore, to verify the reliability of proposed models, eight two-span continuous beam specimens post-tensioned internally with bonded and unbonded tendons were performed. The beam specimens were conducted in the civil engineering laboratory at Rutgers University. The results of beam specimens 1 to 7 were compared to validate the proposed model for the third-point load, while the model for the single concentrated load at midspan was validated by using beam specimen 8. To compare the results of the analytical models with experimental, the load-deformation relationships and the stress in the unbonded tendon were considered. In fact, load versus deflection at  $L/3$ , midspan, and  $2L/3$  from the exterior support relationships were compared for beams subjected to a third-point load. However, deflection at midspan location was considered for the single-point load.

The comparison of the load-deflection relationships between the analytical and experimental results exhibits a good agreement in terms of flexural behavior as shown in Fig. 6.1 to Fig. 6.25. The excellent agreement occurs with beam no. 2 because this beam specimen has the same amount of reinforcing steel at top and bottom of the section at the maximum positive and negative moment locations as illustrated in Fig. 6.4. It can be observed from the load-deflection relationships that the proposed approach usually overestimates the deflection comparing with the experimental results. Also, experimental results of beam specimens 1 and 3 exhibits less load capacity compared with the analytical



results and that because these two beams have very low non-prestressed reinforcement at the middle support location (two #2 rebar) which yield to observing only one big crack at the negative moment zone.

On the other hand, the results from the second model that subjected to a single-point load demonstrate good agreement with experimental results of beam specimen 8 as shown in Fig. 6.22. Also, some beams from the technical literature were investigated to validate the presented approach. The load versus deflection relationships for beams testing by Tan and Tjandra (2007) and Lou et al. (2016) show a good correlation as well, as shown in Fig. 6.23, Fig. 6.24 and Fig. 6.25.

Generally, in each test beam, it is hard to identify the exact curvature distribution for the entire span which this approach based on to calculate the deflection. But, even with all different prestressing ratio for each beam specimens, the proposed approaches demonstrate very good compatibility with the experiments. In addition, it is important to use the real stress-strain curve for non-prestressed steel and prestressing strands in the model to get the most accurate results comparing with beam specimen response.

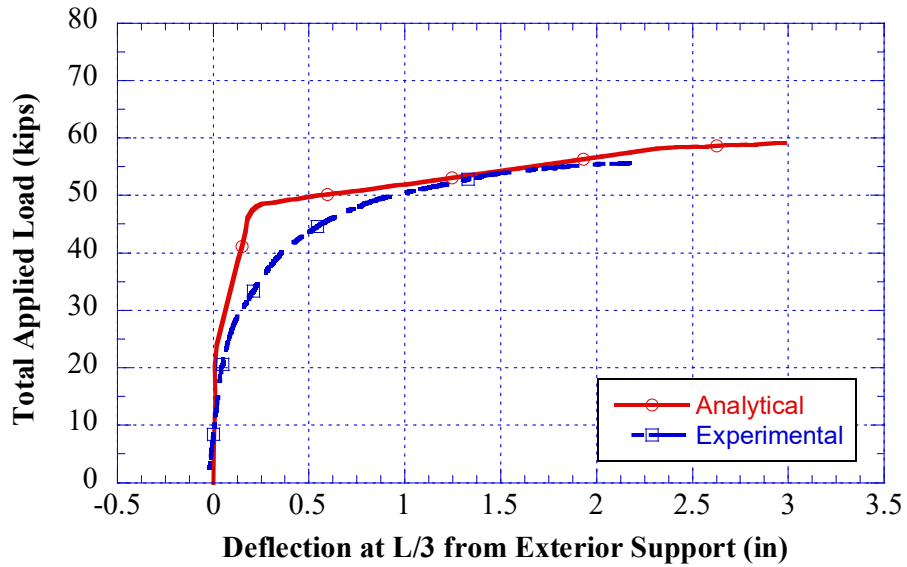


**Fig. 6.1 Applied load and deflection relationship of beam no. 1 in this Investigation: Analytical and experimental results**

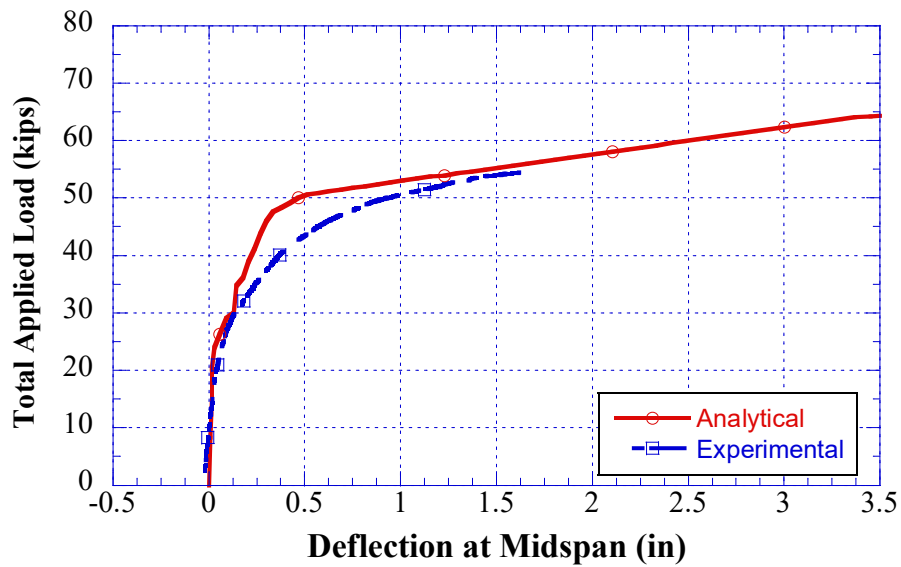


**Fig. 6.2 Applied load and deflection relationship of beam no. 1 in this Investigation: Analytical and experimental results**

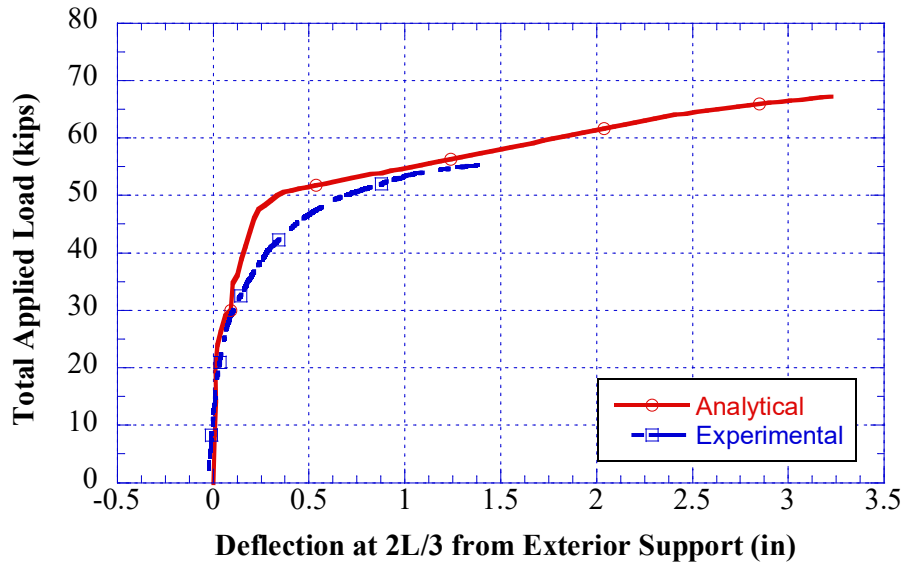


**Fig. 6.3 Applied load and deflection relationship of beam no. 1 in this Investigation: Analytical and experimental results**

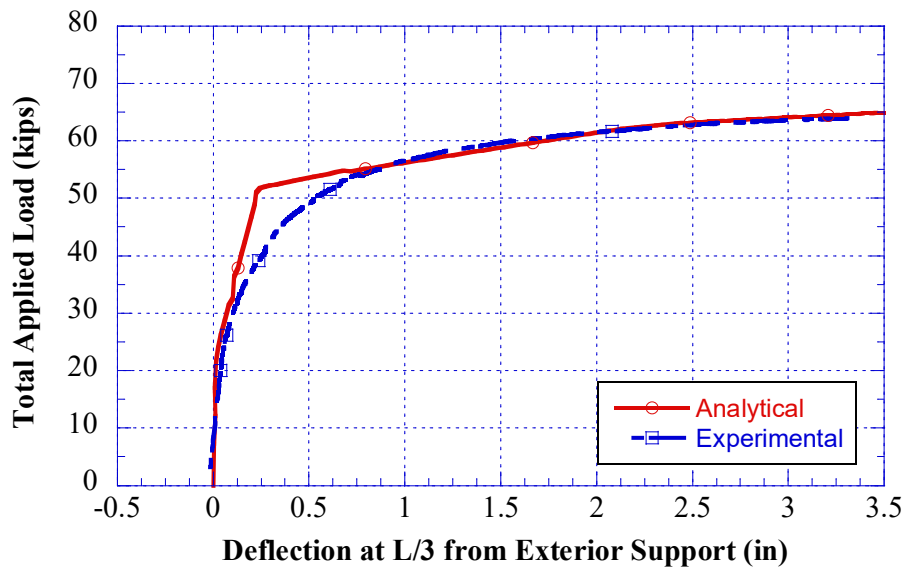


**Fig. 6.4 Applied load and deflection relationship of beam no. 2 in this Investigation: Analytical and experimental results**

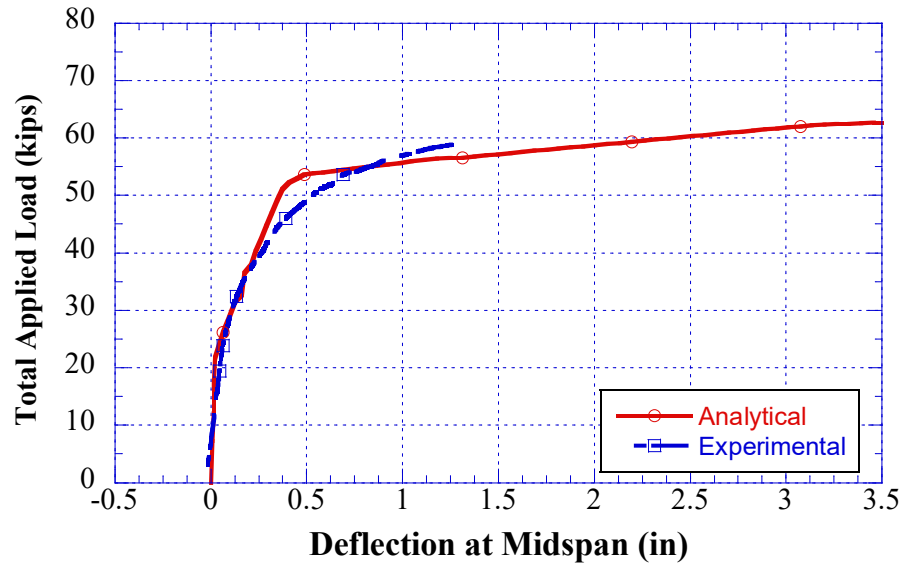


**Fig. 6.5 Applied load and deflection relationship of beam no. 2 in this Investigation: Analytical and experimental results**

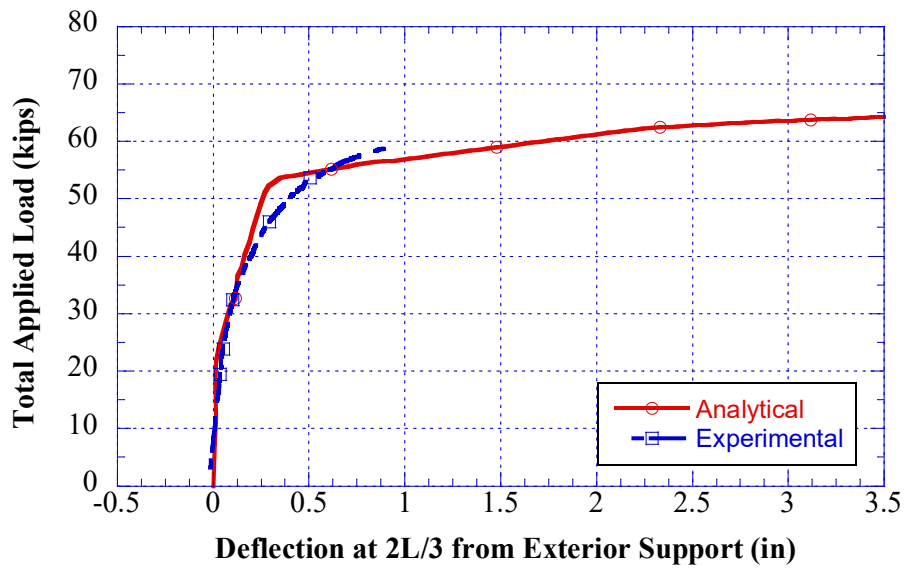


**Fig. 6.6 Applied load and deflection relationship of beam no. 2 in this Investigation: Analytical and experimental results**

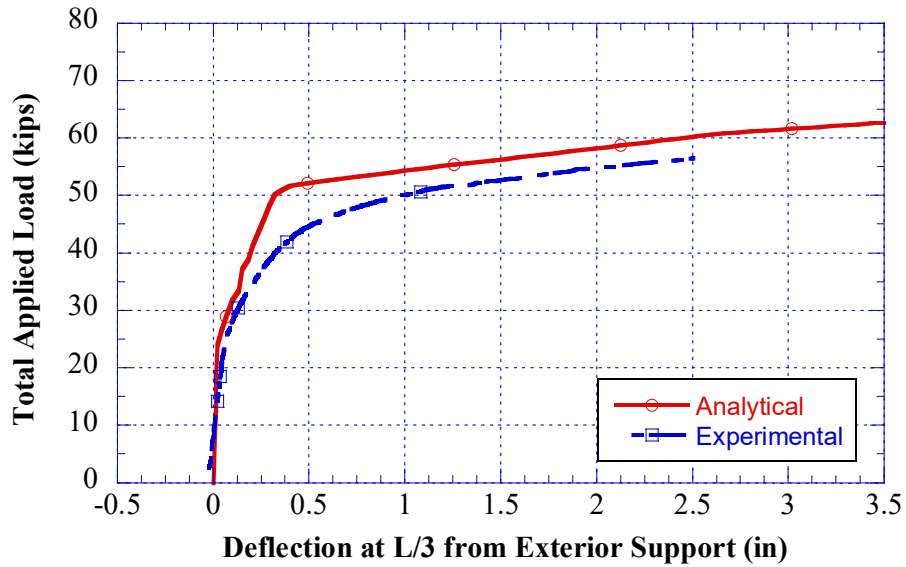


**Fig. 6.7 Applied load and deflection relationship of beam no. 3 in this Investigation: Analytical and experimental results**

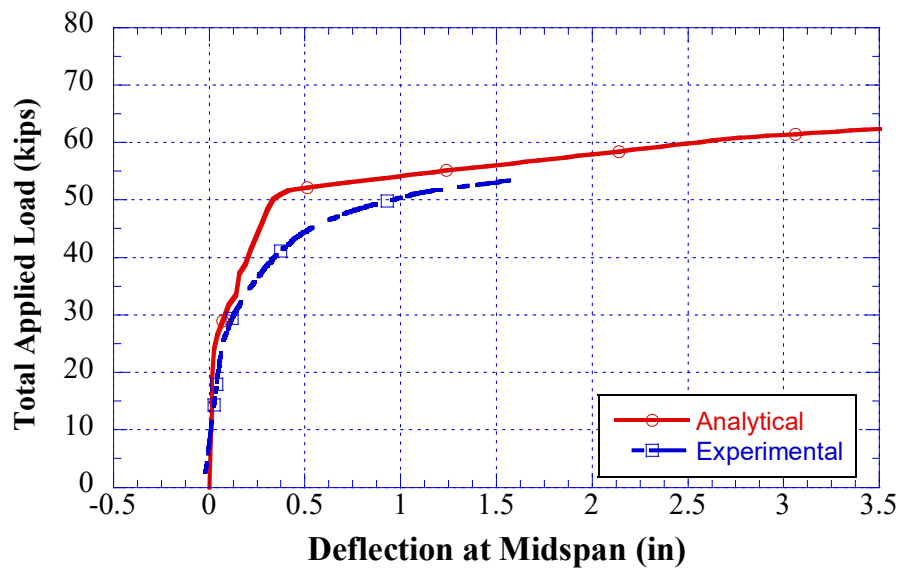


**Fig. 6.8 Applied load and deflection relationship of beam no. 3 in this Investigation: Analytical and experimental results**

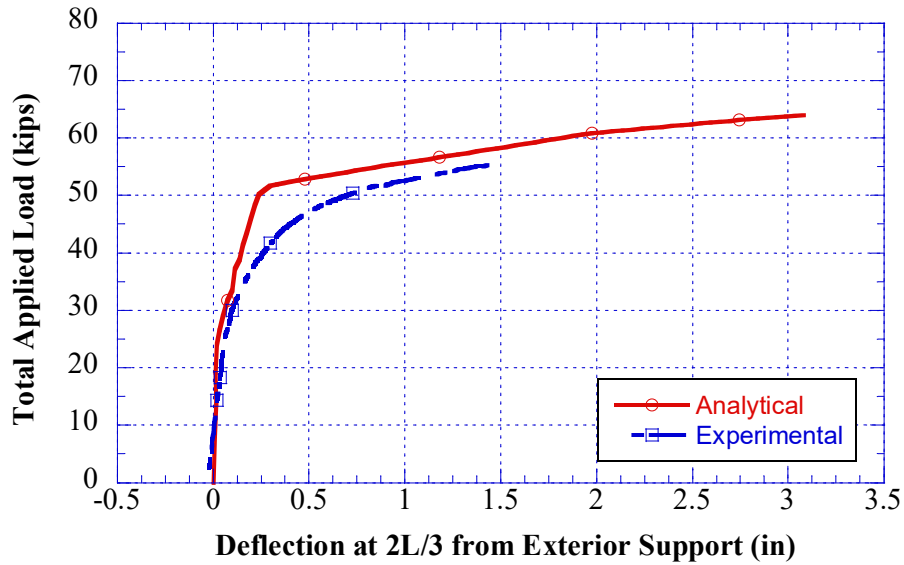


**Fig. 6.9 Applied load and deflection relationship of beam no. 3 in this Investigation: Analytical and experimental results**

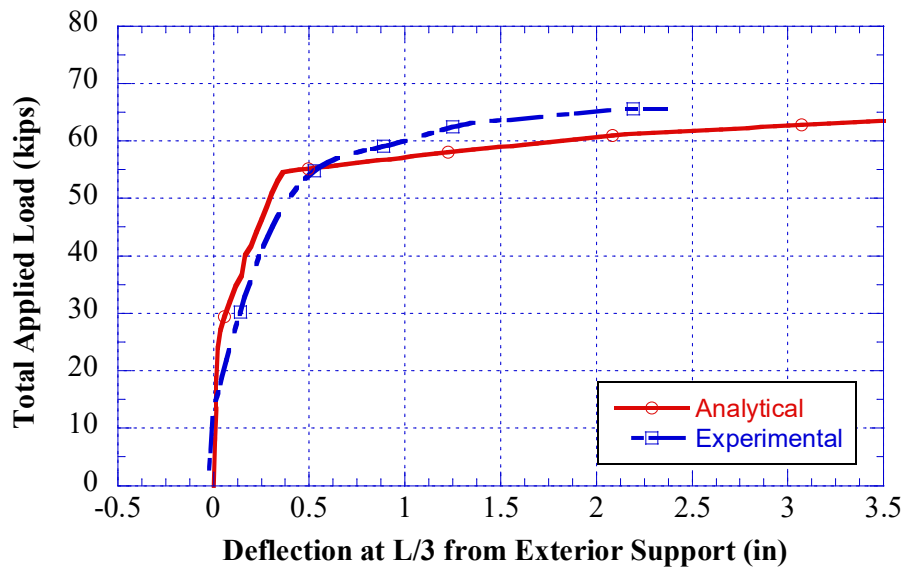


**Fig. 6.10 Applied load and deflection relationship of beam no. 4 in this Investigation: Analytical and experimental results**

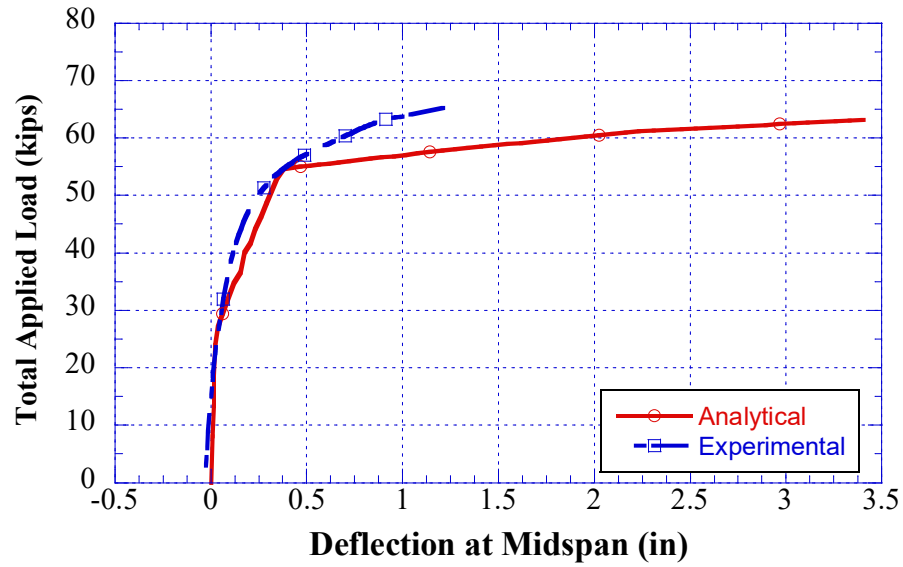


**Fig. 6.11 Applied load and deflection relationship of beam no. 4 in this Investigation: Analytical and experimental results**

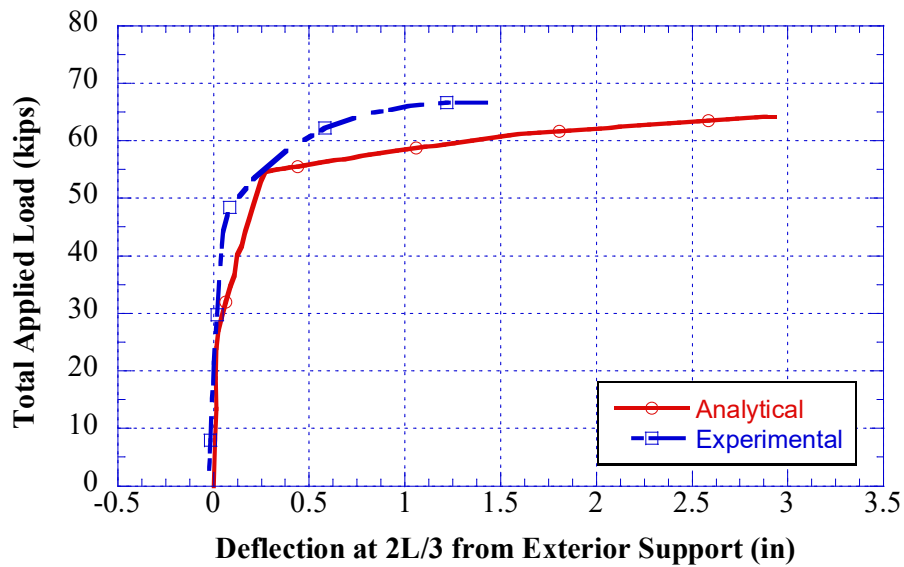


**Fig. 6.12 Applied load and deflection relationship of beam no. 4 in this Investigation: Analytical and experimental results**

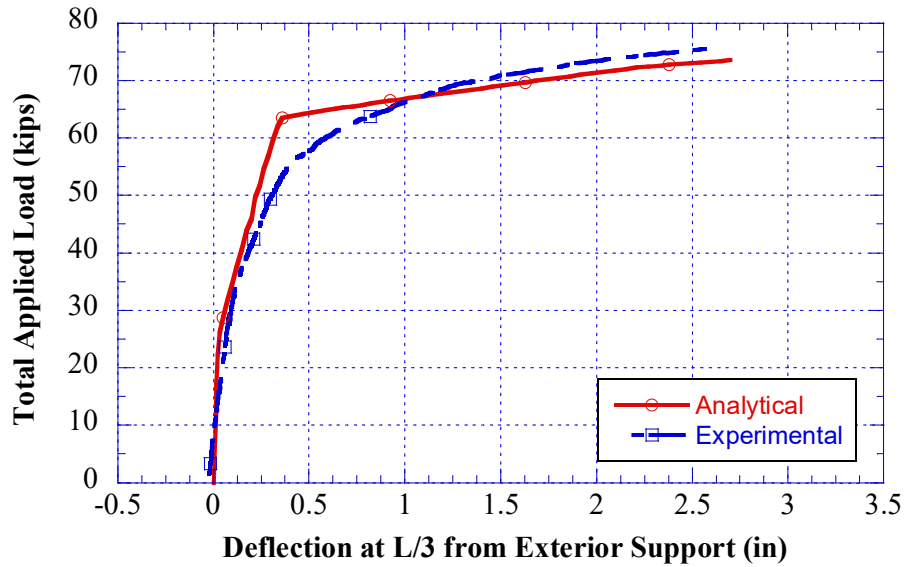


**Fig. 6.13 Applied load and deflection relationship of beam no. 5 in this Investigation: Analytical and experimental results**

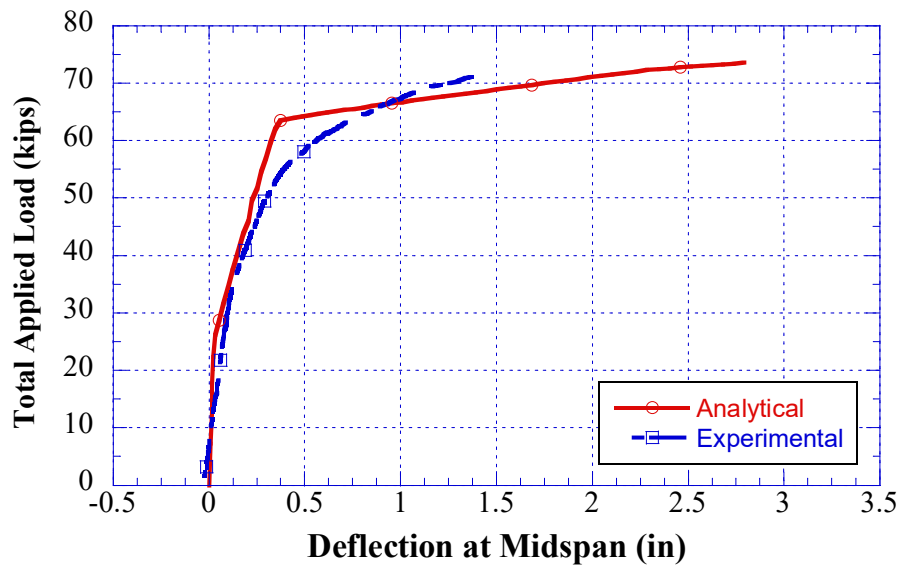


**Fig. 6.14 Applied load and deflection relationship of beam no. 5 in this Investigation: Analytical and experimental results**



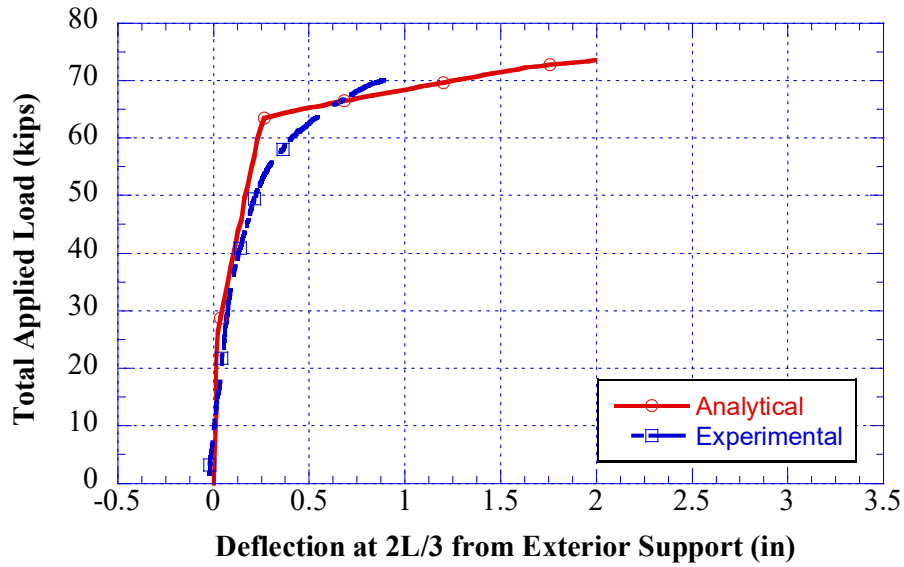


**Fig. 6.15 Applied load and deflection relationship of beam no. 5 in this Investigation: Analytical and experimental results**

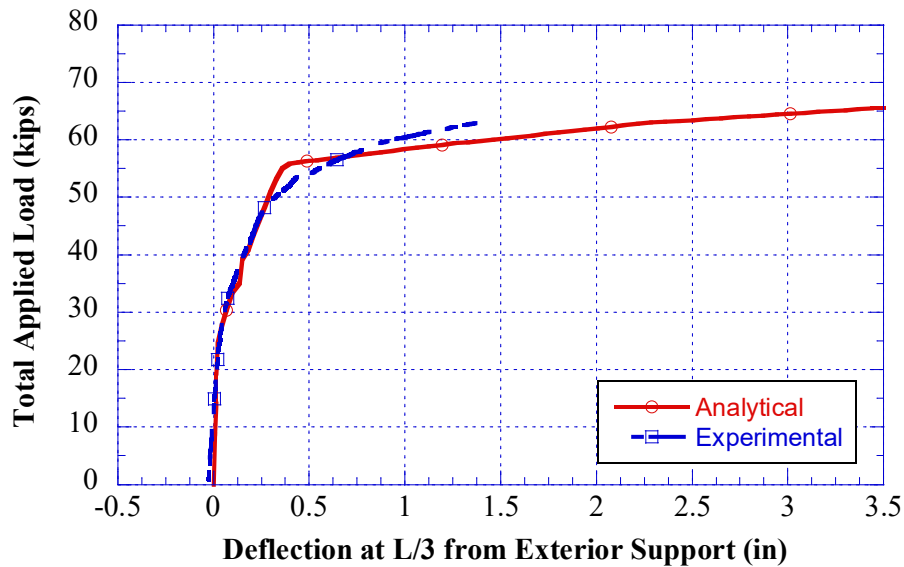


**Fig. 6.16 Applied load and deflection relationship of beam no. 6 in this Investigation: Analytical and experimental results**

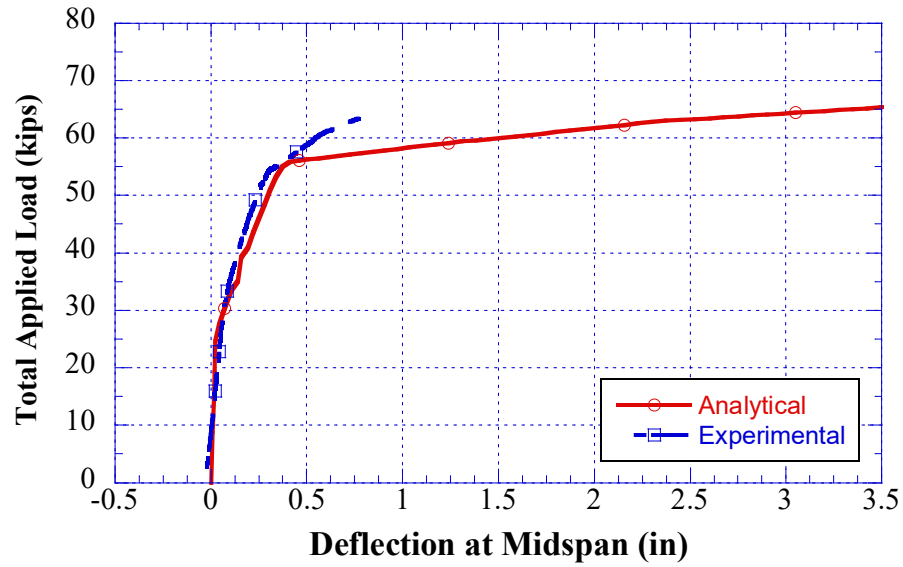


**Fig. 6.17 Applied load and deflection relationship of beam no. 6 in this Investigation: Analytical and experimental results**

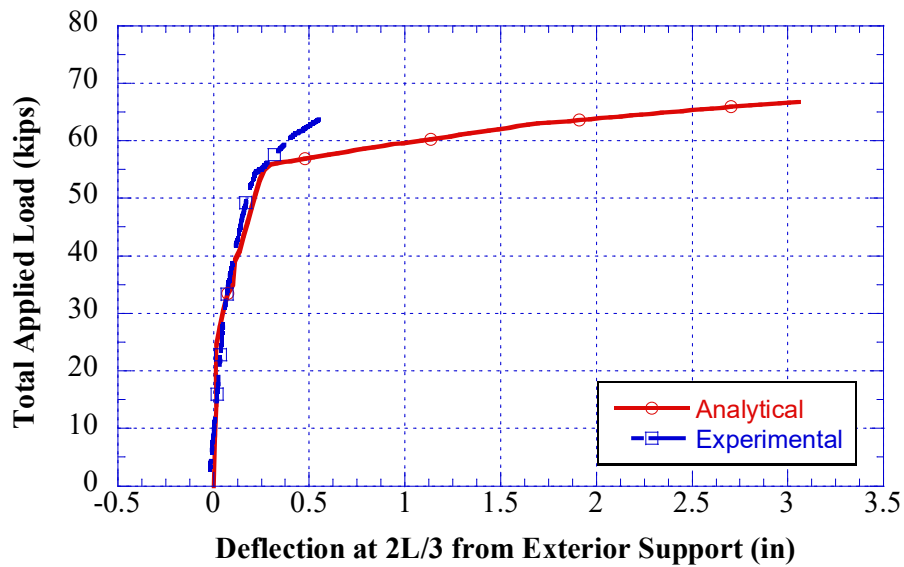


**Fig. 6.18 Applied load and deflection relationship of beam no. 6 in this Investigation: Analytical and experimental results**

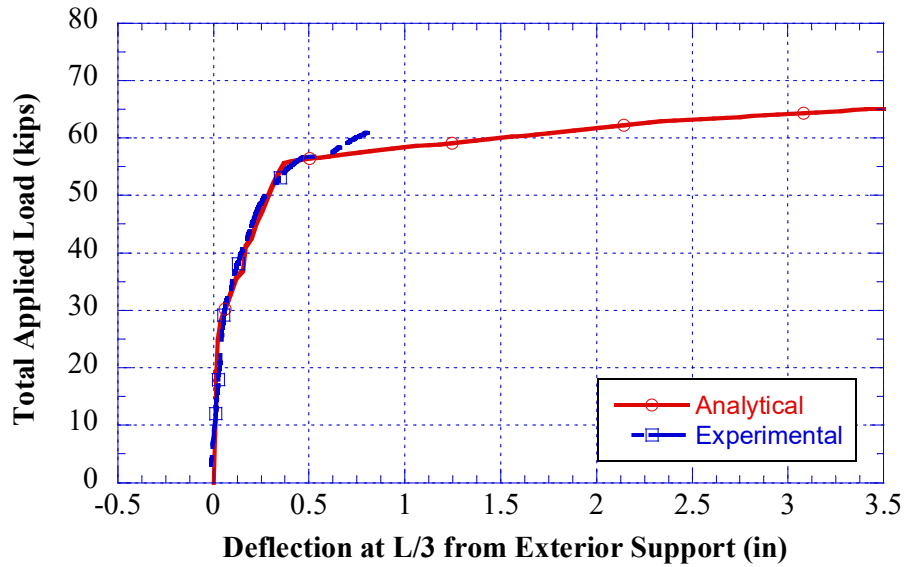


**Fig. 6.19 Applied load and deflection relationship of beam no. 7 in this Investigation: Analytical and experimental results**

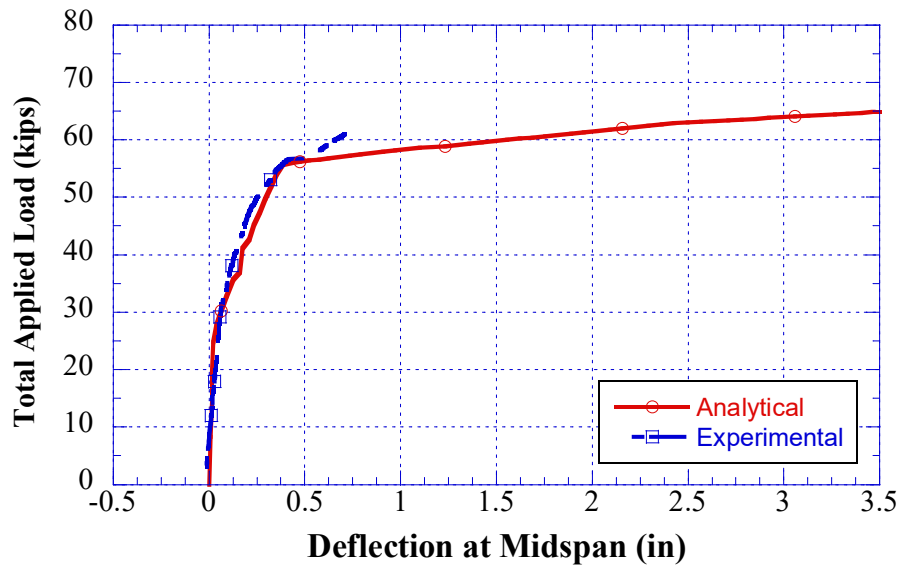


**Fig. 6.20 Applied load and deflection relationship of beam no. 7 in this Investigation: Analytical and experimental results**

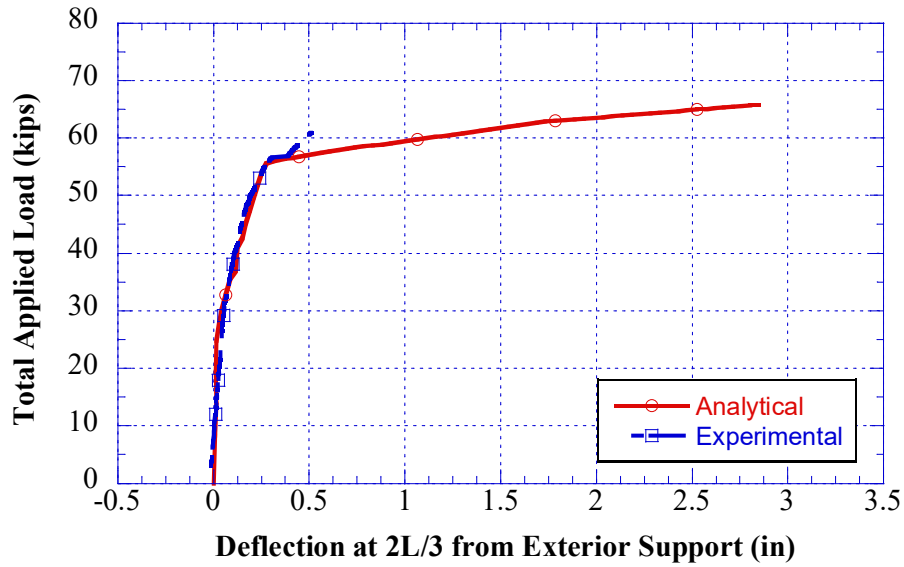


**Fig. 6.21 Applied load and deflection relationship of beam no. 7 in this Investigation: Analytical and experimental results**

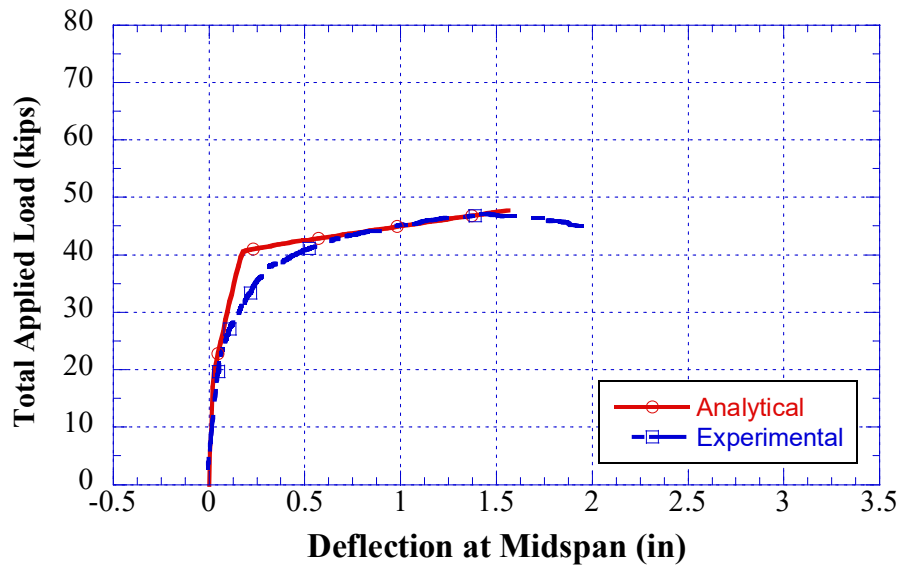


**Fig. 6.22 Applied load and deflection relationship of beam no. 8 in this Investigation: Analytical and experimental results**

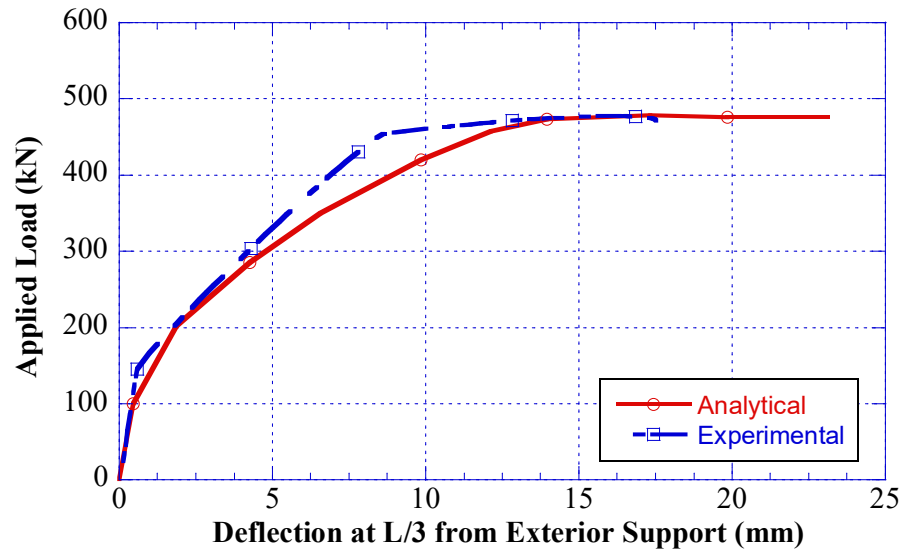


**Fig. 6.23 Applied load and deflection relationship of beam C2 Tested by Tan and Tjandra (2007): Analytical and experimental results**

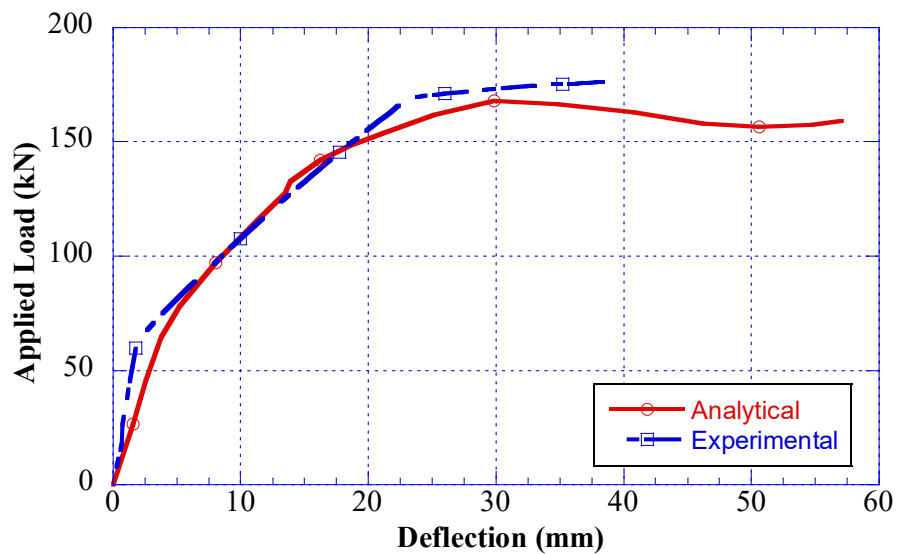


**Fig. 6.24 Applied load and deflection relationship of beam YLB3 Tested by Lou et al. (2016): Analytical and experimental results**

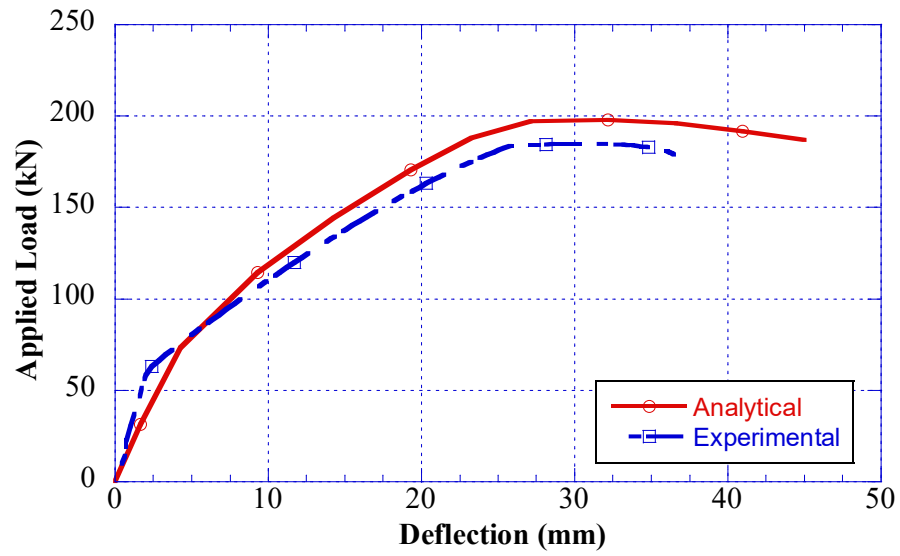


**Fig. 6.25 Applied load and deflection relationship of beam YLC3 Tested by Lou et al. (2016): Analytical and experimental results**

### 6.3 Comparison of Stress in Unbonded Tendon

Since calculating the stress in the unbonded tendon is a challenging aspect of this topic because of the lack of bond between the unbonded tendons and surrounding concrete. Therefore, one of the main objectives of this study is to present a new equation to calculate the stress in the unbonded tendon with acceptable accuracy and reliability. Thus, in addition to validate the presented models through the load-deformation relationships, the stress in the unbonded tendon is compared with the experimental results herein. Load cells were placed at the dead end for all test specimens to observe the force in the tendons during the post-tensioning and applied loads in the test.

The failure of all beams occurred due to the crushing of concrete in compression except beams 6 and 7 where the tests stopped due to observing an excessive crack at one span at the end of additional rebar at the middle support location. The program based on increment in concrete strain in compression, thus, for each beam the program ran according to the actual strain in concrete.

The stress calculation in the unbonded tendon from the analytical models is based on estimating the curvature diagram and moment energy of the plastic hinges. Thus the models predict excellent estimation of the stress in the tendon at failure rather than other limit states. Therefore, it can be noticed from Table 6.1 that the first model shows an excellent estimation of the stress in the unbonded tendon with an error less than 2% except beams 6 and 7 where the comparison was not at ultimate. In addition, the second model for beams subjected to a concentrated load at midspan also exhibits an error less than 3%. Table 6.1 shows the experimental and prediction value of the stress in the unbonded tendon.

The coefficient of variation (COV) of the difference between the calculated and predicted value of the stress in the unbonded tendon is 0.96.

**Table 6.1 Experimental and Predicted Comparison of Stress in Unbonded Tendon**

Beam No.	Load location	$f_{psU}$		Diff. %
		exp.	pred.	
1	Third-Point	265.0	262.53	0.9
2	Third-Point	270.9	265.63	1.9
3	Third-Point	274.6	270.93	1.3
4	Third-Point	261.9	265.29	1.3
5	Third-Point	266.7	265.55	0.4
6	Third-Point	251.5	266.6	6.0
7	Third-Point	246.9	266.2	7.8
8	Midspan	259.9	253.12	2.6



## 6.4 Study the Effect of Design Parameters

Once the proposed models were validated with the experimental results, Different design variables were investigated to test the influence of these parameters on the global behavior of the proposed models. The effect of variation in various design parameters such as non-prestressed steel in tension at the maximum positive moment location  $A_{sI}$ , area of prestressed unbonded tendon  $A_{psU}$ , area of prestressed bonded tendon  $A_{psB}$ , and the effective stress in the prestressing tendon  $f_{pe}$  was investigated herein. To show the influence of each studied variable, it is varied three times by keeping all other parameters constant.

The reliability of both proposed models was tested. The cross-section, material properties and two-harped point tendon profile for beam specimen 2 were considered to check the first model. However, same properties except for the one-harped point at midspan tendon profile were considered for the second model. Twelve case study was examined for each model as shown in Table 6.2. The compressive concrete strength, the eccentricities of the bonded and unbonded tendon, yielding stress for all steels and tendon were constant for all case studies. Also, to notice the variation in the analysis response, case study no. 1 considered as the control for comparison.

The maximum load carrying capacity and deflection predicted in both proposed models were based on the location of the maximum positive moment which takes place at  $L/3$  from the exterior support for third-point load and at midspan for the single-point load. To show the correlation between the investigated variables and the beam response, load-deformation relationship and the stress increase in the unbonded tendon were considered. The analytical results for both models demonstrate a rational response in the load versus deflection relationships as shown in Fig. 6.26 to Fig. 6.33.

Increasing the amount of non-prestressed steel  $A_{sl}$  exhibits a significant increase in carrying capacity with a reduction in the deflection at ultimate. Also, it can be noticed in **Fig. 6.26** and Fig. 6.30, that the cracking load remains the same for all three cases because it depends on the modulus of rupture which basically is based on the compression strength of the concrete  $f'_c$  which is constant for all cases as mention previously. Furthermore, it obviously can be seen that the effect of increasing the area of the bonded tendon on the beam load capacity is more than the influence of increasing the same percentage of the area of the unbonded tendon as illustrated in Fig. 6.27 -Fig. 6.28 and Fig. 6.31 -Fig. 6.32. However, changing the value of the effective prestress in the prestressing tendons does not reflect a significant increase in the load carrying capacity and reduction in the deflection.

**Table 6.2 Material Properties and Dimensions of Case Study Beams**

Case no.	Concrete Beam				Unbonded Tendon			Bonded Tendon		
	$f'_c$ (ksi)	$f_y$ (ksi)	$d_s$ (in)	$A_{sI}$ (in <sup>2</sup> )	$A_{psU}$ (in <sup>2</sup> )	$d_{psU}$ (in)	$f_{peU}/f_{pu}$	$A_{psB}$ (in <sup>2</sup> )	$d_{psB}$ (in)	$f_{peB}/f_{pu}$
1	10	78.6	9.25	0.22	0.058	7.0	0.6	0.058	8.5	0.6
2				0.33						
3				0.4						
4	10	78.6	9.25	0.22	0.058	7.0	0.6	0.058	8.5	0.6
5					0.085					
6					0.153					
7	10	78.6	9.25	0.22	0.058	7.0	0.6	0.058	8.5	0.6
8								0.085		
9								0.153		
10	10	78.6	9.25	0.22	0.058	7.0	0.5	0.058	8.5	0.5
11							0.6			0.6
12							0.7			0.7

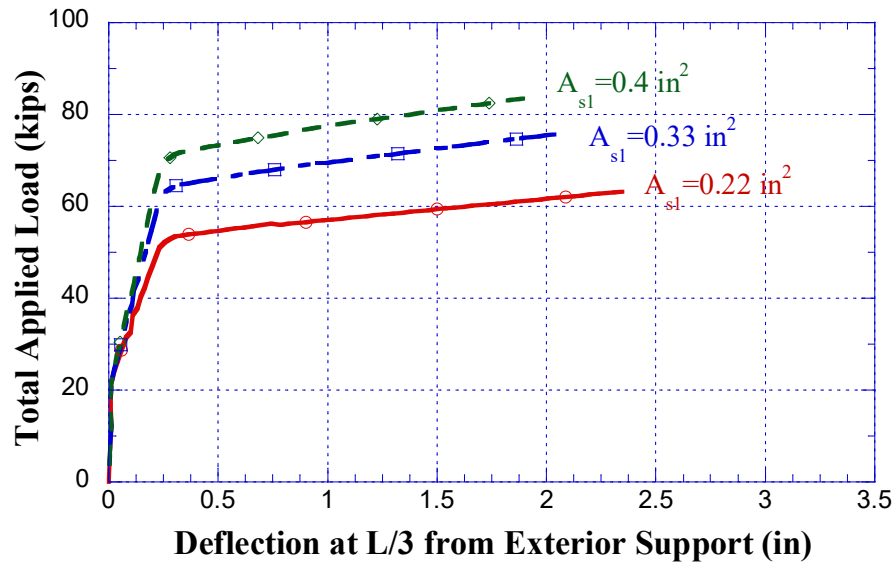


**Fig. 6.26 Relationship Between Applied Load and Deflection at L/3 from Exterior Support for varying Reinforcing Steel  $A_{sl}$**

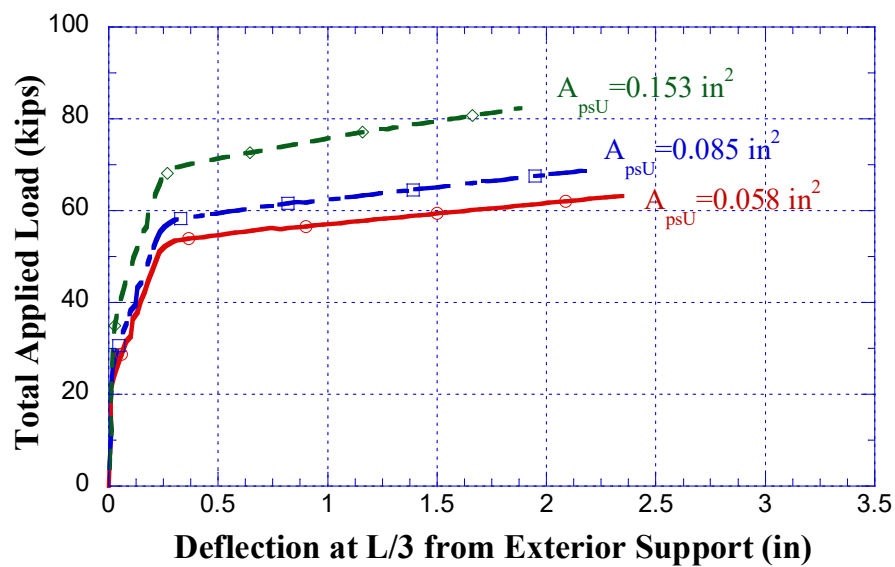


**Fig. 6.27 Relationship Between Applied Load and Deflection at L/3 from Exterior Support for varying Unbonded Tendon Area  $A_{psU}$**

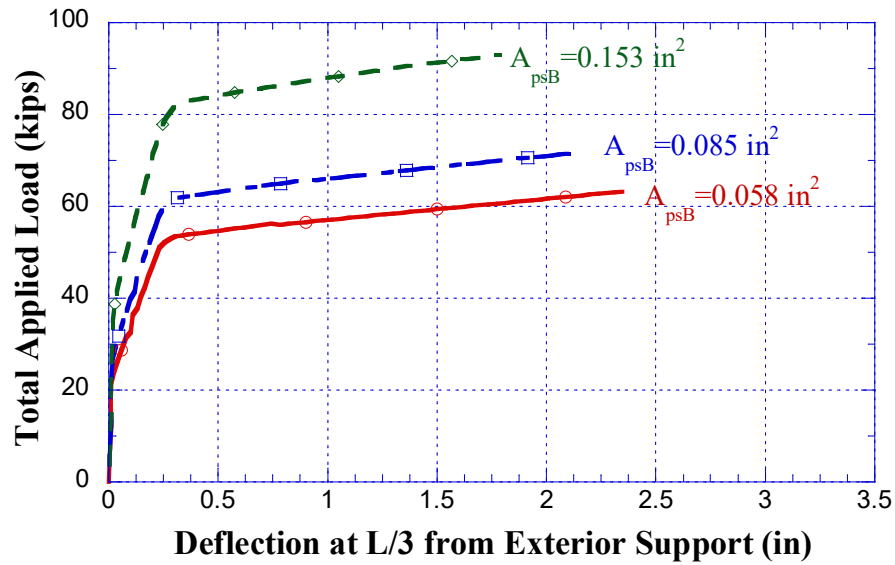


**Fig. 6.28 Relationship Between Applied Load and Deflection at L/3 from Exterior Support for varying Bonded Tendon Area  $A_{psB}$**

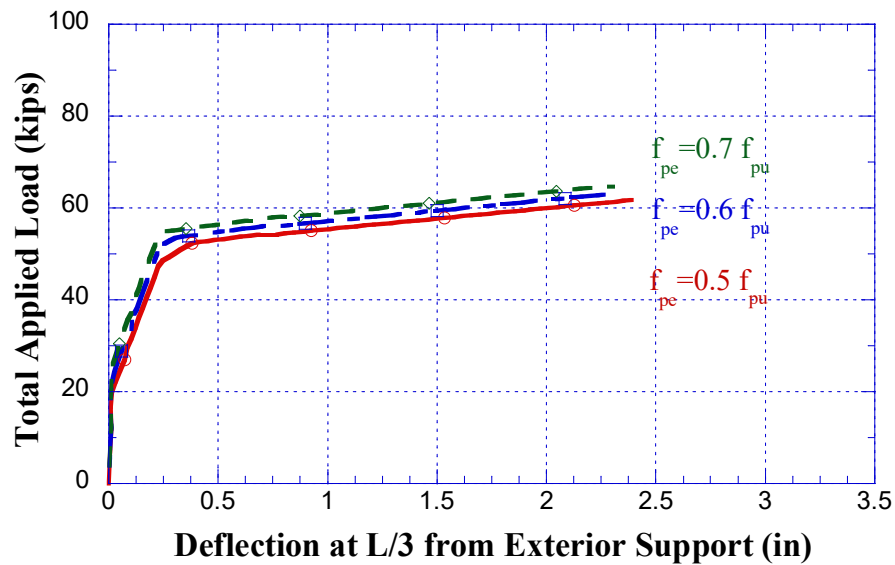


**Fig. 6.29 Relationship Between Applied Load and Deflection at L/3 from Exterior Support for varying Effective Stress  $f_{pe}$**

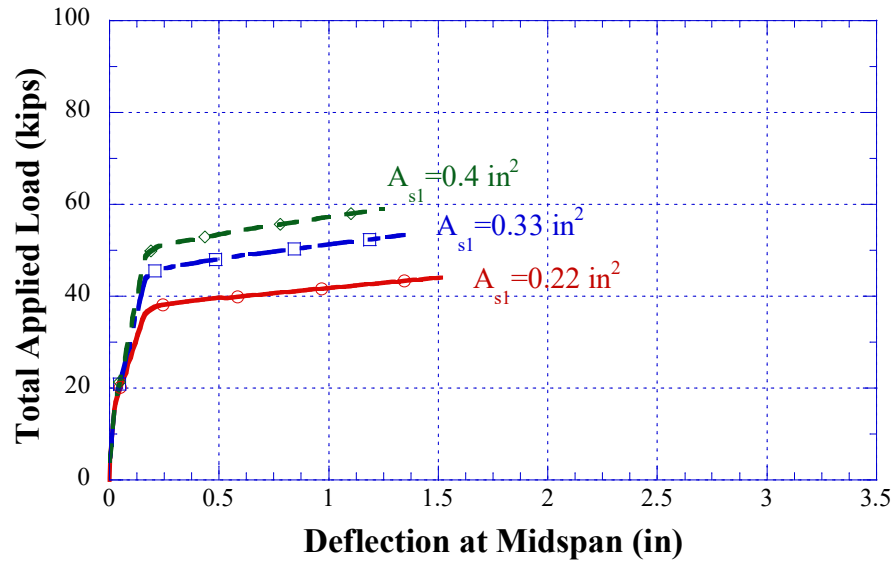


**Fig. 6.30 Relationship Between Applied Load and Midspan Deflection for varying Reinforcing Steel  $A_{sl}$**

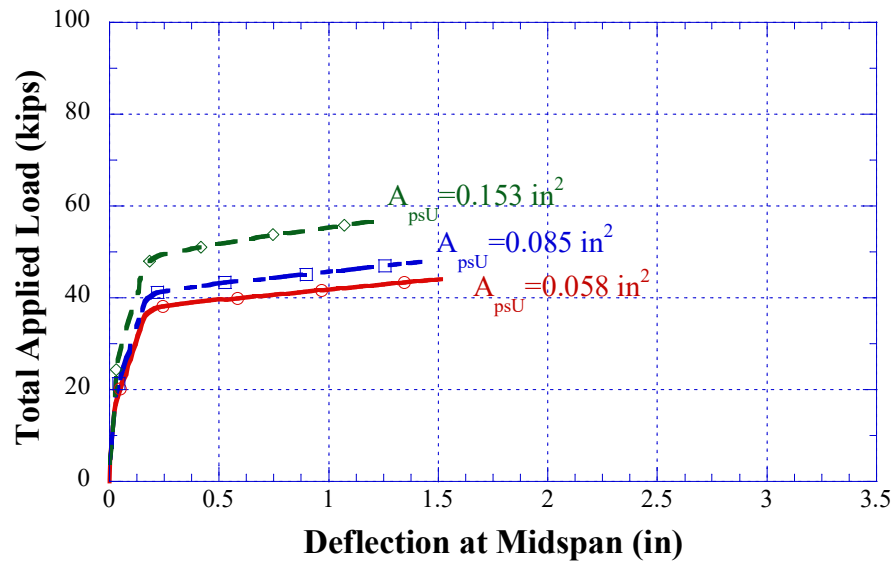


**Fig. 6.31 Relationship Between Applied Load and Midspan Deflection for varying Unbonded Tendon Area  $A_{psU}$**

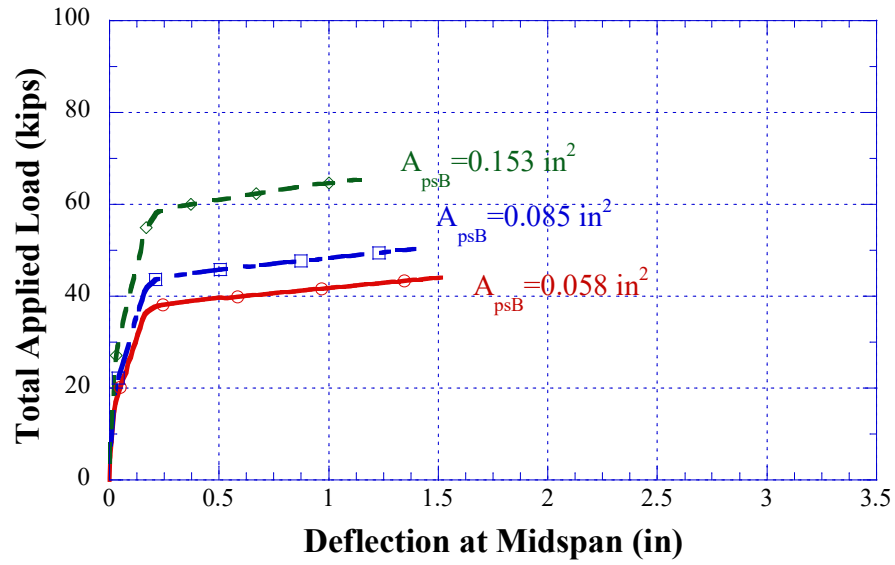


**Fig. 6.32 Relationship Between Applied Load and Midspan Deflection for varying Bonded Tendon Area  $A_{psB}$**

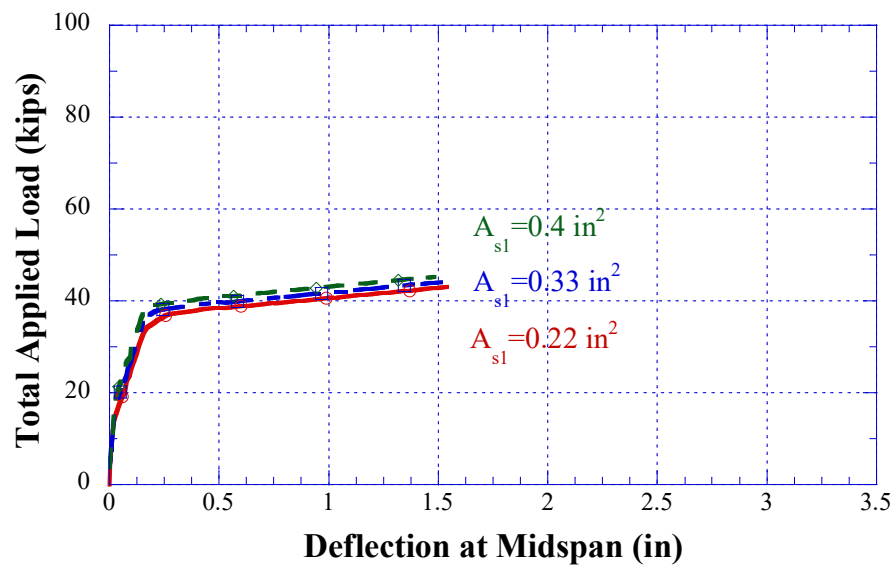


**Fig. 6.33 Relationship Between Applied Load and Midspan Deflection for varying Effective Prestress  $f_{pe}$**

Because of one of the most important aspects in the design of prestressed concrete members is to predict the accuracy of the stress increase in the unbonded tendon. Therefore, this parameter was observed closely herein. By reviewing the stress increase in the unbonded tendon as summarized in Table 6.3 and Table 6.4, it is obvious to notice that it is sensitive to the variation of the  $A_{sI}$ ,  $A_{psU}$  and  $A_{psB}$ , on the other hand, ignorable response to changing of  $f_{pe}$  except case study 12 of the first model. Moreover, all the beams fail due to the crushing of concrete in compression except beam 12 in the first model.

**Table 6.3 Summary of Stress Increase in the Unbonded Tendon for the First Proposed Model**

Case No.	Investigated Parameter	Parameter Value	$f_{pe}$ (ksi)	$f_{psU}$ (ksi)	Diff. of $f_{psU}$ %	$\Delta f_{psU}$ (ksi)	Diff. of $\Delta f_{psU}$ %
1	$A_{sI}$	0.22	173	239.8	0.0	66.80	0.0
2		0.33	173	232.9	3.0	59.90	11.5
3		0.40	173	229.1	4.7	56.10	19.1
4	$A_{psU}$	0.058	173	239.8	0.0	66.80	0.0
5		0.085	173	235.5	1.8	62.53	6.8
6		0.153	173	226.6	5.8	53.60	24.6
7	$A_{psB}$	0.058	173	239.8	0.0	66.82	0.0
8		0.085	173	234.6	2.2	61.60	8.4
9		0.153	173	223.9	7.1	50.88	31.3
10	$f_{pe}/f_{pu}$	0.5	145	213.0	12.6	68.05	1.8
11		0.6	173	240.8	0.4	67.78	0.0
12		0.7	203	265.1	9.5	62.11	7.6



**Table 6.4 Summary of Stress Increase in the Unbonded Tendon for the Second  
Proposed Model**

Case No.	Investigated Parameter	Parameter Value	$f_{pe}$ (ksi)	$f_{psU}$ (ksi)	Diff. of $f_{psU}$ %	$\Delta f_{psU}$ (ksi)	Diff. of $\Delta f_{psU}$ %
1	$A_{sl}$	0.22	173	217.7	0.0	44.67	0.0
2		0.33	173	212.6	2.4	39.60	12.8
3		0.40	173	209.9	3.7	36.87	21.2
4	$A_{psU}$	0.058	173	217.7	0.0	44.67	0.0
5		0.085	173	214.8	1.3	41.84	6.8
6		0.153	173	208.9	4.2	35.88	24.5
7	$A_{psB}$	0.058	173	217.7	0.0	44.67	0.0
8		0.085	173	214.0	1.7	41.04	8.9
9		0.153	173	206.7	5.3	33.70	32.5
10	$f_{pe}/f_{pu}$	0.5	145	190.5	14.3	45.49	1.8
11		0.6	173	217.7	0.0	44.67	0.0
12		0.7	203	246.8	11.8	43.82	1.9

## CHAPTER VII

### CONCLUSIONS

#### 7.1 Summary

The main objective of this study to investigate the analytical and experimental of the flexural behavior for high strength two-span continuous concrete members prestressed with hybrid (bonded and unbonded) tendons. Introducing an approach to predict the stress in the unbonded tendon and validating the model with full-scale specimens are accomplished.

A literature review is performed in chapter II to analyze and compile the most relevant existing research on continuous span members with unbonded and hybrid tendons. Literature related to predicting the stress in the unbonded tendon and solving the issue of strain incompatibility between the tendon and adjusted concrete including the most popular code revisions are performed.

To build a full database about the actual behavior of continuous post-tensioned members, an experimental program is conducted in chapter III. This includes performing 9 two-span 20 ft. long high strength concrete continuous beam specimens post-tensioned internally with bonded (grouted) and unbonded tendons subjected to third-point and single-point applied load. All the materials used in each beam specimen are tested individually to understand the actual strength capacity of the used components, these tests include the tensile strength for non-prestressed and prestressing tendon, compression test for grout and compression, tension and modulus of elasticity for concrete cylinders at different ages.

Also, a two-span trail beam with a rectangular cross-section is built to test the new beam test setup. Moreover, all applied loads, prestressing forces, deflections and strains instrumentations are presented.

All observations and measurements of the experimental program are presented in chapter IV. Crack behavior at the location of maximum positive and negative moments under different load patterns is observed. Also, the load corresponding to the appearance of the first crack at locations of maximum moments is observed. Load versus deflections at midspan and under the location of point loads, load versus strain in non-prestressed steel, beam camber, curvature, and stress increase in the unbonded tendon are demonstrated.

The derivation of the analytical models is presented and illustrated in chapter V. The combinations of both bonded and unbonded tendon with different tendon profiles are considered in the analysis. Two models are presented, one for beams subjected to a third-point load, and another one for the single-point load at midspan. The assumptions and considerations to produce the models are listed. In addition, this chapter described the trussed-beam model and applied to two-span continuous beams. All the potential curvature diagrams at different load levels and limit states and the flowchart of the programming are presented.

Validation of the results of each proposed approach with the results produced by the experimental program is introduced in chapter VI. The validity and reliability of the two approaches are examined by comparing the load versus deflection at the location of the maximum positive moment and the stress in the unbonded tendon. All section dimensions and material properties which tested individually are used in comparison to obtaining more accuracy and simulation. The comparison shows an excellent correlation

between the analytical and experimental results. After validating the models, the reliability is tested by investigating the effect of different design parameters and observing the flexural response. The investigation demonstrates that some design parameters have a significant influence on the results while the impact of other variables can be unremarkable.

## 7.2 Conclusions

The following conclusions can be made base on the analytical and experimental results in this study:

1. Non-prestressed reinforcement is the main parameter for spreading the length of plastic hinges at locations of maximum positive and negative moments as illustrated in chapter IV.
2. Further experimental work is required to investigate the actual plastic hinge length at locations of maximum moments at cracking, yielding non-prestressed steel, yielding prestressing strand and ultimate limit states.
3. The failure of all beam tests occurred due to the crushing of concrete in compression. Also, the stress in the unbonded tendon was around yielding stress  $f_{psy}$ . However, the stress in the bonded (grouted) tendon almost reached the stress at ultimate  $f_{pu}$ .
4. The presented analytical approaches can be applied for two-span continuous concrete beams prestressed with unbonded or hybrid (bonded and unbonded) tendons. Moreover, beams subjected to third-point and single-point load with different tendon profiles can be analyzed by the proposed models.

5. Both analytical models show a good correlation with the experimental results. The prediction of deflection, load carrying capacity and the stress in the unbonded tendon were good estimated.
6. The models were rational and reliable for most test beams and at most load levels, especially at ultimate limit state.
7. Reinforcing steel, prestressing bonded and unbonded strands have a significant impact on the flexural behavior such as load versus deflection and stress increase in the unbonded tendon, however, the influence of the effective stress in the prestressing tendons  $f_{pe}$  can affect the stress in the unbonded tendon while the influence on the load-deflection relationship can be ignorable.

## REFERENCES

## REFERENCES

1. A. A. Maghsudi and Y. Askari D., Ultimate Unbonded Tendon Stress in CFRP Strengthened Post-Tensioned Indeterminate I-Beams Cast with HSCs, *International Journal of Engineering (IJE)*, TRANSACTIONS C: Aspects Vol. 28, No. 3, (March 2015), pp. 350-359
2. ACI 318. Building code requirements for structural concrete and commentary. Michigan (USA): American Concrete Institute; 2014.
3. ACI Committee 363, "State-of-the-Art Report on High-Strength Concrete (ACI 363R-10)," American Concrete Institute, Farmington Hills, Michigan, 2010.
4. Aravinthan, T., Witchukreangkrai, E., and Mutsuyoshi, H. (2005), "Flexural Behavior of Two-Span continuous Prestressed Concrete Girders with Highly Eccentric External Tendons," *ACI Structural Journal*, Vol.102, No.3, May-Jun., pp. 402-411.
5. BS8110. Structural use of concrete-Part 1: Code of practice for design and construction. London (UK): British Standards Institution BSI; 1997.
6. Chakrabarti, P.R., "Ultimate Stress for Unbonded Post-Tensioning Tendons in Partially Prestressed Beams," *ACI Structural Journal*, V. 92, No. 6, Nov.-Dec. 1995, pp. 689-697.
7. Chan, K. E. (2008). Experimental and numerical studies of concrete beams prestressed with unbonded tendons. (Thesis). University of Hong Kong, Pokfulam, Hong Kong SAR.
8. Cooke, N., Park, R., and Yong, P., "Flexural Strength of Prestressed Concrete Members with Unbonded Tendons," *PCI Journal*, V. 26, No. 6, Nov.-Dec. 1981, pp. 52-80.
9. Decheng, K., "Strengthening of RC Beams and Frames by External Prestressing," M.Sc. National University of Singapore, 2009.
10. Du J. S., Au F. T. K., Cheung Y. K. & Kwan A. K. H. (2008), "Ductility analysis of prestressed concrete beams with unbonded tendons," *Engineering Structures*, 30, No. 1, 13-21.
11. Du, G., and Tao, X., "Ultimate Stress of Unbonded Tendons in Partially Prestressed Concrete Beams," *PCI Journal*, V. 30, No. 6, Nov.-Dec. 1985, pp. 72-91.
12. Du, J.S., Au, Francis T.K., Chan, Enoch K.H., Liu, L. "Deflection of unbonded partially prestressed concrete continuous beams." *Engineering Structures* 118 (2016): 89-96.

13. Harajli M. H., Mabsout M. E. & Al-Hajj J. A. (2002), "Response of externally post-tensioned continuous members", *ACI Structural Journal*, 99, No. 5, 671-680.
14. Harajli, M. H., and Kanj, M. Y., "Service Load Behavior of Concrete Members Prestressed with Unbonded Tendons," *Journal of Structural Engineering, ASCE*, V. 118, No. 9, Sep. 1992, pp. 2569-2588.
15. Lou, Tiejiong, Sergio M.R. Lopes, and Adelino V. Lopes. "Response of continuous concrete beams internally prestressed with unbonded FRP and steel tendons." *Composite Structures* 154 (2016): 92-105.
16. Machida, A., and Bamrungwong, C., "Flexural Behavior of Two-Span Partially Continuous Prestressed Concrete Beams with External Tendons," *Proceedings, IABSE Colloquium, Concrete Model Code for Asia, Structural Concrete: Design, Materials and Construction, and Maintenance, Phuket, Thailand, 1999*, pp. 191-196.
17. Mattock, A. H., discussion of "Rotational Capacity of Concrete Beams," by W. Corley, *Proceedings, ASCE*, Vol. 93, ST2, April 1967, pp. 519-522.
18. Myers, J. J., and Carrasquillo, R. L., 1998, "The Production and Quality Control of High Performance Concrete in Texas Bridge Structures," Report No. FHWA/TX-05/9-580/589-1, Center for Transportation Research, University of Texas at Austin, Austin, TX, Dec., pp. 32-33, 226-231, 424.
19. Nassif, H. H., and Ozkul, O., "Flexural Behavior of Externally Prestressed Beams," *Proceedings of the First Annual Concrete Bridge Conference, Nashville, Tennessee, October 6-9, 2002*.
20. Nassif, H., Ozkul, O., and Harajli, M. H. "Flexural Behavior of Beams Prestressed with Bonded and Unbonded," *PTI Journal*, V. 1, No. 1, Jan. 2003, pp. 60-71.
21. Nassif, H., Ozkul, O., Hwang, E. - S., and Han, M. Y., "Design and Analysis of Incrementally Prestressed Concrete (IPC) Bridge Girders," *Proceedings of the Concrete Bridge Conference, Charlotte, North Carolina, May 17-18, 2004*.
22. Nawy, E. G., "Prestressed Concrete – A Fundamental Approach", Fifth Edition Update, Upper Saddle River, N.J.: Prentice Hall, 2010.
23. Ozkul, O., Nassif, H. H., and Malhas, F., "Deflection Prediction and Cracking of High Strength Concrete Beams Prestressed with Unbonded Tendons," *Serviceability of Concrete, ACI SP-225-7, American Concrete Institute, Farmington Hills, MI, 2004*.
24. Ozkul, O., "A New Methodology for the Analysis of Concrete Beams Prestressed with Unbonded Tendons," Ph.D. Thesis, Rutgers, The State University of NJ, New Brunswick, NJ, 2007.



25. Ozkul, O., Nassif, H., Tanchan, P. and Harajli, M., "Rational Approach for Predicting Stress in Beams with Unbonded Tendons," ACI Structural Journal, Vol. 105, No. 3, May 2008, pp. 338-347.
26. Park, R., and Paulay, T., "Reinforced Concrete Structures," John Wiley & Sons, New York, NY, 1975.
27. Tan, K. H., and Tjandra, R. A., 2003b,. "Strengthening of precast concrete girder bridges by post-tensioning for continuity." PCI J., 48(3), 56-71.
28. Tanchan, P., "Flexural Behavior of High Strength Concrete Beams Prestressed with Unbonded Tendons," PhD Thesis, Rutgers, The State University of NJ, New Brunswick, NJ, 2001.
29. Unal, G., "Simplified Prediction Equation for Ultimate Stress in Beams Prestressed with Hybrid Tendons," M.Sc. Thesis, Rutgers, The State University of NJ, New Brunswick, NJ, 2011.
30. Warwaruk, J., Sozen, M. A., and Siess, C. P., "Investigation of Prestressed Reinforced Concrete for Highway Bridges, Part III: Strength and Behavior in Flexure of Prestressed Concrete Beams," Bulletin No. 464, University of Illinois Engineering Experiment Station, Urbana, Ill., Aug. 1962, pp.105.
31. Six, P., "Continuous Unbonded Post-Tensioned Members: Quantifying Strand Stress Increase," M.Sc. Thesis, Utah State University, Logan, UT, 2015.